2010

REAL-TIME MODEL PREDICTIVE CONTROL OF QUASI-KEYHOLE PIPE WELDING

Kun Qian
University of Kentucky, qkun2@uky.edu

ABSTRACT OF DISSERTATION

Kun Qian

The Graduate School
University of Kentucky
2010

REAL-TIME MODEL PREDICTIVE CONTROL OF QUASI-KEYHOLE PIPE WELDING

ABSTRACT OF DISSERTATION

A dissertation submitted in partial fulfillment of the
requirements for the degree of Doctor of Philosophy in the
College of Engineering
at the University of Kentucky

By

Kun Qian

Lexington, Kentucky

Director: Dr. YuMing Zhang, Professor of Electrical Engineering

Lexington, Kentucky

2010

ABSTRACT OF DISSERTATION

REAL-TIME MODEL PREDICTIVE CONTROL OF QUASI-KEYHOLE PIPE WELDING

Quasi-keyhole, including plasma keyhole and double-sided welding, is a novel approach proposed to operate the keyhole arc welding process. It can result in a high quality weld, but also raise higher demand of the operator. A computer control system to detect the keyhole and control the arc current can improve the performance of the welding process. To this effect, developing automatic pipe welding, instead of manual welding, is a hot research topic in the welding field.

The objective of this research is to design an automatic quasi-keyhole pipe welding system that can monitor the keyhole and control its establishment time to track the reference trajectory as the dynamic behavior of welding processes changes. For this reason, an automatic plasma welding system is proposed, in which an additional electrode is added on the back side of the workpiece to detect the keyhole, as well as to provide the double-side arc in the double-sided arc welding mode. In the automatic pipe welding system the arc current can be controlled by the computer controller.

Based on the designed automatic plasma pipe welding system, two kinds of model predictive controller − linear and bilinear − are developed, and an optimal algorithm is designed to optimize the keyhole weld process. The result of the proposed approach has been verified by using both linear and bilinear model

structures in the quasi-keyhole plasma welding (QKPW) process experiments, both in normal plasma keyhole and double-sided arc welding modes.

KEYWORDS: Quasi-keyhole welding, Model predictive control, real-time, linear model, bilinear model

Kun Qian

07/14/2010

REAL-TIME MODEL PREDICTIVE CONTROL OF QUASI-KEYHOLE PIPE WELDING

By

Kun Qian

Dr. YuMing Zhang
Director of Dissertation

Dr. Stephen Gedney
Director of Graduate Studies

07/15/2010
Date

RULES FOR THE USE OF DISSERTATIONS

Unpublished dissertations submitted for the Doctor's degree and deposited in the University of Kentucky Library are as a rule open for inspection, but are to be used only with due regard to the rights of the authors. Bibliographical references may be noted, but quotations or summaries of parts may be published only with the permission of the author, and with the usual scholarly acknowledgements.

Extensive copying or publication of the dissertation in whole or in part also requires the consent of the Dean of the Graduate School of the University of Kentucky.

A library that borrows this dissertation for use by its patrons is expected to secure the signature of each user.

Name	Date

DISSERTATION

Kun Qian

The Graduate School

University of Kentucky

2010

REAL-TIME MODEL PREDICTIVE CONTROL OF QUASI-KEYHOLE PIPE WELDING

DISSERTATION

A dissertation submitted in partial fulfillment of the
requirements for the degree of Doctor of Philosophy in the
College of Engineering
at the University of Kentucky

By
Kun Qian

Lexington, Kentucky

Director: Dr. YuMing Zhang, Professor of Electrical Engineering

Lexington, Kentucky

2010

DEDICATED TO MY FAMILY

ACKNOWLEDGEMENT

The research work in this dissertation is funded by the National Science Foundation Project under grant DMI-0527889 and University of Kentucky Center for Manufacturing.

Firstly I would like to sincerely thank my advisor Dr. YuMing Zhang for his invaluable guidance, continuous encouragement and constructive instructions. I am also grateful to Drs. Larry Holloway, Alan T. Male and JingShan Li for their helpful insight and supervision. I want to thank all of my colleagues in the Welding Research Lab: JinSong Chen, Yi Huang, XiangRong Li, Yi Lu, Yan Shao, XiaoJi Ma, GuoHong Ma, ZhenZhou Wang, YuKang Liu and ZhiJiang Wang for their helpful suggestions for my work.

In addition, I want to give my thanks to my parents and brother/sister for their endless love and support throughout all my life. Also I'd like to express my great appreciation to my wife, Ding, for supporting and sharing with me so many wonderful things in my life. Lastly, I'd like to thank my son, Allen, for giving me the happiness in the past two years.

TABLE OF CONTENTS

LIST OF TABLES

LIST OF FIGURES

CHAPTER 1 Introduction

1.1 Background

Welding is one of the simplest and easiest ways to join pipe sections. Compared to other mechanical joint ways − such as the flanged joints, threaded joint etc. − welding can eliminate the complicated joint designs and special threading equipment, resulting in reduction in overall joint cost. Another important advantage of welding is that it can achieve the best joint quality. This is an important aspect, since modern processes impose higher and tougher demands on the pushing pressure, flow, and temperature requirements on today's pipe systems than they were decades ago. The joint defects, such as leaks that were once considered nuisances, are now classified as hazardous spills and dangerous, since these problems are so serious that sometimes can shut down plants or even jeopardize human life. The welding can provide the best sealing and fastening quality in the pipe joint, thus it has manifold application in the industry.

Quasi-keyhole arc welding (QKAW), including plasma arc welding [1] and patented keyhole double-sided arc welding − developed at the University of Kentucky [2], is a novel approach proposed to operate the keyhole arc welding process that has significant advantages over laser welding in industrial applications in terms of cost, application range, safety, joint preparation, etc. [3]. It uses highly constrained plasma arc, coming from the nozzle of the plasma torch, to establish the keyholes, subsequently closed with melted metal after keyholes are confirmed along the butted line to realize the joint of workpieces. Compared with other welding methods, such as Gas Metal Arc Welding (GMAW), QKAW can easily achieve full penetration, typically required in high quality pipe welding. There are many other advantages to QKAW, which will be discussed in next chapter, increasing the range of QKAW

applications in the pipe welding joint processes.

Conventionally, welding processes are highly labor-intensive and need skilled operators. In addition the pipe welding, compared to plate welding, imposes higher skill requirement on operators. Furthermore, due to the harsh environment and intense process disturbance, sound welds are not guaranteed to be repeatable from weld to weld. Thus, automated arc welding becomes important for productivity, quality and cost-efficiency. In orbital automated pipe welding (OAPW) the torch moves with a computer controlled weld head (a traveler to install the torch) on the orbit rail ring during the weld process, instead of manually. Since many factors, such as the torch position and weld speed, can affect the result of weld, most of OAPW cannot handle so many factors online to adapt the change of conditions during the weld. This is in contrast to experienced welders that can adjust various factors during the manual welding to guarantee the full penetration and prevent burn-through and get a satisfying weld result. This limitation of OAPW prevents its wider application, especially on some critical weld jobs, in which experienced welder is still irreplaceable. In order to get a good weld quality in the orbital pipe welding, a suitable control system must be developed.

Some successful quasi-keyhole welding controllers, based on the interval model [7], have been reported in the past [3, 4, 5, 6] by University of Kentucky, and these controllers are developed. This is a time-domain algorithm and is proposed to control the interval plants described by the impulse response function [8], that means the impulse response process boundaries $\{h_{\max}(k), h_{\min}(k)\}$ need to be known. Although the interval models can take into account the widely varying conditions and consequently have wide application, too wide or inaccurate intervals are still an issue. In this dissertation, a new kind of control algorithm, based on the MPC is proposed to control QKAW process.

Another deficiency of the former designs is that only peak current is controlled

in the process and other parameters are set to empirical constants. Optimization of selected performance indices by adjusting specific parameters online, would achieve better results in the automatic welding process. In this dissertation, one optimization method is proposed and experimentally verified.

1.2 Objective

The objective of this study is focused on developing an automatic control system to improve the productivity, quality and efficiency of the quasi-keyhole pipe arc welding (QKPAW) process. This control system should be able to adjust the weld arc current to prevent burn-through and establish the keyhole in reference time to ensure the welding quality and overcome the process variability, fluctuation and disturbance. The result of the study has good potential to be used as a promising and commercial product.

Therefore, the specific dissertation objective can be summarized to following three components:

- Design a control system for the QKPAW, including the sensor, the controller, the online monitor/control software;
- Develop an advanced control algorithm for the controller and verify it's performance from experiments;
- Find a feasible method to optimize the weld quality to workpiece during the welding process.

1.3 Outline of dissertation

This dissertation is organized as follows:

Chapter 1 introduces the background, the objective and the outline of the dissertation.

Chapter 2 provides a review of quasi-keyhole pipe welding process. It evaluates

the common arc welding methods, followed by the introduction of the quasi-keyhole welding process and its comparison with other arc welding methods. Some concepts of the pipe welding are also given.

Chapter 3 reviews the popular control methods in the industry, followed by specifics of the model predictive control (MPC).

In chapter 4, the QKPAW system developed in this study is introduced, as well as the methodology for its realization. Chapter 5 introduces the process modeling and simulation. The basic modeling theories are reviewed first, followed by the linear and bilinear model structures. The simulations conducted on the basis of the identified models are also presented.

Chapter 6 and 7 describe the linear and bilinear model predictive controller design, followed by the experimental results.

Chapter 8 introduces the improved MPC to optimize the process heat input..

In Chapter 9, the description of double-sided arc welding experiments, conducted on the thicker pipe to test the performance of the control system, is given.

Chapter 10 concludes this study and proposes suggestions for future work. It summarizes the results and contribution of this research and gives the future direction of this research.

CHAPTER 2 Quasi-keyhole Pipe Welding

The quasi-keyhole welding (QKW) process[5, 9] including the plasma arc welding[1, 10] and double-sided arc welding[4], uses a highly constrained plasma jet coming from the plasma arc torch to establish the keyhole, and then maintains and closes the keyhole by switching from the peak current to a lower arc current − called the base current (in plasma welding model) or double-side current (in double-sided welding model) − after the keyhole establishment is confirmed, so the melted metal solidified in the keyhole to realize the joint. With an effective keyhole sensor, QKW can assure the desired full penetration and, if well controlled, avoid burn-through − a condition under which the melted metal detaches from the work-piece. This process has significant advantages over laser welding in industrial application in terms of cost and complexity.

To present a concept of quasi-keyhole pipe welding, in this chapter, some basic welding methods are introduced first, followed by the introduction of plasma arc welding and the double-sided arc welding process, and finally, the characteristics of the pipe welding process.

2.1 Arc Welding Method

Arc welding uses the arc, created by one or more welding power supplies, between an electrode and the base material to melt the metals at the welding area. There are many welding methods used in the industry, which can be divided into two main classes: (1) Consumable electrode method, such as gas metal arc welding (GMAW), which uses the melted metal from electrode as well as the melted base material with optional addition of filler material, to realize the metal joint. (2) Non-consumable electrode method, such as Gas tungsten arc welding (GTAW), which

uses the tungsten as the electrode not melted in the welding.

2.1.1 GMAW welding

Gas metal arc welding, sometimes is referred to by its subtype metal inert gas (MIG) welding, or metal active gas (MAG) welding, is a semi-automatic or automatic arc welding process in which a continuous and consumable wire electrode and a shielding gas are fed through a welding gun. A constant voltage and direct current power source is most commonly used with GMAW, but constant current systems, as well as alternating current, are also be used. There are four primary methods of metal transfer in GMAW − globular, short-circuiting, spray, and pulsed-spray − each of which has distinct properties and corresponding advantages and limitations [11].

GMAW was originally developed for welding aluminum and other non-ferrous materials in the 1940s. Although it was soon applied to steel welding, as it allowed for lower welding time compared with other welding processes, the high cost of inert gas limited its wide-spread use in steels until several years later, when the use of semi-inert gases such as carbon dioxide became common. Today, GMAW is the most common industrial welding process, preferred for its versatility, speed and the relative ease of robotic automation. The automobile industry in particular uses GMAW welding almost exclusively. Unlike welding processes that do not employ a shielding gas, such as shielded metal arc welding, GMAW is rarely used outdoors or in other areas of air volatility. A related process, flux cored arc welding, often does not utilize a shielding gas, employing a hollow electrode wire filled with flux on the inside instead [12].

There are many benefits of GMAW that will ensure its popular application in the industry:

1. The welding can be performed in almost any position;
2. Higher deposition rates compared to other welding methods;
3. Lower operator skill required ;

4. Long welds can be made without starts and stops;
5. Minimal post weld cleaning is required;

GMAW also has some disadvantages, such as difficult arc starting, unstable arc, easily burn back and irregular wire feed, two of the most prevalent quality problems are:

1. Heavily oxidized weld deposit, also called dross. It is caused by oxygen of any origin, whether from the atmosphere or the shielding gas, in contact with the weld pool. As a result, sufficient flow of inert shielding gases is necessary, and welding in volatile air should be avoided;
2. Porosity. Porosity is caused by the gas that enters the metal in the process and cannot escape before the metal is solidified. Keeping the arc steady and reducing the cooling rate are effective ways to eliminate the porosity.

2.1.2 Gas tungsten arc welding

Gas tungsten arc welding (GTAW), also known as tungsten inert gas (TIG) welding, is an arc welding process that uses a non-consumable tungsten electrode to produce the weld. The weld area is protected from the shielding gas (usually an inert gas such as argon), and a filler metal is normally, but not necessarily, used in the process. A constant-current welding power supply produces energy that is conducted across the arc through a column of highly ionized gas and metal vapors known as the plasma [13].

GTAW has popular application in welding of thin sections of stainless steel and light metals such as aluminum, magnesium, and copper alloys. It grants the operator greater control over the weld than other welding methods such as shielded metal arc welding and gas metal arc welding, allowing for stronger, higher quality welds. However, GTAW is comparatively more complex and difficult to master, and furthermore, it is significantly slower than most other welding techniques.

Compared to other welding methods, GTAW welding benefits can be

summarized as follows:

1. Superior quality welds. GTAW can achieve clean, high-quality weld results, demonstrated by a small distortion of the welded workpiece;
2. Precise control of welding variables; such as the heat and the width of the weld line.
3. Clean weld process. There is little spatter or slag, sparks, or smoke produced during the GTAW;
4. Application in wide range of metals.

The shortcomings of GTAW are well known, some of limitations are:

1. Requires greater welder dexterity than in MIG or stick welding;
2. Lower deposition rates;
3. Higher level of UV rays;
4. More costly for welding thick sections.

2.1.3 Plasma arc welding

To improve the performance of GTAW, a related process, plasma arc welding, uses a slightly different welding torch to create a more focused welding arc and as a result is often automated [10]. Plasma arc welding (PAW) is an advanced version of GTAW or TIG welding process. GTAW welding has a free-burning arc, which is unstable and tends to wander in the low current range. With an increase in current, the arc power and diameter also increases. This leads to a lack of concentrated power in the work-piece, which results in a bigger seam and a larger heat-affected zone [14]. To overcome this limitation, The PAW method employs a plasma gas and a shielding gas in the PAW torch. The arc comes from the electrode, generally made of tungsten, goes through the constricting nozzle, which highly constrained the arc to be a narrow columnar shape, as Figure 2-1 shows.

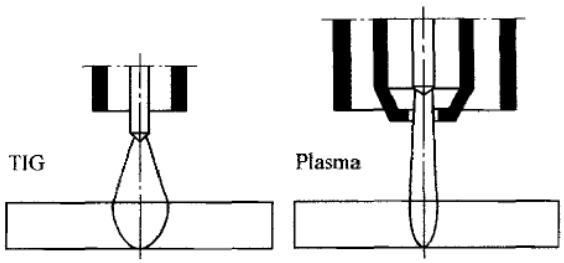

Figure 2-1 Comparison of TIG and Plasma

Figure 2-2 shows a simple plasma welding structure, in which the cooling water is recycled to extract the heat created by arc, in order to cool the torch and prevent the nozzle burnout. The plasma gas and shielding gas flow through the inner and outer part of the plasma nozzle respectively.

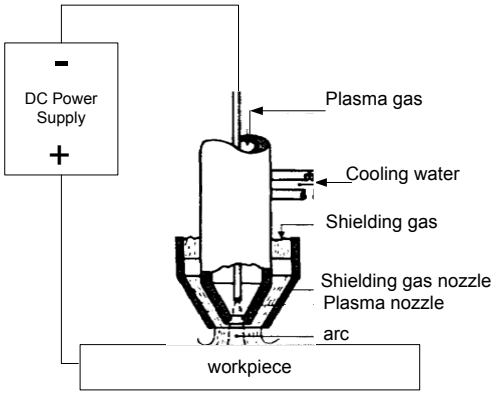

Figure 2-2 Plasma arc welding

In PAW, the plasma arc torch electrode is recessed into the nozzle. In order to bridge the arc current between the electrode and the welded workpiece, a pilot arc, ignited from electrode tungsten to nozzle and blown out by the orifice gas, is needed before the PAW process can start. The pilot arc, generated between tungsten (cathode) and torch nozzle (anode), is forced through a fine-bore copper nozzle that constricts the arc and the plasma that exits the orifice at high velocities (approaching the speed of sound) and temperatures approaching 20,000 °C [10]. In the PAW process, the main arc is constrained by the small orifice to ensure that the plasma jet is more directionally stable than the gas tungsten arc welding.

The most important advantage of PAW is that its arc is straighter and more concentrated than the arc produced by other welding methods, such as TIG and

GMAW hence the method is less sensitive to arc length. In the welding process, the PAW variance of 2-3 mm is acceptable without significantly changing the heat input to the workpiece, which is about ten times greater than that of TIG method [14].

When a current is passed between two electrodes though a gas, the gas molecules accelerate and collide with each other. As the energy increases, it exceeds the binding force between the atom nucleus and electrons and the electrons are released from the atom. The gas now consists of neutral molecules, positively charged atoms, and negative electrons. After the gas is ionized, it is called plasma, the fourth state of matter, and has the capability of conducting current. Plasma occurs in all welding arcs to varying degrees. The characteristic features of PAW include [14]:

1. The reliable penetration with the keyhole method;
2. Butt welds possible in thick materials (up to 8mm) without the use of filler;
3. Weld possibly even in very thin materials;
4. Lower heat affected zone and little distortion;
5. High arc stability at low arc current;
6. Little sensitivity to arc length variations as a result of the concentrate arc;
7. Less filler metal required in keyhole mode significantly reduces porosity;
8. Flexible, due to the ability to perform the keyhole welding and melt-in welding using the same equipment.

2.1.4 Classification of PAW method

According the current range, the PAW can be divided into three different classes [15]:

a. Micro plasma welding:

The current is between 0.1A to 15A, can be used for welding the metal thickness down to about 0.1mm, attractive to aero space industry.

b. Medium plasma welding:

The range of current is (15A − 100A), suitable for welding the sheet materials to

reduce the distortion or unacceptable joints.

c. Keyhole plasma welding:

Welding current >100A, the main benefit of keyhole plasma welding is that it can be used for butt welds up to 8mm and provide full penetration.

Although the PAW is classified based on the current range, it is not the focus of this dissertation. Since the peak currents in our experiments are normally greater or equal to 100A, the keyhole plasma welding is a part of QKAW in this research.

2.2 Keyhole plasma Arc Welding

In the keyhole plasma welding, appropriate selection of the combination of arc current, plasma gas flow and the travel speed will produce a relatively small weld pool with a hole penetrating completely through the base metal. It is called the keyhole plasma welding.

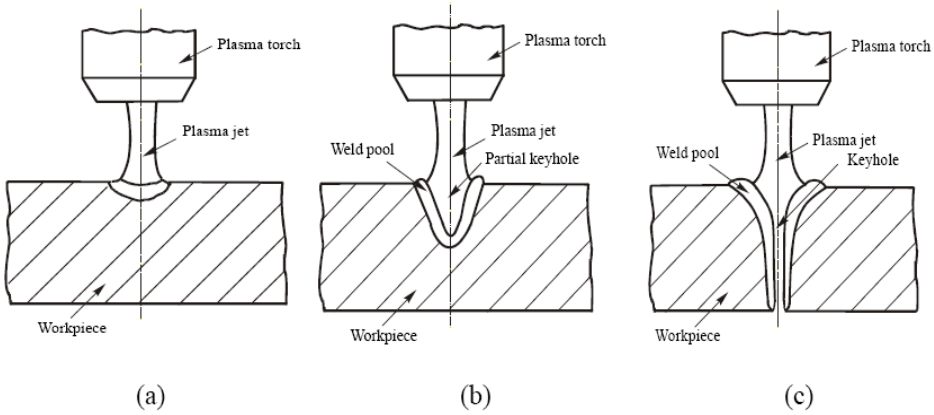

Figure 2-3 Dynamic development in keyhole PAW process [5]

In the keyhole welding operation, the keyhole is formed with the melted metal displaced to the top bead surface by the plasma stream. As the plasma arc torch is then moved forward along the weld joint, the metal melted by the arc at the front side of the keyhole flows around the plasma stream to the rear, where the weld pool progressively solidifies. As the torch continues to move forward, the keyhole progresses with it, leaving the liquid metal solidified behind it. A typical formation of keyhole process is shown in Figure 2-3. In Figure 2-3(a), the plasma arc begins to act

on the workpiece, and the workpiece is barely melted and the weld pool is small. With the increasing energy, the melted metal is blown away, causing the depth of the weld pool and the partial keyhole to increase, as shown in Figure 2-3(b). Figure 2-3(c) shows that the weld pool finally becomes fully penetrated and the full keyhole is established through the work-piece thickness.

The principal advantage of keyhole welding is full penetration of a thicker material than achieved by GTAW in a single pass. Although keyhole PAW involves more process variables and its energy density is lower than laser beam welding or electron beam welding, keyhole PAW is more cost effective and more tolerable to joint preparation, not to mention its advantages over conventional GTAW in terms of penetration depth, joint preparation, welding speed and thermal distortion [16]. Thus, keyhole PAW has the potential to replace GTAW in many applications as a primary process for precise joining.

Despite its merits above, keyhole PAW has narrow operating windows. For example, when the keyhole is barely established, a slight decrease in the welding current and/or the flow rate of the plasma gas, or a slight increase in the welding speed may result in a keyhole failure. This implies that the stable state of the keyhole needs to be improved to prevent the failure. If the welding current and the plasma gas flow rate are increased and/or the welding speed is decreased, the process will withstand larger variations in the welding parameters, such as the welding current, the flow rate of the plasma gas and the welding speed, without a collapse of the keyhole. However, once the welding current and the plasma gas flow rate increase and/or the welding speed decreases to certain levels, further changes in these parameters may cause a burn-through, a phenomenon in which the molten metal is detached from the workpiece by arc pressure. Thus, more operator skill is required for manual operation. Hence automatic plasma arc welding is more critical and challenging [5].

2.2.1 Keyhole PAW waveform description

A typical current waveform and efflux signal recorded quasi-keyhole welding process can be designed as illustrated in Figure 2-4. Figure (a) shows base current I_b and peak current I_p measured from the process and they are illustrated in Figure (b). At the beginning of a cycle, the arc current is switched to I_p to establish the keyhole on the workpiece. After the keyhole is established and the efflux plasma reaches the detection pipe as the result, the main welding power supply (power supply 1) switches the arc current from I_p to I_b. The keyhole would be closed slowly during the base current period, as the heat input and the arc pressure reduces to allow the melted metal to fill the keyhole and solidifies in it. After a specified period of base current T_b and when the torch moves forward to a required position, the peak current is applied again to re-establish the keyhole, beginning a new pulse cycle. As this result, the process is not maintained in the keyhole mode as it is classically defined, but in a repeated establishing-closing-solidifying mode which is termed quasi-keyhole [17].

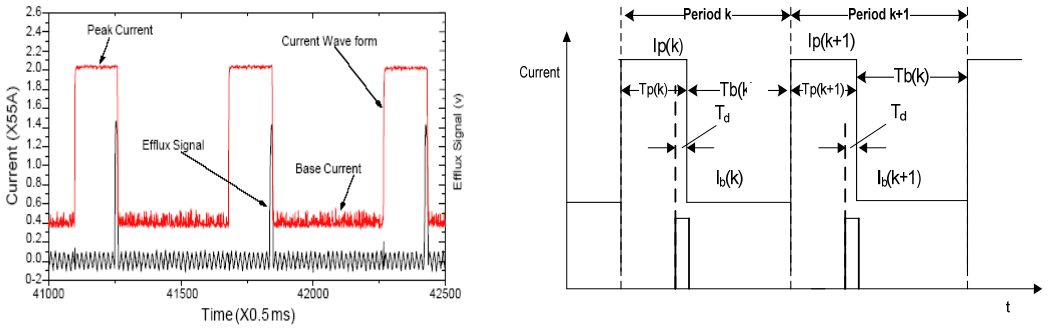

(a)Measured current signal (b) Graphical representation of signal

Figure 2-4 Keyhole PAW process waveforms

The base current time, T_b， is typically set to be constant and remains the same in every period. Hence, when $I_b(k-1)$ increases, more heat is input into the workpiece, resulting in higher temperature around the area where the keyhole would be established. As a result, less heat input would be needed to establish the keyhole in the keyhole-establish time, so that $T_p(k+1)$ is shortened in determinate $I_p(k+1)$.

2.3 Double-Sided Arc Welding (DSAW)

DSAW, a novel welding process developed and proposed in the University of Kentucky [9] [4], is another quasi-keyhole arc welding. Based on the regular keyhole PAW, DSAW is realized by inserting another electrode on the other side of the welded workpiece, when the keyhole exists, the plasma arc can go through the keyhole instead of dispersing on the welded metal. The theoretical design can be explained by the Figure 2-5

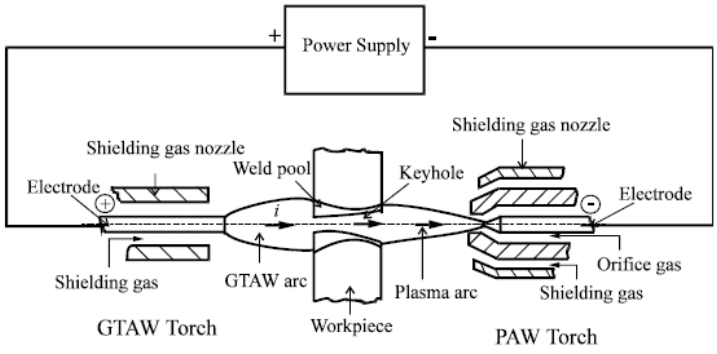

Figure 2-5 DSAW system structure [9]

In the DSAW, before the keyhole is established, the main weld current goes through the PAW torch to the surface of the welded workpiece, as in regular PAW welding. After the keyhole is established, the arc flow through the thickness of the workpiece and arrives at the rear electrode. In this case, the direction of the arc is referred to as “through the thickness.” Since the arc is concentrated in the keyhole instead of dispersing on the surface of the welded workpiece, the DSAW achieves unique energy concentration and radial heating mechanism. In addition to having the same advantages as the keyhole PAW, DSAW has some additional benefits as following [9]:

1. DSAW can get a symmetric and hourglass butt shape on both sides of the welded workpiece.
2. DSAW has a proven capability of achieving the deeper, narrower joint penetration on thick workpiece up to 12.7mm (1/2 inch) in a single pass.

3. DSAW can reduce the heat input into the workpiece by at least 70%, compared to the regular plasma arc welding.

These characters make DSAW more suitable for joining thick workpiece up to 12.7mm (1/2inch), while other arc welding methods normally need the workpiece to be coved and welded in multiple pass. Although high power laser can realize the one pass welding of 10mm thickness steel, its high cost, high pre-weld preparation and complicated system prevent its wide-spread application in the industry.

2.3.1 Waveform of DSAW

Since the DSAW is a component of the quasi-keyhole welding, its waveform is similar with the waveform of the keyhole PAW: It also uses the high current (I_p) pulse to establish the keyhole, and after the keyhole is detected, the high current is switched to a low current. The difference between them is that DSAW switches I_p to a lower current than I_b in keyhole PAW, and uses the double-side arc (I_d) to maintain the keyhole instead of the base current. The Figure 2-6 shows the current waveform of the DSAW, including (a) the waveform measured from the experiment and it is illustrated by the (b).

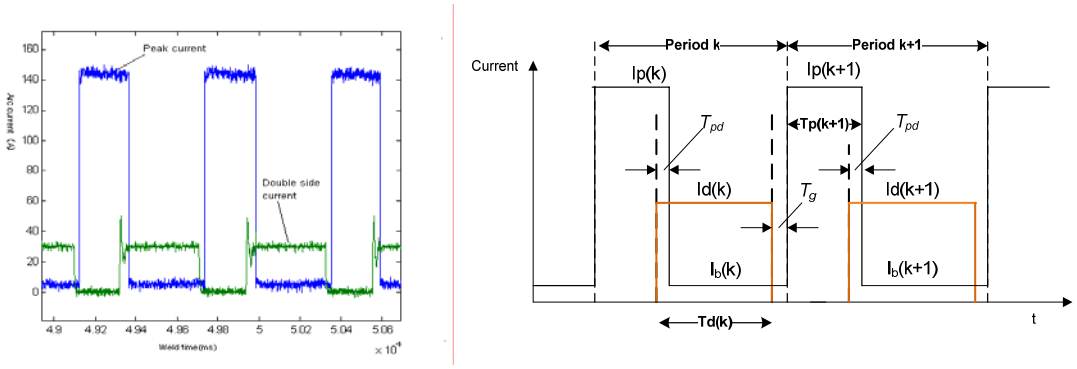

(a) Measured current waveform (b) Waveform illustration

Figure 2-6 DSAW current wave form

In this current waveform, I_p is used to establish the keyhole. When the keyhole is opened entirely by the plasma arc, some plasma can emerge through the keyhole and

reach the rear electrode to bridge the arc between the two electrodes. Due to the voltage difference between the two electrodes, I_d is stepped up from zero when the keyhole is detected, and I_p is switched down to I_b after T_{pd}, a short time in which I_p and I_d coexist to make sure keyhole can be kept open until I_d becomes stable. T_{pd} is determined by the electrical performance of the power supply. Figure 2-6(a) shows that in the experiment, I_d becomes stable in around 30ms after it is switched on, as the resulting T_{pd} is set as 30ms in the following experiment. After keyhole is detected, I_d is kept for T_d − a constant double-side current time set before weld − then it is shut off. After T_g − another short time interval ensuring that the keyhole can be closed before the new I_p is applied − the main current is switched back to the peak current to establish new keyhole and begin a new weld cycle.

In the quasi-keyhole welding, T_p is one of important variables. To get the full penetration, the distance between neighbor keyholes l must be longer than the minimum diameter of the keyhole R, which is normally on the back side of workpiece in quasi-keyhole PAW, as Figure 2-7(a) and (b) shows. If T_p is too long, l may be longer than R and the keyholes cannot superpose the adjacent next keyhole, as Figure 2-7(c) shows, so the full penetration cannot be ensured since the part of the welding line between adjacent keyholes cannot be fully melted, as the Figure 2.7(d) shows. On the other hand, if T_p is too short, excessive superpose occurs in adjacent keyholes, thus the weld pool area may be blown open too many times by I_p. In addition, the shorter T_p implies higher than necessary I_p may be applied, resulting in the large arc pressure − proportional to the square of the current – that may easily cause a burn-through. In order to get a satisfactory weld line, the peak current should be just sufficient to achieve the desired keyhole establishment time. Thus, the objective of the control system is to keep the output of the system T_p tracking the

trajectory of a desired reference T_p^*.

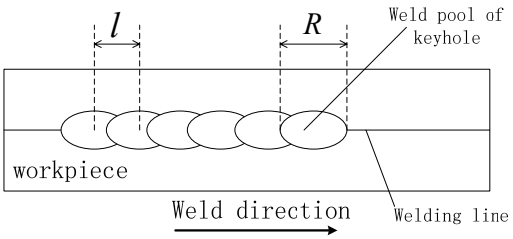

(a) Full penetration

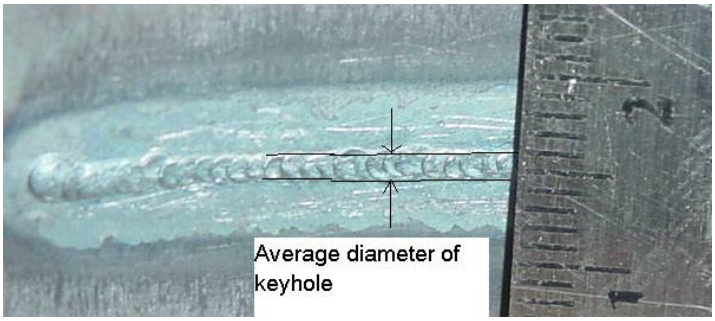

(b) Full penetration practical example

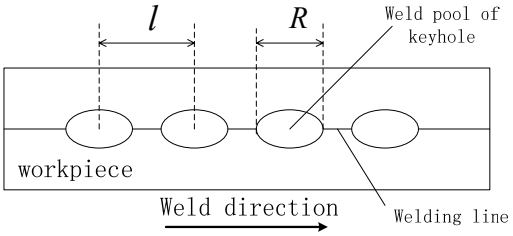

(c) Non-Full penetration

(d) Non-Full penetration practical example

Figure 2-7 Keyholes in the welded workpiece

2.4 Pipe Welding

Since this study is focused on the pipe welding, some pipe welding fundamentals

are introduced in this subsection. In contrast to the plate welding, where the angles between the plate, gravity and torch are usually unchanged; in the pipe welding, the weld position is a critical parameter for the weld quality. Although the terms flat, horizontal, vertical, and overhead sufficiently describe the positions for the plate welding, they do not adequately describe the pipe welding positions. In the pipe welding, there are four main positions of pipe weld in the industry, as Figure 2-8 shows, and they are known as the horizontal rolled position (1G), vertical position (2G), inclined position (6G) and horizontal fixed position (5G) [18], i.e. There is no 3G or 4G test position in pipe welding.

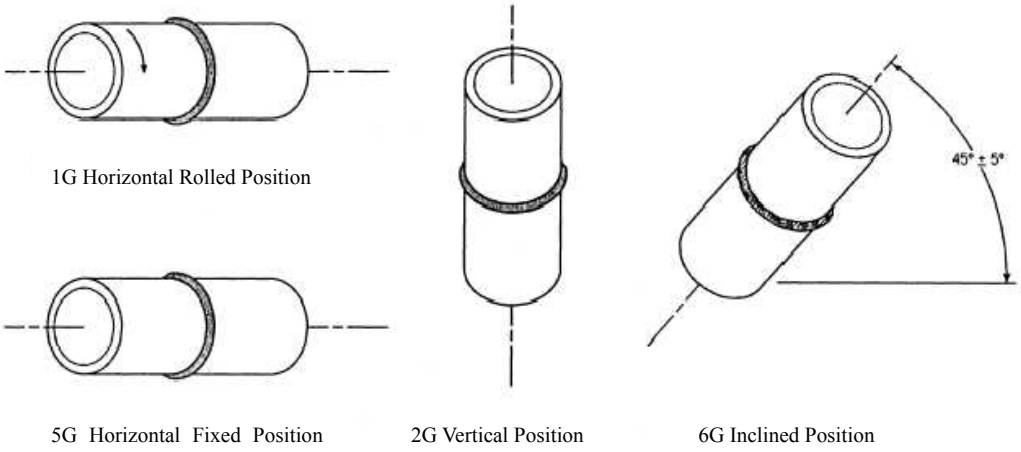

Figure 2-8 Pipe welding positions

The position of weld pool greatly affects the flow of the molten filler metal due to gravity. The 1G position is similar to the plate welding, since the torch is fixed (normally in the top position), and the welded pipe is rolling during the weld. As the gravity draws the molten metal downward into the joint, making the welding faster and easier, unfortunately 1G position welding can only be used in short pipe welding in which the welded pipes can rotate easily. In the pipe line welding in the field, or the pipe joint in manufacturing such as in construction and ship yard, the pipes to be welded are too long to rotate or at least one of the welded pipes is fixed in position that cannot move in the welding process. In this situation, of interest in this research,

5G position welding is used, where welded pipes are fixed and the torch is moved around the pipes to realize the whole position welding that is more practical and important in the industry.

It is obvious that 5G position welding is much more difficult than 1G position welding. Since the torch moves around the pipe, the weld changes from flat (top position) to vertical, and finally to overhead position weld. During this process, the model parameters may change greatly to increase the difficulty of weld control. The remaining 2G − vertical welding, and 6G − inclined position welding, are more difficult than the horizontal position welding and require considerable practice to produce good quality welds, they are outside of scope of this research. This dissertation is focused on the horizontal welding since it is the most popular welding position in the industry.

When the pipe is welded in the 5G position, in order to identify the torch and weld pool position in the weld process and easily illustrate them in this paper, the pipe positions are consistently numbered from 1 to 12 as shown in Figure 2-9, the top of the pipe is called 12'oclock position and the bottom of the pipe is called 6'oclock position.

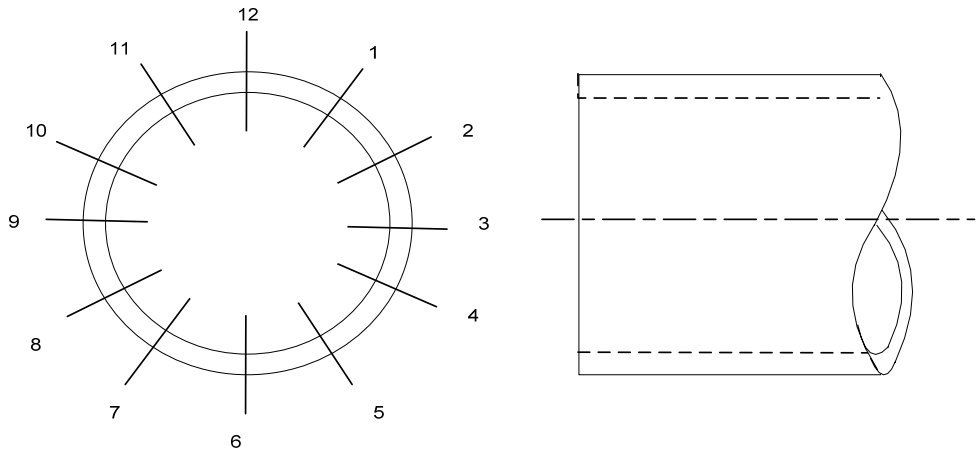

Figure 2-9 Number position around the pipe

CHAPTER 3 Model Predictive Control

Before introducing the MPC controller developed in this study, some key concepts of MPC, necessary for better understanding the designed controller, are presented. In this chapter, the development and principles of MPC are reviewed first, followed by the introduction of some popular MPC algorithms in the industry. In the third section, nonlinear MPC is summarized and its two algorithms are presented.

3.1 Introducing the MPC

The objective of predictive analysis is to estimate future and unknown results based on the analysis of the past and current information. The modern control theory based on the state space method has been developing since the beginning of 1960's, and has prompted the evolution of the automatic control technology, but there is still a gap between its theory and application. To overcome the problem, scientists began to develop alternative control algorithms that dispense with complex models and enable easy online computation, resulting in the Predictive control.

In the predictive control, MPC is one of the most important algorithms and is a subject of extensive research in the academia and industry. MPC has been studied since the end of 1980s [28]; it determines the online control input by solving a finite horizon open loop control optimization problem [29]. It can explicitly account for model uncertainties and has been widely used in industrial applications [30].

MPC refers to a class of computer control algorithms that do not designate a specific control strategy; instead they make explicit use of the process model to obtain the control signal by minimizing an objective function. At each control interval, an MPC algorithm determines a sequence of manipulated variable adjustments that optimize future plant behavior. The first input in the optimal sequence is then sent

into the plant as an instant control signal, and the entire optimization is repeated at subsequent control intervals; where at each instant the horizon is displaced towards the future by applying the first control signal of the sequence calculated at each step [31].

MPC is capable of considering both constant and varying future set-points. The objective of the predictive control law is to drive future plant outputs $y(k+j)$ close to the reference outputs $y_r(k+j)$ as the main control problem. This is done by using a receding-horizon approach for which at each sample-instant k, as shown in Figure 3-1 [32]. The future set-point sequence $y_r(k+j)$ is calculated in the algorithm, where a prediction model is used to generate a set of predicted outputs and obtain the corresponding predicted system error. The appropriate quadratic function of the future errors and controls is subsequently selected to be minimized in the calculation, assuming that after some control horizon further increments in control are zeros. A suggested sequence of future controls can be provided after the calculation above. The first element of the future sequence and output to the controlled process − the appropriate data vector shifts – are asserted, so that the calculations can be repeated at the next control instant.

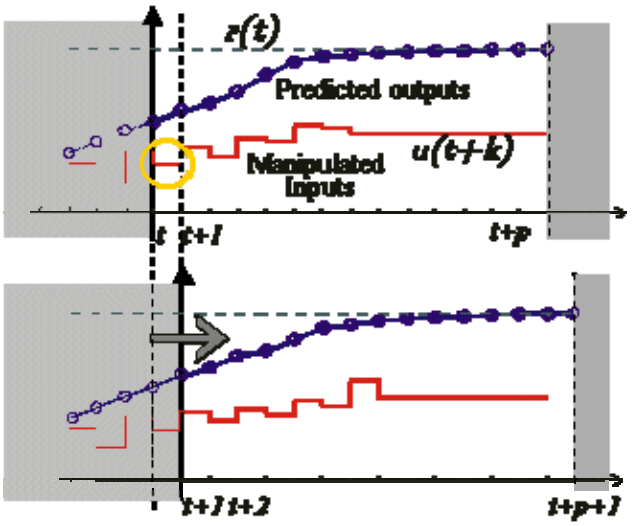

Figure 3-1 Receding-horizon approach

Since the model predictive control is a type computer control based on the model, it not only uses the current and past errors, but the future errors predicted by predictive model to calculate the optimal input, as shown in Figure 3-2. To resolve the MPC control problem, the typical quadratic function mentioned above is typically selected, given by:

$$J = \sum_{j=0}^{n-1} \left(\| y_{k+j|k} - y_{ref} \|_Q^2 + \| \Delta u_{k+j|k} \|_S^2 \right) \quad \text{(Eq.3-1)}$$

The objective function in Eq.3-1 illustrates some of the commonly used terminology in the MPC literature. Outputs and controls are usually doubly indexed as $y_{k+j|k}$ and $u_{k+j|k}$ to indicate values at time $k+j$, given information up to and including time k. Since MPC requires prediction, the double subscript also carries the connotation of prediction when the first index is larger than the second. Variables that are singly indexed may be used to represent controls or outputs that have already been implemented, computed or measured up to the current time k. An optimal sequence of controls is often indicated using an asterisk $(u^*_{k+j|k})$. The corresponding output values then become $y^*_{k+j|k}$. The $\Delta u_{k+j|k}$ illustrated in the equation is $\Delta u_{k+j|k} = u_{k+j|k} - u_{k+j-1|k}$.

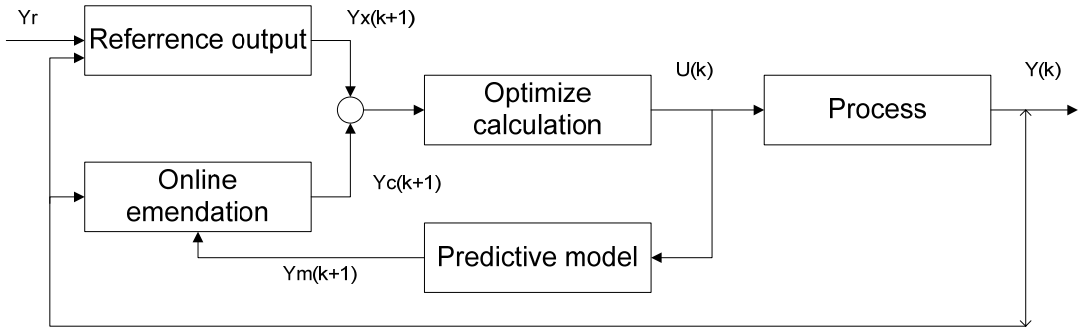

Figure 3-2 Structure diagram of predictive control

3.2 Development of MPC

Model Predictive Control originated and appeared in industry about 30 years ago as an effective means for addressing multivariable constrained control problems. Although the idea of receding horizon control and model predictive control can be traced back to 1960's, interest in this field increased only in 1980's after publication of the first paper on Dynamic Matrix Control(DMC), and the first comprehensive exposition of Generalized Predictive Control(GPC) [33] [34, 35]. Thus since late 1970s, various articles have appeared showing an incipient interest in MPC in industry, principally the Richalet *et al.* publications [36] presenting Model Predictive Heuristic Control (MPHC) (later known as Model Algorithmic Control (MAC)) and those of Cutler and Ramakter[37] with Dynamic Matrix Control (DMC).

The success of MPC, particularly in chemical process industries, is due to the simplicity of the algorithm and the use of the impulse or step response model which, although possessing many more parameters than the formulations in the state space or input-output domain, is usually preferred as being more intuitive and requiring less priori information for its identification. The use of a finite-horizon strategy allowed the explicit handling of process and operational constraints by the MPC, and their heuristic and algorithmic formulations, and took advantage of the increasing potential of digital computers of that time.

Another line of work on adaptive control ideas emerged independently, developing strategies essentially for mono-variable processes formulated with input-output models. Some examples of these strategies are Extended Prediction Self Adaptive Control (EPSAC) by De Keyser and Van Cuawenberghe [38] or Generalized Predictive Control (GPC) developed by Clarke *et al.* in 1987 [34, 35]. In the early time of the development, MPC was considered to be a technique suitable to linear and rather slow systems like those usually encountered in the process industry; more complex systems − such as nonlinear, hybrid, or very fast processes − were

considered beyond the realm of MPC, until publication of some recent impressive results in these fields. Applications of MPC to nonlinear and to hybrid processes have also appeared in the literature, the majority of applications (see surveys by Qin and Badgwell [39]) are in the area of refining, one of the original application fields of MPC, where it has a solid background. An important number of applications can be found in petrochemical and chemical industry. Although MPC technology has not yet penetrated deeply into areas where process nonlinearities are strong and frequent changes in operation conditions occur, the number of nonlinear MPC applications is clearly increasing.

Historically, the models of choice in linear industrial MPC applications were time domain, input/output, step, or impulse response models [36, 37]. Continuous-time models may be more familiar to those with a classical control background in transfer functions, but discrete-time models are very convenient for digital computer implementation. Linear models in the process industries are, by their nature, empirical models and identified from input/output. The ideal model form for identification purposes is perhaps best left to the experts in identification theory, but a survey of that literature indicates no disadvantages to using state-space models inside the MPC controller. In this research the discrete-time input/output models MPC is a chose method for resolving the QKPAW problem.

3.3 The Popular MPC Algorithm

The predictive control has greatly progressed since the model predictive heuristic control (MPHC) was introduced by Richalet in 1978. Many model predictive control algorithms have been proposed and have successful application [40]. Amongst these algorithms, DMC, MAC and GPC are the most successful and have important influence in the industry, and they are introduced in the subsequent subsections.

3.3.1 Model Algorithmic Control (MAC)

MAC uses the inner model based on the impulse response, and takes advantage of the past and future input and output information to predict the future output. It completes the feedback emendation with the output error of the model, compared with the reference output, and optimizes it with the quadratic form performance index to calculate the input control signal to the process in the current cycle. Figure 3-3 shows the MAC structure diagram.

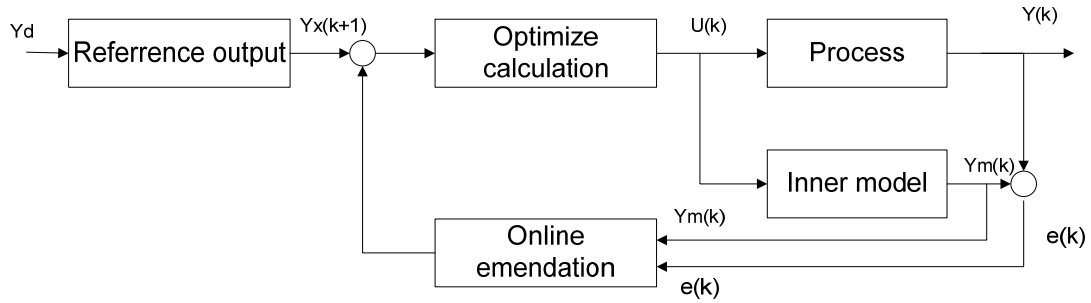

Figure 3-3 Structure diagram of MAC

3.3.2 Dynamic Matrix Control (DMC)

DMC is an algorithm that uses the optimization to achieve the control strategy. It is different from MAC in that it uses the step response, which is easier to be measured in the industry, has the advantages of less computation and strong robustness. It is a multiple variable optimal control algorithm with constraints proposed by C.Culter [37] and was first applied at Shell at 1974.

The predictive model of the DMC can be expressed as follows:

At every instant k, controlled increase in the future M horizon $\Delta u(k),\cdots,\Delta u(k+M-1)$ needs to be determined to create the system output in the future P horizon $y_M(k+i\,|\,k)$, which under these circumstances, can be close to the reference output $y_r(k+i)$. Here, M and P are denoted as control horizon and optimal horizon.

When a control signal increment is added into the input, the output serials can be measured in each sample time. The output serials can be expressed as the dynamic coefficients: $\hat{a}_1, \hat{a}_2, \ldots, \hat{a}_N$.

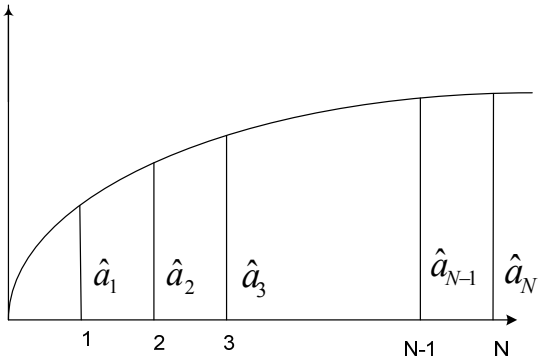

Figure 3-4 Dynamic coefficients of step signal

The output of the predictive model in the future *P* times will be:

$$\begin{aligned} y_m(k+1/k) &= y_0(k+1/k) + \hat{a}_1 \Delta u(k) \\ y_m(k+2/k) &= y_0(k+2/k) + \hat{a}_2 \Delta u(k) + \hat{a}_1 \Delta u(k+1) \\ &\vdots \\ y_m(k+P/k) &= y_0(k+P/k) + \hat{a}_P \Delta u(k) + \hat{a}_{P-1} \Delta u(k+1) + \cdots + \hat{a}_{P-M+1} \Delta u(k+M-1) \end{aligned} \quad \text{(Eq.3-2)}$$

Here $y_m(k+j/k)$ are the predictive outputs of the future *N* steps at *k* when $\Delta u(k)$ was added into the model and $y_0(k+j/k)$ are the predictive outputs of future *N* steps at k without $\Delta u(k)$.

Eq.3-2 can be rewritten in a matrix form:

$$Y_m(k+1) = Y_0(k+1) + A\Delta U(k) \quad \text{(Eq.3-3)}$$

where

$$Y_m(k+1) = \left[y_m(k+1/k), y_m(k+2/k), \ldots, y_m(k+P/k) \right]^T \quad \text{(Eq.3-4)}$$

$$Y_0(k+1) = \left[y_0(k+1/k), y_0(k+2/k), \ldots, y_0(k+P/k) \right]^T \quad \text{(Eq.3-5)}$$

$$A=\begin{bmatrix} \hat{a}_1 & 0 & 0 & 0 \\ \hat{a}_2 & \hat{a}_1 & 0 & 0 \\ \vdots & \vdots & \vdots & 0 \\ \hat{a}_P & \hat{a}_{P-1} & \cdots & \hat{a}_{P-M+1} \end{bmatrix}_{P\times M} \quad \text{(Eq.3-6)}$$

here A is composed of the step response coefficients, and is called Dynamic Matrix, and $Y_0(k+1)$ is the initial output of the predictive model. It comes from the control increment before the time *k*. The control increments from $k-1$ are assumed to be $\Delta u(k-N), \Delta u(k-N+1), \cdots, \Delta u(k-1)$, while $\Delta u(k-N-1)=\Delta u(k-N-2)=0$.

The initial output can be expressed as:

$$\begin{aligned} y_0(k+1/k) &= \hat{a}_N\Delta u(k-N)+\hat{a}_N\Delta u(k-N+1)+\hat{a}_{N-1}\Delta u(k-N+2)+ \\ &\quad \cdots+\hat{a}_2\Delta u(k-2)+\hat{a}_2\Delta u(k-1) \\ y_0(k+2/k) &= \hat{a}_N\Delta u(k-N)+\hat{a}_N\Delta u(k-N+1)+\hat{a}_N\Delta u(k-N+2)+ \\ &\quad \hat{a}_{N-1}\Delta u(k-N+3)+\cdots+\hat{a}_2\Delta u(k-2)+\hat{a}_2\Delta u(k-1) \\ y_0(k+P/k) &= \hat{a}_N\Delta u(k-N)+\hat{a}_N\Delta u(k-N+1)+\cdots+\hat{a}_N\Delta u(k-N+P) \end{aligned} \quad \text{(Eq.3-7)}$$

Since

$$\begin{aligned} &\Delta u(k-N)=u(k-N)-u(k-N-1) \\ &\Delta u(k-N+1)=u(k-N+1)-u(k-N) \\ &\qquad\vdots \\ &\Delta u(k-1)=u(k-1)-u(k-2) \end{aligned} \quad \text{(Eq.3-8)}$$

Thus the initial output can be expressed as

$$Y_0(k+1)=A_0U(k-1) \quad \text{(Eq.3-9)}$$

here

$$U(k-1)=[u(k-N+1),u(k-N+2),\cdots,u(k-1)]^T$$

$$A_0=\begin{bmatrix} \hat{a}_N-\hat{a}_{N-1} & \hat{a}_{N-1}-\hat{a}_{N-2} & \hat{a}_{N-2}-\hat{a}_{N-3} & \cdots & \hat{a}_3-\hat{a}_2 & \hat{a}_2 \\ & \hat{a}_N-\hat{a}_{N-1} & \hat{a}_{N-1}-\hat{a}_{N-2} & \cdots & \hat{a}_4-\hat{a}_3 & \hat{a}_3 \\ 0 & \ddots & & & \vdots & \vdots \\ & \hat{a}_N-\hat{a}_{N-1} & \hat{a}_{N-1}-\hat{a}_{N-2} & \cdots & \hat{a}_{P+2}-\hat{a}_{P+1} & \hat{a}_{P+1} \end{bmatrix} \quad \text{(Eq.3-10)}$$

By substituting Eq.3-9 into Eq.3-3, the predictive model can be expressed by the control input:

$$Y_m(k+1)=A_0U(k-1)+A\Delta U(k) \quad \text{(Eq.3-11)}$$

In order to reduce the effects caused by disturbance and the unmatched model, the predictive system output should be the sum of the predictive output of the model and the measure error:

$$Y_p(k+1) = Y_m(k+1) + h\left[y(k) - y_m(k)\right] = A\Delta U(k) + A_0 U(k-1) + he(k) \qquad \text{(Eq.3-12)}$$

Since in the control process the control increase Δu does not normally change enough to cause the oscillation, it can be realized by adding a constraint in the performance index. As the result, the performance index can be chosen as:

$$J = \left[Y_p(k+1) - Y_r(k+1)\right]^T Q\left[Y_p(k+1) - Y_r(k+1)\right] + \Delta U^T(k)\lambda\Delta U(k) \qquad \text{(Eq.3-13)}$$

here λ is a weight coefficient, used to constrain the change of control input u .

Since in the k instant, $Y_p(k+1)$ and $Y_r(k+1)$ are already known, the J can be minimized by ΔU, then the control law can be obtained by solving $\partial J_p / \partial \Delta U(k) = 0$ to get

$$\Delta U(k) = (A^T QA + \lambda)^{-1} A^T Q[Y_r(k+1) - A_0 U(k-1) - he(k)] \qquad \text{(Eq.3-14)}$$

This yields all the optimal input increments $\Delta u(k), \cdots, \Delta u(k+M-1)$, even though the DMC does not need all of them and only the first increase $\Delta u(k)$ is selected to be control input to the controlled system. In the next instant, the algorithm above is repeated to obtain $\Delta u(k+1)$. That is the 'rolling optimization' mentioned before.

3.3.3 Generalized Predictive Control (GPC)

Generalized Predictive Control is a predictive control algorithm developed in the adaptive control research. It adopts the CARIMA (Controlled Auto-Regressive Integrated Moving Average) or CARMA (Controlled Auto-Regressive Moving Average) as the predictive model, and overcomes the shortcoming of the impulse response model and step response model that cannot describe unstable processes and are hard to implement online. GPC keeps the model prediction of the

minimum-variance self-tuning controller and introduces the concept of multi-step prediction in the optimization to the parameters of slowly varying system. Since GPC uses the traditional model, the model parameters can be identified online to achieve adaptive control.

There are numerous algorithms aimed at resolving the GPC problem; here a typical simple GPC algorithm, based on the original model parameters, is introduced. The advantage of this algorithm is that, unlike other GPC algorithms, it does not need to resolve the Diophantine equation that requires substantial computational effort that may prohibit its on-line applications.

The mathematical model of the controlled objective is a discrete-difference function:

$$A(z^{-1})y(k) = B(z^{-1})u(k-1) + C(z^{-1})\xi(k)/\Delta \qquad \text{(Eq.3-15)}$$

where y, u, ξ are system input, system output and white-noise respectively, with 0 mean value, $\Delta = 1 - z^{-1}$, $A(z^{-1}) = \sum_{i=1}^{n_a} a_i z^{-i}$, $B(z^{-1}) = \sum_{i=0}^{n_b} b_i z^{-i}$

Consider a CARIMA model:

$$y_{k+1} = -A_1 y_k - \cdots - A_{n+1} y_{k-n} + B_1 \Delta u_k + \cdots + B_{n-1} \Delta u_{k-n+1} \qquad \text{(Eq.3-16)}$$

where y is the output vector, and Δu is the input vector.

Writing out the difference equation for the next n_y sampling instants yields:

$$\begin{aligned}
y_{k+1} + A_1 y_{k+1} + \cdots + A_{n+1} y_{k-n} &= B_1 \Delta u_k + B_2 \Delta u_{k-1} + \cdots + B_{n-1} \Delta u_{k-n+1} \\
y_{k+2} + A_1 y_{k+2} + \cdots + A_{n+1} y_{k-n+1} &= B_1 \Delta u_{k+1} + B_2 \Delta u_{k-1} + \cdots + B_{n-1} \Delta u_{k-n+2} \\
&\vdots \\
y_{k+1} + A_1 y_{k+n_y} + \cdots + A_{n+1} y_{k-n+n_y+1} &= B_1 \Delta u_{k+n_y-1} + \cdots + B_{n-1} \Delta u_{k-n+n_y}
\end{aligned} \qquad \text{(Eq.3-17)}$$

The matrix form of the upper equation is given as:

$$\underbrace{\begin{bmatrix} I & 0 & \cdots & 0 \\ A_1 & I & \cdots & 0 \\ A_2 & A_1 & \cdots & 0 \\ \vdots & \vdots & \vdots & \vdots \end{bmatrix}}_{C_A} \underbrace{\begin{bmatrix} y_{k+1} \\ y_{k+2} \\ \vdots \\ y_{k+n_y} \end{bmatrix}}_{\underset{\rightarrow}{y}_k} + \underbrace{\begin{bmatrix} A_1 & A_2 & \cdots & A_{n+1} \\ A_2 & A_3 & \cdots & 0 \\ A_3 & A_4 & \cdots & 0 \\ \vdots & \vdots & \vdots & \vdots \end{bmatrix}}_{H_A} \underbrace{\begin{bmatrix} y_k \\ y_{k-1} \\ \vdots \\ y_{k-n} \end{bmatrix}}_{\underset{\leftarrow}{y}_k}$$

$$= \underbrace{\begin{bmatrix} B_1 & 0 & \cdots & 0 \\ B_2 & B_1 & \cdots & 0 \\ B_3 & B_2 & \cdots & 0 \\ \vdots & \vdots & \vdots & \vdots \end{bmatrix}}_{C_{zb}} \underbrace{\begin{bmatrix} \Delta u_k \\ \Delta u_{k+1} \\ \vdots \\ \Delta u_{k+n_y-1} \end{bmatrix}}_{\Delta \underset{\rightarrow}{u}_{k-1}} + \underbrace{\begin{bmatrix} B_2 & B_3 & \cdots & B_n \\ B_3 & B_4 & \cdots & 0 \\ B_4 & B_5 & \cdots & 0 \\ \vdots & \vdots & \vdots & \vdots \end{bmatrix}}_{H_{zb}} \underbrace{\begin{bmatrix} \Delta u_{k-1} \\ \Delta u_{k-2} \\ \vdots \\ \Delta u_{k-n+1} \end{bmatrix}}_{\Delta \underset{\leftarrow}{u}_{k-1}} \quad \text{(Eq.3-18)}$$

Simplifying the Eq.3-18 to

$$C_A \underset{\rightarrow}{y}_k + H_A \underset{\leftarrow}{y}_k = C_{zb} \Delta \underset{\rightarrow}{u}_{k-1} + H_{zb} \Delta \underset{\leftarrow}{u}_{k-1} \quad \text{(Eq.3-19)}$$

yields the output predictions obtained by shifting the items in Eq.3-19

$$\underset{\rightarrow}{y}_k = H \Delta \underset{\rightarrow}{u}_{k-1} + P \Delta \underset{\leftarrow}{u}_{k-1} + Q \underset{\leftarrow}{y}_k \quad \text{(Eq.3-20)}$$

where $H = C_A^{-1} C_{zb}$, $P = C_A^{-1} H_{zb}$, $Q = -C_A^{-1} H_A$

In order to formulate the GPC control law, the vector formulation of the cost equation should be firstly defined.

$$J = \left\| \underset{\rightarrow}{r} - \underset{\rightarrow}{y} \right\|_2^2 + \lambda \left\| \Delta \underset{\rightarrow}{u} \right\|_2^2 \quad \text{(Eq.3-21)}$$

Substitute Eq.3-20 into Eq.3-21

$$J = \left\| \underset{\rightarrow}{r} - H \Delta \underset{\rightarrow}{u}_{k-1} + P \Delta \underset{\leftarrow}{u}_{k-1} + Q \underset{\leftarrow}{y}_k \right\|_2^2 + \lambda \left\| \Delta \underset{\rightarrow}{u} \right\|_2^2 \quad \text{(Eq.3-22)}$$

Since the performance index is quadratic and positive, the unique minimum J can be calculated by setting the first derivative to zero.

$$\frac{dJ}{d\Delta \underset{\rightarrow}{u}} = 2\left(H^T H + \lambda I\right) \Delta \underset{\rightarrow}{u} + 2H^T \left[Q \underset{\leftarrow}{y} + P \underset{\leftarrow}{\Delta u} - \underset{\rightarrow}{r} \right] = 0$$
$$\Rightarrow \Delta \underset{\rightarrow}{u} = \left(H^T H + \lambda I\right)^{-1} H^T \left[\underset{\rightarrow}{r} - Q \underset{\leftarrow}{y} - P \Delta \underset{\leftarrow}{u} \right] \quad \text{(Eq.3-23)}$$

Thus the current control law is

$$\Delta u_k = g_1 \left(H^T H + \lambda I \right)^{-1} H^T \left[\underset{\rightarrow}{r} - Q \underset{\leftarrow}{y} - P \Delta \underset{\leftarrow}{u} \right] \quad \text{(Eq.3-24)}$$

where $g_1 = [\mathrm{I}_m, 0, 0, \cdots, 0]$

3.4 Nonlinear MPC

In general, industrial processes are nonlinear, but many MPC applications are based on the use of linear models. There are two main reasons for this: on one hand, the identification of a linear model based on process data is relatively easy and, on the other hand, linear models provide good results when the plant is operating in the neighborhood of the operating point. In addition, the use of a linear model together with a quadratic objective function gives rise to a convex problem whose solution is well studied, with many commercial applications available.

In many practical situations the process requires frequent changes from one operation point to another and, therefore, a nonlinear model must be employed. The use of Nonlinear Model Predictive Control (NMPC) is justified in those areas where process nonlinearities are strong and process demands require frequent changes in operation regimes. Although the number of applications of NMPC is still limited (see [41], [19]), its potential is excellent, and MPC using nonlinear models is likely to become more common as users demand higher performance and new software tools make nonlinear models more readily available.

From a theoretical point of view, when a nonlinear model changes the control problem from a convex QP to a non-convex Non-Linear Program (NLP), the solution of which is much more difficult. There is no guarantee, for example, that the global optimum can be found.

In a highly nonlinear system, there are two main MPC control methods reported in the real application: Neural Networks and fuzzy predictive control, and their basic algorithms can be introduced as follows.

3.4.1 Neural Networks

The nonlinear dynamics of the process can also be captured by an artificial Neural Network (NN). Neural networks are general and attractive tools for modeling nonlinear processes, since they have the ability to approximate any nonlinear function to an arbitrary degree of accuracy [42]. This, together with the availability of training techniques, has made them very successful in many predictive control applications and commercial products. The potential of NN for practical application lies in their following properties: (1) they can be used to approximate any continuous mapping, (2) they achieve this approximation through learning, (3) parallel processing and non-linear interpolation can easily be accomplished with NN [32];

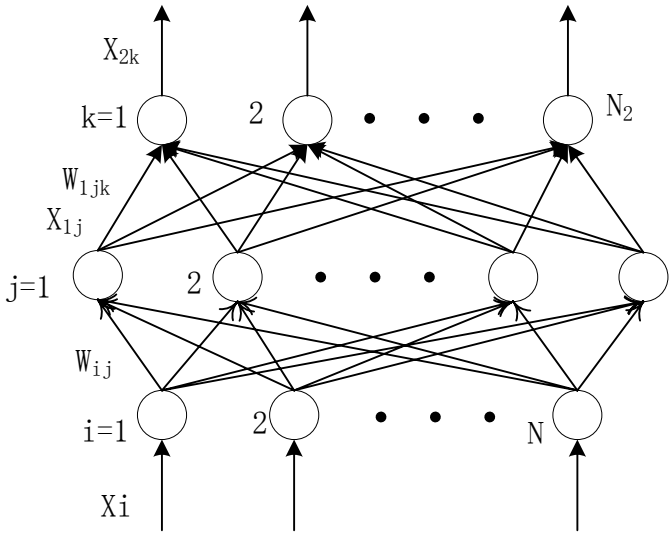

Figure 3-5 Three layer Neural Network structure

Neural Networks are usually combined with linear models in practical applications, since they are not able to extrapolate beyond the range of their training data set. Based on a model confidence index, the NN is gradually turned off when its prediction appears unreliable, whereby the predictions continue relying on the linear part.

One of the well-developed NN is a three-layer perceptron, Figure 3-5 shows the basic structure of this network. It has been proven that a three layer NN can

approximate any continuous function to the desired accuracy.

The output of the three-layer NN can be described by

$$W_{2k} = f(X;W) = \sum_{h=1}^{N_1} \sigma \left[\sum_{j=1}^{N} \left[W_{ijk} \sigma \left[\sum_{i=1}^{N_0} W_{ij} X_i + \theta_{0j} \right] + \theta_{1k} \right] \right] + \theta_2 \qquad \text{(Eq.3-24)}$$

$k = 1, \cdots, N_2$

where X is a regression vector given by

$$X = \left[y(t), \cdots, y(t-n_y), u(t), \cdots, u(t-n_u) \right]^T$$

$\sigma(.)$ is the activation function, W_{ij} the first-to-second layer interconnection weights, W_{1ij} the second-to-third layer interconnection weights, and θ_{ij}, θ_{2k}, are threshold offsets. It is usually desirable to adapt the NN weights and thresholds off-line or on-line in real-time to achieve the required approximation performance of the net. That is, the NN should have the learning ability. The back-propagation (BP) algorithm has been used to give the NN this ability. The basic idea of BP algorithm is to use the gradient algorithm to minimize the network-output error. Using the structure presented in Figure 3-5, the computation of BP can summarized as follows:

1. compute the output of the HIDDEN layer, X_{1j}

   $\bar{X}_{1j} = \dfrac{1}{1+\exp(-\bar{O}_{1j} + \bar{\theta}_{1j})}$, where $\bar{O}_{1j} = \sum_{i=1}^{N} W_{ij} X_i$, and X_i is the input of NN.

2. Compute the output of OUTPUT layer, X_{21}

   $X_{21} = \dfrac{1}{1+\exp(-O_{21} + \theta_{21})}$, where X_{21} is the output of the NN, and

   $O_{21} = \sum_{j=1}^{N_1} W_{1j1} X_{1j}$

3. Update the weights from HIDDEN to OUTPUT layer, W_{1j1} by

   $W_{1j1}^{t+1} = W_{1j1}^{t} + \eta_1 \delta_{11} X_{1j}$, where $\delta_{11} = -(X_{21}^d - X_{21})$ with X_{21}^d is the desired

output, and X_{21} is the NN output.

4. Update the weights from INPUT to HIDDEN layer, W_{ij}

   $W_{ij}^{t+1} = W_{ij}^{t} + \eta_2 \delta_j \bar{X}_i$, where $\delta j = [\delta_{11} W_{1j1}] W_{1j}(1 - X_{1j})$

5. Update the thresholds, θ_{21}, θ_{1j} by $\theta_{21}^{t+1} = \theta_{21}^{t} + \eta_{1\theta}\delta_{11}, \theta_{1j}^{t+1} = \theta_{1j}^{t} + \eta_{2\theta}\delta_j$, where $\eta_{1\theta}$ and $\eta_{2\theta}$ are gain factors.

To decide when to end the training process, a terminating condition for the training process is usually formulated as $\varepsilon = \frac{1}{2}\sum_{l=1}^{M}(X_{21}^{dl} - X_{21}^{l})^2$, where l is the sample number. The iterative tuning process is terminated when ε is smaller than a specified threshold and the optimum weight W is obtained.

Based on the NN model presented above, the linear model, required in MPC, can be extracted at each time instant by dynamic linearization. The dynamic linearization in this context implies that the system is linearized at each time instant regardless of whether the system is in a steady or in a transient state.

Linear transfer function obtained by dynamic linearization is described as

$$G(z,t) = \frac{b_1 z^{-1} + b_2 z^{-2} + \cdots + b_n z^{-n}}{1 + a_1 z^{-1} + a_2 z^{-2} + \cdots + a_n z^{-n}} \qquad \text{(Eq.3-25)}$$

where a, b are the parameters of the model and can be obtained by using a first-order Taylor series approximation of the non-linear model:

$$a_k(t) = -\frac{\partial y(t)}{\partial y(t-k)} \qquad \text{(Eq.3-26)}$$

$$b_k(t) = -\frac{\partial y(t)}{\partial u(t-k)} \qquad \text{(Eq.3-27)}$$

Since the detailed structure and parameters of the mapping between the input and output are known from the NN model, a, b can be calculated with Eq.3-26 and Eq.3-27.

The NN model predictive control can be illustrated as in Figure 3-6. After NN model is identified and linearized, the linear MPC can be called to calculate the input control signal.

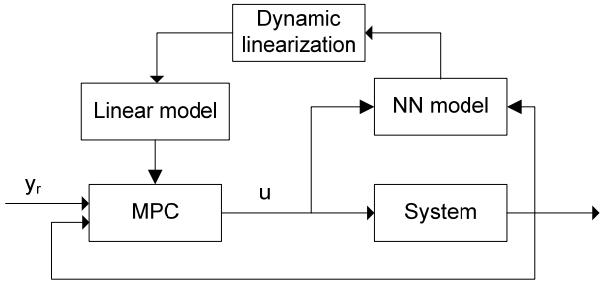

Figure 3-6 Predictive control diagram based on NN model

3.4.2 Fuzzy predictive control

A highly nonlinear system controlled by a linear model predictive controller (MPC) may not exhibit a satisfactory dynamic performance. This has led to the development of a number of nonlinear MPC (NMPC) approaches that permit the use of first principles-based nonlinear models. Such models can be accurate over a wide range of operating conditions, but may be difficult to develop in many industrial applications. Moreover, an NMPC usually requires tremendous computational effort that may prohibit its on-line applications.

Fuzzy predictive control is a fuzzy control based on the prediction of the predictive model, and according the objective error and the experience of the operator, using the fuzzy decision method to decide the output online. This method is applied in the Endpoint Dynamic Control of some complicated processes. Another type of fuzzy predictive control, comprised of the fuzzy identification and the GPC, is the multi-viable predictive control based on identification of the fuzzy model. It can use the linear system theory to design the GPC, which simplifies the design and achieves fast tracking performance and good robustness [43]. In this method, a nonlinear system is divided into a number of linear, or nearly linear, subsystems. Thus a quasi linear empirical model is developed by fuzzy logic for each subsystem where the

output is rewritten in the weighted average value of the output:

$$y(k+1)=\frac{\sum_{j=1}^{P} w^j y^j(k+1)}{\sum_{j=1}^{P} w^j} \quad \text{(Eq.3-28)}$$

$$\Delta u(k+i)=\sum_{j=1}^{P} w^j \Delta u^j(k+i) \quad \text{(Eq.3-29)}$$

where w^j are the weights of output, and

$$J(k)=\sum_{i=1}^{Ny}\sum_{j=1}^{P}\mu_i\left(w^j\left(y^j(k+i)-yr(k+i)\right)\right)^2+\sum_{i=1}^{Nu}\sum_{j=1}^{P}v_i\left(w^j\Delta u^j(k+i)\right)^2 \quad \text{(Eq.3-30)}$$

Then the controller design can be accomplished through a two layer iterative process. The upper layer design is decomposed into the derivation of local controllers. In the lower layer design, for the j_{th} subsystem, the optimization problem is defined as follows:

$$\min_{\Delta u^j(k+1),\Delta u^j(k+2),\cdots,\Delta u^j(k+Nu)} J^j(k)$$

Subject to

$$R^j: \text{If } y(n+k-1)\text{is } A_0^j, y(n+k-2)\text{is } A_1^j,\cdots,y(n+k-m)\text{is } A_{m-1}^j$$
$$\text{and } u(n+k-1)\text{is } B_0^j, u(n+k-2)\text{is } B_1^j,\cdots,u(n+k-l)\text{is } B_{l-1}^j$$

$$\text{Then } y^j(n+k)=y^j(n+k-1)+\sum_{i=1}^{T}h_i^j\Delta u(n+k-1)+\varepsilon^j(n+k-1)$$

The predictive output can be obtained as:

$$\hat{Y}(k)=\left(\sum_{j=1}^{P}w^j y^j(k+1),\sum_{j=1}^{P}w^j y^j(k+2),\cdots,\sum_{j=1}^{P}w^j y^j(k+N_y)\right)^T$$

After resolving the optimization problem, the control input can be calculated as

$$\Delta U(k)=\left(\sum_{j=1}^{P}w^j \Delta u^j(k+1),\sum_{j=1}^{P}w^j \Delta u^j(k+2),\cdots,\sum_{j=1}^{P}w^j \Delta u^j(k+N_u)\right)^T$$

3.5 Constraints of MPC

Nearly every application imposes constraints; actuators are naturally limited in the force (or equivalent) they can apply. Safety limits − such as maximum temperature,

pressure and velocity and efficiency − often dictate steady-state operation close to the boundary of the set of permissible states [31], and have an important effect to the feasibility of the designed controller.

In MPC design, three types of constraints exist: hard, soft and terminal constraints.

Hard constraints are constraints which must be satisfied, such as the limits on actuators (which must lie between 0% and 100%). In the welding process, two types of hard constraints exist: input and output constraint. The input constraint is an obvious hard constraint is the current output limit, since the output of the weld power supply is limited by its electrical performance. In the welding system proposed in this paper, the weld current cannot exceed 450A, the upper limit of the power supply, or be lower than 0A. As the result, hard constraint can be defined between (0A, 450 A).

Soft constraints are those which should be satisfied if possible, to prevent fatigue damage to equipment or to ensure quality, but can be violated if necessary. In most traditional controlled objectives, the gradual change of control variables is preferred in order to achieve a smooth process. This desired performance is achieved by adding penalizing violation of soft constraints in the formulation. In the quasi-keyhole welding, some soft constraints should be added on the peak current and the peak current time. The reason for that is that although the power supply can output the current up to its limit and hold it constant for a long time, the nozzle of the weld torch usually cannot endure the heat created and passed from the arc; hence with the increase of the peak current and the peak current time, the nozzle is burned quickly.

CHAPTER 4 Quasi-keyhole Welding System design

A good welding system is a key to get a satisfying welding quality in the welding process. The quasi-keyhole, just as the name implies, must have a practical and efficient keyhole sensor to detect the keyhole establishment. Another requirement of the welding system is that it needs a fast response of the controller, in order to control the welding process. In this chapter, the designed experiment system is described in detail. In the first section, the hardware composition is introduced, followed by the explanation of the program used to realize the automatic control process.

4.1 System Component

The proposed experimental system is shown in the Figure 4-1. The improved system mainly consists of three power supplies, two desktop computers, two current sensors, and voltage isolation modules. [54]:

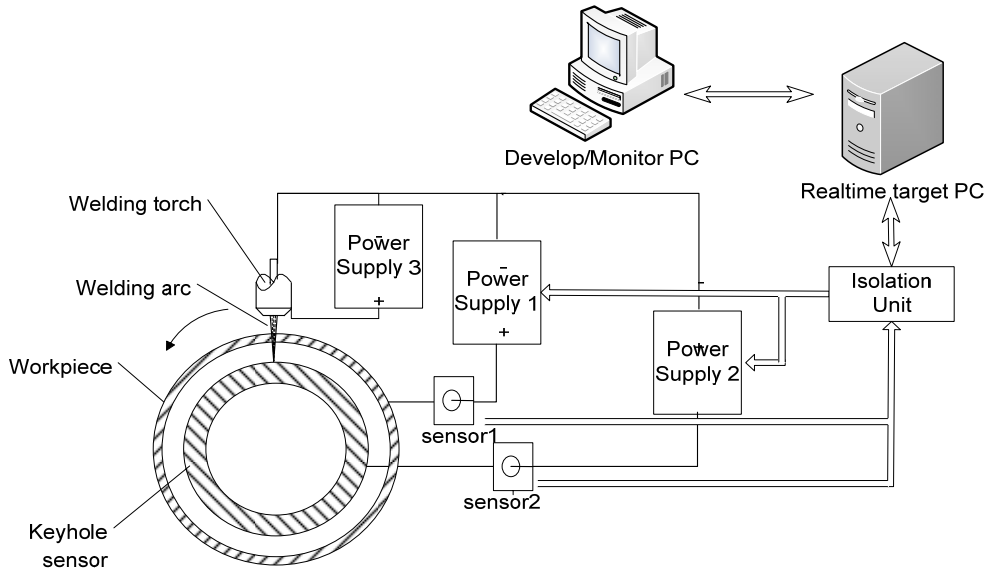

Figure 4-1 System structure of QKAPW

4.1.1 Power supply

Power supplies, the devices that provide electrical current, are the key component in the welding process. Welding power supplies are usually classified as constant current (CC) or constant voltage (CV). CC power supply adjusts its output voltage to maintain a steady current; whilst the CV power supply, in contrast, maintains the voltage by adjusting the output current. In this experimental system, as Figure 4-1 shows, three different power supplies − all operating in the CC mode − are used, and their purposes in the system are stated as follows:

The pilot arc power supply (power supply 3 in Figure 4-1) in the QKAW system is used to start the pilot arc before beginning the welding process. Maxstar 150 STH, produced by Miller Electric MFG. Co. was chosen. It is a compact TIG/STICK weld power supply with high frequency arc start for non-contact TIG. In this experimental arrangement, the positive output of the pilot is connected to the plasma torch nozzle, and the negative pole is connected to the torch tungsten electrode.

Figure 4-2 Maxstar 150 STH

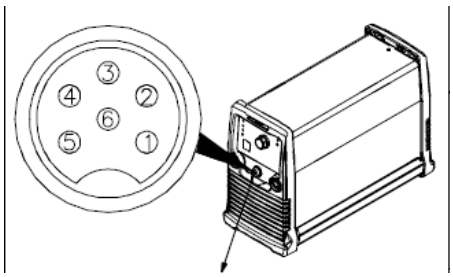

Figure 4-3 Connecter of Maxstar 150 STH

Physically, the pilot arc is a small current between the tungsten and the nozzle, blown out the orifice by the gas and has a return electrical path built into the torch

head. The pilot arc will be self-maintained until it is brought into proximity of the workpiece, whereby the main plasma welding arc is ignited. There are two main approaches to producing pilot arc plasma in the application. The first one, used in our early QKPAW system, is manually contact-started. In this method, the nozzle and electrode are manually short-circuited by using a tungsten rod, which is moved away quickly after the pilot arc is generated. When the plasma gas begins to flow, the nozzle is blown forward to produce the pilot arc plasma. The second approach is a high frequency (HF) self-start method, used in the improved system. Here, a high-voltage, high-frequency and low current circuit is used to initialize a very small high-intensity spark within the torch body, thereby generating small pilot arc plasma. This method is adopted in the QKPAW, due to its advantages: the pilot arc is stared easily, and – in contrast to the manual start − in the event of arc break-off, there is no need to move the torch off the weld head to start the arc. This method does have some disadvantages, such as the risk of electrocution associated with the high voltage pulse, and the large amount of radio frequency emissions − which greatly disturb the electrical signals or even damage the sensitive electronics (electric hardware or computers) when the pilot arc is ignited. To resolve this issue, the voltage isolation modules, introduce later, are used to separate the power supply signals from the computer signals.

On the Maxstar 150 front panel, there is one 5-pin connector used to remote control the power supply; to enable the output, the pin 1 and pin 2 must to be short circuited. In the QKPAW system, a relay is connected to pin 1 and pin 2. When the system is electrified, the relay short circuits the two pins, thus achieving a small pilot arc current of around 10A in the weld process.

The function of the main power supply (power supply 1 in Figure 4-1) is to produce plasma arc to establish the keyhole in the process. The arc current is adjusted by the computer through the machine remote control connector, and can be

maintained in the preset current by the machine inner control circuit. In the first step, Miller MAXTRON 450, as Figure 4-4(a) shows was used as the main power supply. It is a DC CC/CV Inverter MIG power supply, which can output up to 450A current and can be controlled by computer through a remoter connector. Since Miller MAXTRON 450, as a MIG power supply, does not integrate the cooler that is needed to cool the torch in the TIG and PAW welding, an external cooler is needed to cool the torch in the QKAPW system. To improve the system, in the later phase in the research, Miller MAXTRON 450 was replaced by the Dynasty® 350 Series power supply, as the Figure 4-4(b) shows, from Miller Electric MFG. Co. Dynasty® 350 can output exceptionally smooth and precise arc and can achieve high-speed DC TIG pulse controls [55]. The advantage of using Dynasty® 350 Series is that it can integrate the cooler and gas to simplify the system.

(a) MAXTRON 450 (b) Dynasty® 350

Figure 4-4 Main power supply

The last power supply, referred to as keyhole power supply in the system, is used to offer the rear arc when the keyhole is established. If the system works in the plasma welding mode, it can be treated as a keyhole sensor power supply; whereas if the system works in the double-sided arc welding, it can also provide the double-side arc

current. In this system, PM200 power supply is chosen, as shown in Figure 4-5.

Figure 4-5 PM200 power supply

4.1.2 High current plasma torch

Since the torch can determine the weld quality as well as power supply does, a high performance plasma torch is also important for the plasma welding. In this system, a torch developed and patented by B&B Precision Machine. Co. is adopted. This torch is initially developed to find a suitable torch for the Variable Polarity Plasma Arc (VPPA) welding as a component of NASA's External Tank welding system [56] .

Figure 4-6 High current plasma torch

4.1.3 Keyhole sensor

The keyhole sensor is another necessary component in the welding since the detection of the keyhole establishment is a crucial foundation in the process to assure the full penetration in the keyhole welding system. To ensure a good quality, a suitable penetration monitoring method must be applied. Several different methods have been developed, such as the measuring the light emitted from the keyhole [57], measuring the infrared radiation from workpiece [58, 59], measuring the oscillations in the weld pool [60], using the ultrasonic sensors [61], measuring the reflected plasma [62, 63] etc. In this paper a simple sensor has been developed based on the efflux plasma in the Welding Research Lab at University of Kentucky [64]. Its principle is shown in Figure 4-7.

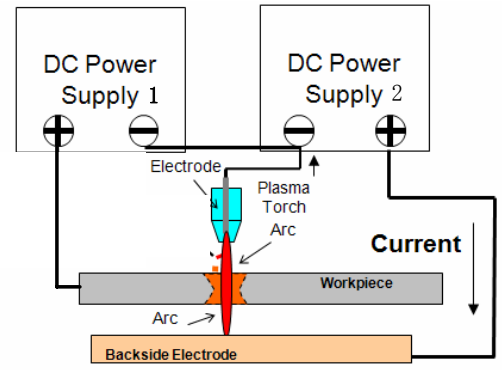

Figure 4-7 Theory of keyhole sensor

As Figure 4-7 shows, when the keyhole is established through entire thickness of the workpiece, the plasma efflux can pass through the keyhole and workpiece to reach the detection pipe. As a result, a current loop is formed for the detection power supply (power supply 2 in the Figure 4-1), and the establishment of the keyhole can be detected from the current (zero or nonzero) flowing through the detection power supply. Compared with other penetration sensors − such as the weld pool oscillation sensor, ultrasonic, infrared, or vision based sensor [65] − this sensor is simpler and can detect the keyhole as soon as it is opened. Although the integrated keyhole sensor [3] can use just one power supply to detect the keyhole, the sensor proposed in this

study has an advantage that it can be used in the double-sided arc welding process to offer the rear arc, as well as a sensor to detect keyhole . The rear electrode, in the pipe welding system, is designed as shown in Figure 4-8. Two homocentric short copper pipes were manufactured into a hollow pipe, so that water can flow in from the inlet fitting and out from the outlet fitting.

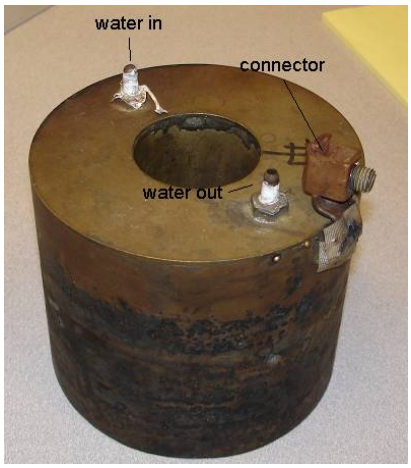

Figure 4-8 Backside electrode

4.1.4 Current sensors

The purpose of the current sensor is to measure the arc current online. In the earlier system, two current sensors were used to measure the main current and the back arc current respectively. In proposed system, since the main power supply can feed back the weld current from its interface connector, only one current sensor, Models CLN-500 closed-loop Hall Effect current sensor, is used in the system to measure the back arc current. It can accurately measure DC and AC currents and provide electrical isolation between the current carrying conductor and the output of the sensor.

The turn ratio of CLN-500 is 1:5000, meaning its O/P outputs the 1/5000 of the measured current. Since the voltage signal is easier to sample in the proposed QKPAW system, a 50Ω resistor is connected between O/P and the GND of the DC supply, so that the resistor voltage difference can be measured by the computer

through the I/O module. As a result, the ratio of the voltage difference and the measured current is 1:100.

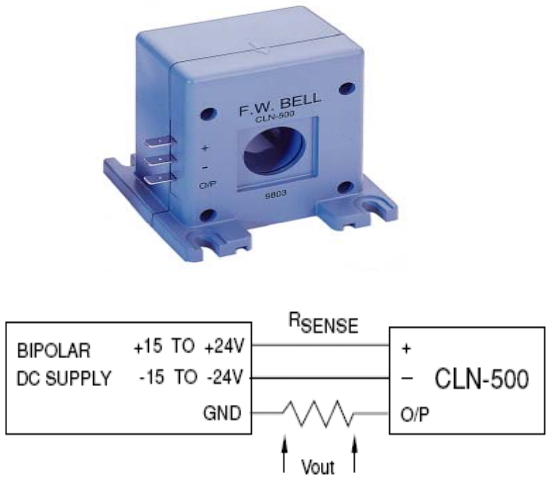

Figure 4-9 Current sensor

4.1.5 Traveler system

The function of the traveler system is to hold the plasma torch and move around the welded pipe on two parallel trails with it. Since the research focuses on the 5G position pipe welding, where the pipe is fixed and torch is moving around the pipe in the weld, a traveler that can move the torch around the pipe is necessary.

In the proposed system, one 4" long, schedule 40 steel pipe with six inch inner diameter (ID) is fixed on a self-make table to support the weld head. Two parallel guide ring rails are installed around the pipe, and a weld head called T-head produced by Magnatech. Co. can move on them around the pipe. On one side of the weld head, a DC motor driving extended arm is used to install a plasma torch, as shown in Figure 4-10.

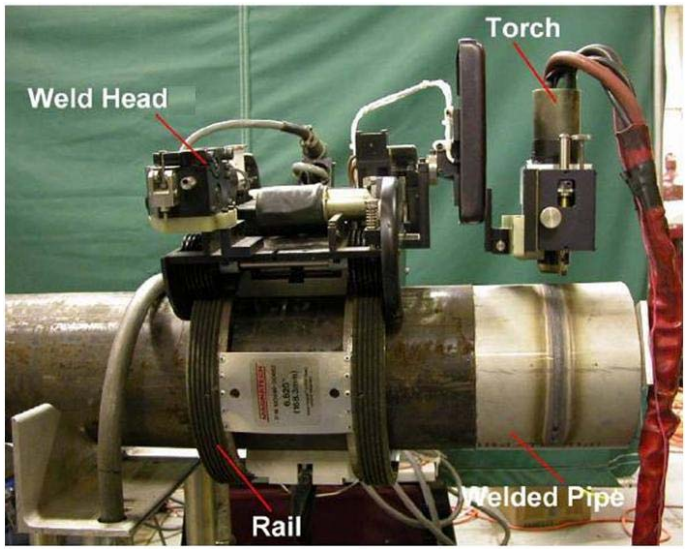

Figure 4-10 Traveler system

The arm of the weld head has three degrees of freedom relative to the welded pipe. To conveniently illustrate the torch position and movement, a coordinate base on the weld head is defined as shown in Figure 4-11. The X axis is parallel with the welded pipe, Y axis is normal to the surface of the welded pipe, and Z axis is tangent to the pipe surface.

Although the T-head is supplied with the connector to the Pipemaster Power Supply to realize the control of the T-head by the controller inside the power supply, the eventual movement actuators are three DC motors inside the weld head. In order to simplify the system and lower the cost, in the experimental system, the T-head is modified to be controlled by an adjustable DC power supply whose output can be controlled by a computer instead of by the Pipemaster power supply.

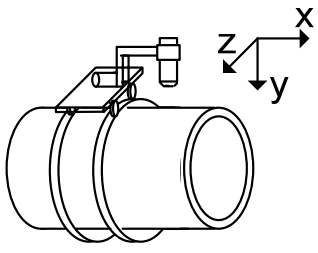

Figure 4-11 Coordination of traveler system

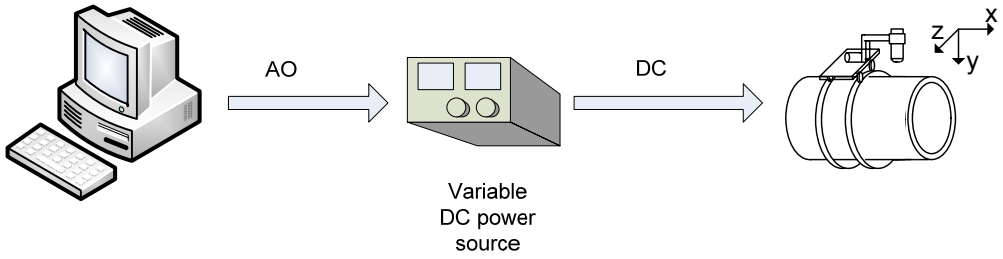

Figure 4-12 DC motor control

To conveniently describe the three DC motors in the weld head, they are called X-Motor, Y-Motor and Z-Motor respectively for the direction of movement they control. In the direction of Z axis, since the torch only needs to move in one direction without return during the weld, in this system, the Z-Motor is controlled by a 0-30V variable DC-power source, whose output can be controlled by the computer, isolated by a voltage isolation module to realize the welding speed control. Table 4-1 shows the calibration between the computer analog output (AO) voltage, output voltage of DC source and the weld-head speed. The calibration shows that the control voltage coming from computer has the linear relationship with the moving weld-head speed, with the ratio of around 1:2.5.

Table 4-1 Calibration between voltage and speed

AO voltage (V)	Voltage of DC source (V)	Speed of weld-head(mm/s)
0.2	3.5	0.5
0.4	7.2	1.0
0.6	10.6	1.5
0.8	13.8	2

To control the torch movement in the direction of *X*, a simple electric circuit board, shown in the Figure 4-13, is used in the system. In the board, the V_{in} is the input of the DC power supply, V_{out} is the output to the motors, D0.0 and D0.1 of the *Jcontrol* are the control input from digital I/O of the computer. When D0.0 is low, the left relay is in the default position and no voltage is output to V_{out}, thus the motor is in the stop

state. When D0.0 is switched to high level and D0.1 is in low level, the V_{out+} equals to the V_{in}, and V_{out} equals to the GND; this implies that the motor will run in the positive direction of axis. If D0.0 is high and D0.1 is low, the right relay would be switched, and as the result, V_{out+} equals to GND and V_{out-} equals to V_{in}, implying that the motor would moves in the negative direction of axis.

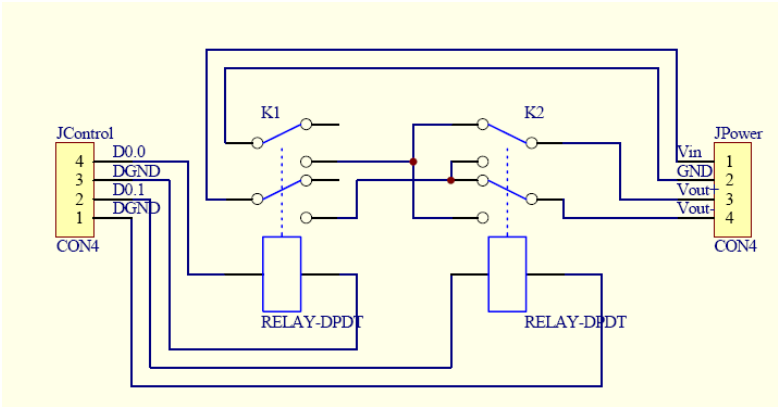

Figure 4-13 X motor control circuit

4.1.6 Real-time controller.

Since Windows XP is currently the most popular and easily accessed computer operating system, the development of the control software is based on Windows XP. The shortcomings of Windows XP in real-time applications are obvious, since the Microsoft Windows operating system has been designed as a general-purpose operating system, suitable for using both as an interactive system on the desktop and as a server system on a network, and causes following problems when used in a real-time operation system:

- Too few thread priorities are available for the user.
- Opaque and nondeterministic scheduling decisions.
- Priority inversion, particularly in interrupted processing.

Although faster processors do dramatically increase processing throughput and average response times, thus may lead one to speculate that the system may become

real-time, they cannot make a nondeterministic system deterministic or even consistently improve worst-case response times. Therefore, newer hardware platforms will not make the Windows XP platform real-time.

Due to the shortcomings of Windows operating system, the fast sample time varies greatly. In order to test the real-time performance, a test was conducted prior to the experiment, where a simple program designed with timing sample and output function was run in Windows XP operating system with the I/O module NI PCI-6221The sample and output period is set 1ms, and the result shows that the sample period changes from less than 1ms to 20ms; whilst in the real-time target PC, the sample period can be almost stable at 1ms. In the automatic welding control system, the currents are preferred to be sampled every millisecond; thus, the real-time performance is an important qualification in the process.

A real-time operating system (RTOS) is a multitasking operating system intended for real-time applications. The RTOS guarantees not only the real fast performance, but also the absolute reliability and deterministic performance. The National Instruments Real-Time Module is an add-on component for the LabVIEW (short for Laboratory Virtual Instrumentation Engineering Workbench) Development System. When installed, this software compiles NI LabVIEW graphical code and optimizes it for the selected real-time target. Combined with the LabVIEW Real-Time Module, all NI real-time hardware targets including PXI, Compact FieldPoint, FieldPoint, CompactRIO, and standard desktop PCs can be developed and deployed for application. The embedded RTOS for these targets is a single dedicated kernel that provides maximum reliability for embedded code [66]. In this system, a standard desktop PC is selected as the real-time target, called target PC, since it is the most economical real-time target and can provide the wider extension ability. The target PC is a desktop computer transformed to a real-time controller by installing the NI real-time module operating system, combined with the I/O module NI PCI-6221. The

hardware configuration of the target PC in the system is Intel PII 500 CPU, 128M memory and 12G hard disk.

4.1.7 The I/O module

The purpose of the I/O module is to sample the signals coming from the process, such as the output of the current sensor and the feedback signal of power supply to the computer, and output the control signal − calculated by the computer − to the actuator, to control the process.

In this QKAPW system, a NI PCI-6221 acquisition module from National Instrument Co. is adopted. NI PCI-6221 is a low cost M series Multifunction DAQ PCI board, it has 16 channels 16-Bit Analog Inputs I/O(250 kS/s); two 16-bit analog outputs (833 kS/s); 24 digital I/O and 32-bit counters; and Correlated DIO (8 clocked lines, 1 MHz). It is compatible to C, C++, Visual Basic as well as LabVIEW [67]. One of the advantages to choosing the NI PCI 6221 as the I/O module in the system is that it supports the real-time target PC to realize the real-time control.

Figure 4-14 NI PCI-6221

In QKPAW system, the first three channels in analog input I/O are used for sampling the weld arc current, weld arc voltage and the back electrode current separately; two digital I/O channels (D0 and D1) are used for the power supplies' contact switches, which enable the power supplies' output ; another two digital I/O are used to control the movement direction of the torch; two analog output I/O channels (AO0 and AO1) are used to control the output currents of the main power supply and the keyhole power supply.

4.1.8 Isolation module

The purpose of the isolation modules is to isolate the computer signals from the electrical signals coming from the power supplies. Since the power supplies in the operating mode can cause strong electromagnetic noise and disturbance, and sometimes even a high voltage impulse, which may damage the computer system if there is no isolation electronic circuit between them. To prevent these damages, isolation modules must be used, between the I/O board and power supply, to isolate the electrical signal from the power supplies to computers. Another function of isolation module is to filter the strong noise and disturb coming from the power supplies and weld arc. The QKPAW system uses two voltage output isolation modules for controlling the output of the power supplies, and further two voltage input isolation modules for measuring the main power supply and the keyhole power supply current respectively.

4.2 Software Introduction

The software in the QKPAW is the program combined with the hardware to realize the system function. Although the QKPAW system hardware is selected and integrated as the introduction above, before beginning the experiments, the software was developed for the welding process. In this system, the program was developed mainly with LabVIEW (Version 8.2) except the control algorithm, which is developed in C++.

The flowchart of the program is shown in Figure 4-15. When the weld process begins, the program begins to sample the main current and the rear current I_d with the frequency of 1kHz, and the open-loop high current square waveform pulse, called open-loop keyhole establish phase, is output to establish the keyhole on the pipe until the keyhole sensor detects I_d is switched on, signaling that the first keyhole is established. After the first keyhole is detected, the program calls the control algorithm

to calculate the peak current in the next cycle to equate the keyhole establish-time to the tracking reference time T_r. In the case T_p that is too long, the full-penetration may have failed, as introduced in Chapter 2. To avoid the fail, a restriction T_{pmax} is added to T_p: If the keyhole cannot be opened in T_{pmax}, the program will switch to the keyhole establish phase to establish the keyhole with higher current I_o, which can establish the keyhole in a shorter time. After the keyhole is detected, the program switches the arc current into the base current, and after T_b, the current is switched back to I_p to begin a new weld cycle.

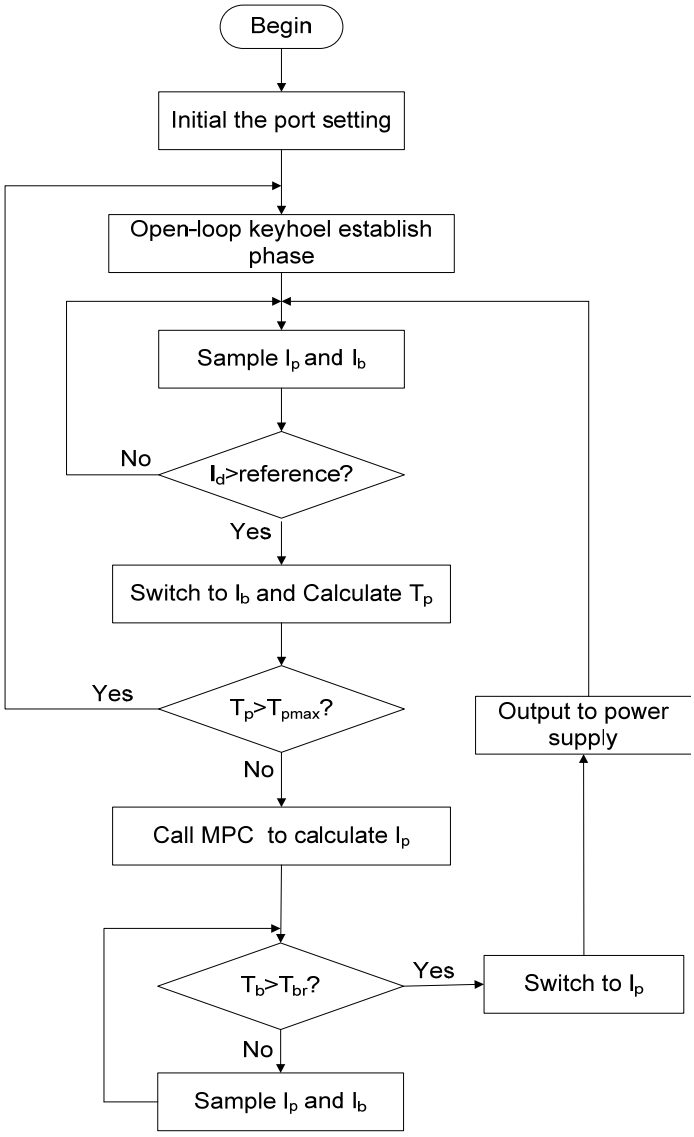

Figure 4-15 Flowchart of the control program

In this control program, mostly functions are realized by the components of LabVIEW, such as I/O date read and write, file save and data display, but the MPC algorithm, which is too complex to be realized in a graphic language, is written in C++ (Visual C++, Version 6.0) and compiled to a dynamic link library (DLL) file. Thus the LabVIEW can call the DLL file to calculate the control signal in the next weld cycle.

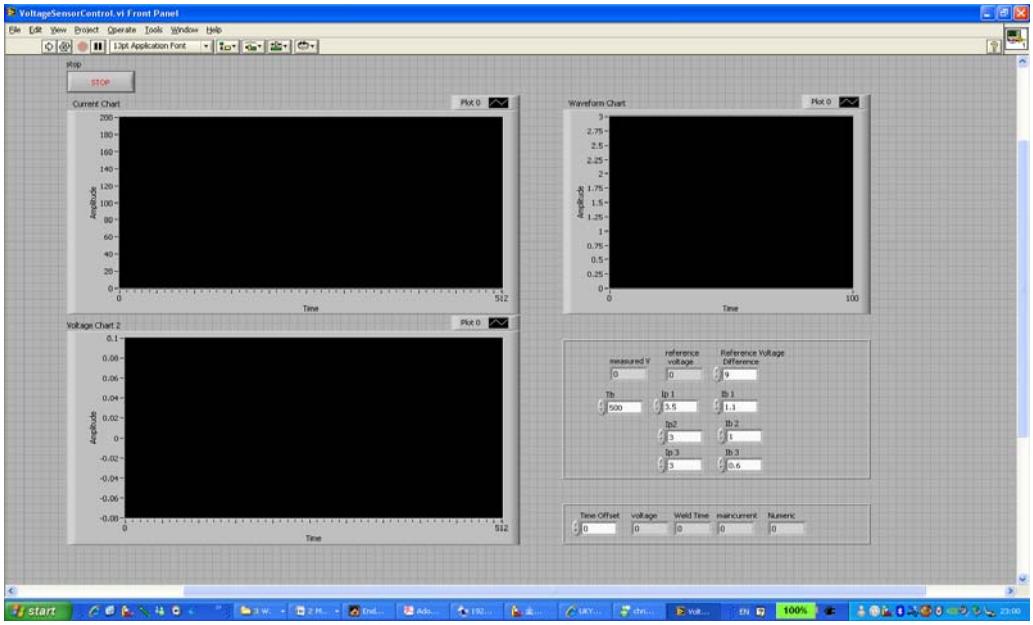

(a) Front panel of LabVIEW

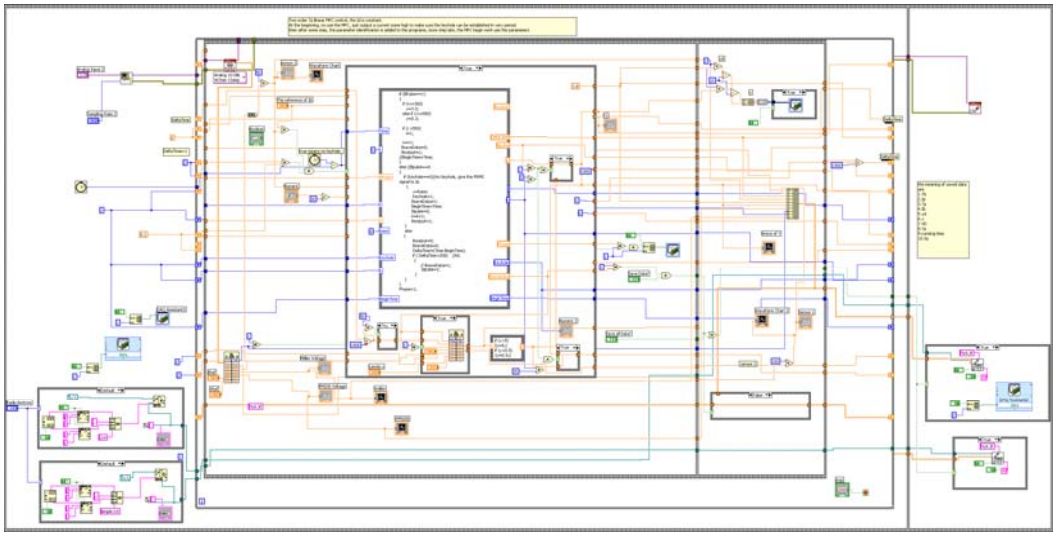

(b) Block diagram of LabVIEW

Figure 4-16 Program interface of LabVIEW

LabVIEW is one of the most widely used graphical development platforms in a virtual instrument − a type of digital measure instrument based on a computer system to realize the functions of traditional hardware measurement instrument − and is becoming most popular development environment for data sampling, analysis, display and control. In contrast to traditional programming languages, LabVIEW depends on the powerful graphical language instead of text code to get a friendly human machine interface (HMI) without the need for professional programming.

The LabVIEW program is comprised of two components: front panel and block diagram. The front panel is a graphical human interface used to set the input and view the output. In the front panel, the input is called control and output is called indicator, they are laid on the front panel in a form consisting of many icons − such as button, knob, switch and graphic chart − to simulate the actual instrument. The block diagram includes the function node and data wire, which perform the data processing and calculation function.

One issue that needs to be considered is the mathematical calculation capability of LabVIEW, since LabVIEW is a graphic language focusing on the virtual instrument instead of mathematical function. Although the formula node can embed C language into LabVIEW, its computation ability is limited. To make up for this shortcoming, LabVIEW provides a Call Library Function Node to call the standard Dynamic Link Library (DLL) file compiled from other programming language with strong mathematic capability, such as C++. In the proposed QKPAW system, the MPC algorithm is developed in C++ and compiled to a DLL file to calculate the control input and is called by LabVIEW in every weld cycle.

4.3 Process Parameters Selection

Before modeling the QKAPW, the basic process parameters need to be selected to get a good weld result on the special welded pipe. These parameters, obtained from

repeating an open-loop experiment, include the peak current time T_p, base current time T_b, the plasma gas flow rate, the distance between the nozzle and the welded workpiece, weld speed, etc.

In the keyhole plasma welding, the shape of the weld pool is an inverse bell and the smallest keyhole is achieved in the rear of the workpiece, as shown in Figure 2-3. From the rear picture of the welded pipe, shown in Figure 2-6(b), the keyhole diameter in a good weld result is around 1.5mm in average. To insure the full penetration and enough superposition of the keyhole, assuming the worst case that the keyhole is opened in the upper limit of the keyhole-establishment time (T_{Pmax}), the distance between the centers of neighboring keyholes should be no larger than the keyhole radius. From the open-loop experiments, a good group of the weld parameters for 3.2mm thick wall carbon steel pipe is selected as shown in Table 4-2:

With these process parameters, if the system can be well controlled and T_p=T_r, the distance between the centers of the neighboring keyholes should be $(T_r + T_b) * V_{weld} = 1mm$. The shortest distance can be calculated in the case of T_p≈0 $l_{min} = T_b * V_{weld} = 0.8mm$, the longest distance is in the case of T_p=T_{pmax} and $l_{max} \approx (T_{P\max} + T_b) * V_{weld} = 1.4mm$. In the case that the minimal diameter is around 1.5*mm* the full penetration can be achieved.

Table 4-2 Common parameters in QPAW experiments

Pipe thickness	3.2 mm
Pipe outer Diameter	145 mm
Shielding gas	Pure argon
Orifice gas	Pure argon
Orifice gas flow rate	1.4L/min (3 ft^3/h)
Shielding gas flow rate	11.5L/min (25ft^3/h)
Electrode to workpiece distance	5mm
Retraction of tungsten	2mm
Back electrode to workpiece distance	10mm
Sample period	1ms
Welding speed	2mm/s
Orifice diameter	1.8mm
Pilot arc current	15 A
Keyhole establish reference time(T_r)	100ms
Base current time (T_b)	400ms
Upper limit of T_{pr} (T_{Pmax})	300ms

CHAPTER 5 System Modeling and Simulation

It is well known that model development is the first and one of the most time consuming activities in model predictive control projects. An appropriate model that can depict the QKPAW process dynamics is a crucial component in the process control, since the model predictive controller, as its names denotes, is developed on the base of the process model.

The description of QKPAW process in Chapter 2 gives a practical image of process implementation. To better understand the designed system and the principles behind it, in this chapter, linear and bilinear structure models are proposed and identified respectively, and in the simulation section, the two model types are simulated to compare the results.

5.1 Modeling Theory Review

In order to better explain the QPAWP modeling process, firstly the model identification theory is briefly introduced.

The modeling and identification is a challenging task, not only in the control application, but in engineering and science in general, and is a popular research topic in these fields. The basic steps that system identification follows are shown in Figure 5-1 [65, 68].

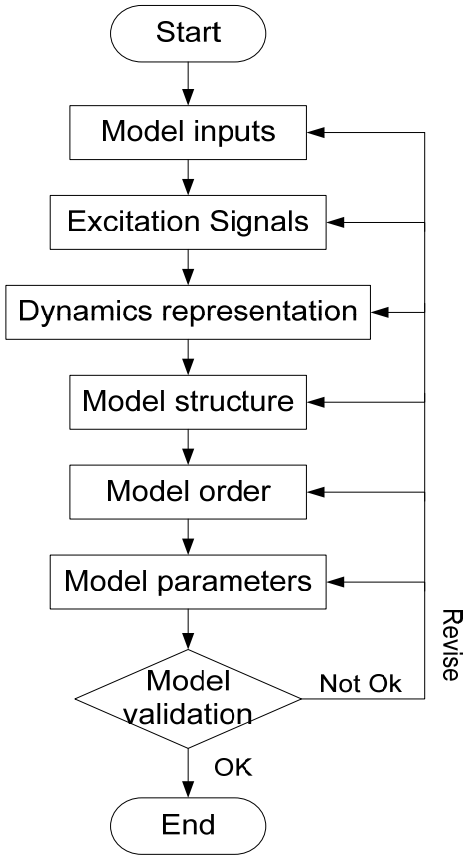

Figure 5-1 Diagram of system identification loop

a) Model inputs

The first step of identification is the choice of model inputs. According the analysis in the previous chapter, in the QKPAW process, I_p and I_b are selected as the input to the model.

b) Excitation signals

The second step, choice the excitation signals, that requires prior knowledge about the process, is made. The common excitation signals in industry are impulse, step and random signal.

c) Dynamic representation

The third step is dynamic representation, which depends on the model application. In this step, choosing the model structure, another most important step of the identification, is the main task.

In the industry control area, there are two possible structure forms − state-space

and polynomial. If no detailed prior knowledge of the system exists, the choice of most appropriate structure may not be obvious. In the absence of any prior knowledge, it is advisable to try out various available choices and use the one that seems to work the best.

d) Model Order

Once a model structure is determined, the next task is to select the model order. The choice of a model order is influenced by sampling frequency and the system delay, but in general, the aim should be to not higher order than necessary.

e) Model Parameter

Parametric models, such as the transfer functions or state-space model, use a group of parameters to capture system dynamics. It usually can be completed automatically by optimal algorithms. The most common algorithm is the least square algorithm (LSA), a method of data fitting in which the least sum of squared residuals − the differences between the observed values and the values given by the model − is achieved with best fit parameters.

The basic LSA parameter identification can be summarized as follows: Take the input sequence into the welding process to produce the process output sequence $\left[T_p(i), T_b(i)\right]^T$ (i=1,2,3,……,N), then the model parameters can be estimated by the least squares method:

$$\hat{\theta}_{uy} = \left[\Phi_{uy}{}^T \Phi_{uy}\right]^{-1} \Phi_{uy}{}^T y \qquad \text{(Eq.5-1)}$$

where $\Phi_{uy} = \begin{bmatrix} \phi_{uy}{}^T(1) \\ \vdots \\ \phi_{uy}{}^T(N) \end{bmatrix}$, ϕ_{uy} is the memory vector, contains the actual and past terms of the input signal, the past terms of the output signal:

$$\phi_{uy}(k) = f_{uy}\left(u(k), \cdots, u(k-n_u), y(k-1), \cdots, y(k-n_y)\right) \qquad \text{(Eq.5-2)}$$

and $\hat{\theta}_{uy}$ is the model parameter estimates .

For complex physical systems, three basic approaches to model development are: fundamental, empirical, and gray-box modeling. Fundamental models are developed from knowledge of physical principles fundamentals and sometimes are called white-box model, as the internal details of these models have clear, direct physical interpretations. Empirical models, on the other hand, are called black-box models, since they depend on the mapping between the system input and the output without any direct physical interpretation. The term gray-box model may be called half-white half -black box model, since it bases on some physical analyses and some input/output data.

Historically, the models of choice in early industrial MPC applications were time domain, input/output, step, or impulse response models [69] [70]. Linear models in the process industries are, by their nature, empirical and identified from input/output data. The discussion of MPC in state-space form has several advantages, including easy generalization to multivariate systems, ease of analysis of closed-loop properties and online computation. Furthermore, starting with this model form, the wealth of linear systems theories − the linear quadratic regulator theory, Kalman filtering theory, internal model principle, etc. − is immediately accessible for use in MPC [71].

f) Model Validation

The last step is model validation. Its purpose is to validate the accuracy of the identified models using independent sets of measured data from a real system. For a given set of inputs, the simulated output of the identified model can be compared with the measured output from the real system. If the produced errors are smaller than the predetermined criterion, the model is accepted to represent the process dynamics.

Model validation is another important step in the model building sequence, but easily overlooked. After the model is identified, it is used to predict the output, given an input sequence; subsequent check is made to determine the goodness of fit

In a standard case, the model is validated by analyzing the residuals of the

identified model, i.e. the differences between the measured and the predicted output from the model. If the model to data fit was correct, the residuals would approximate the random errors, implying statistical nature of the relationship between the measured output and the model predictive output variables. Therefore, if the residuals are relatively small, it suggests that the model fits the data well, or vice versa.

It can be determined by analyzing the improvement percentage goodness of fit as a function of model order and when doing this, a separate and independent dataset is advised to be used for validation. Choosing an independent validation data set would improve the detection of over-fitting.

There are many statistical tools for model validation, but the primary tool for most modeling applications is Graphical residual and Quantitative analysis of residuals analysis.

In model validation, graphical methods have an advantage over numerical methods, as they readily illustrate a broad range of complex aspects of the relationship between the model and the data.

Quantitative analysis of residuals − also called Numerical methods for model validation − is another important model validation tool , it tends to be narrowly focused on a particular aspect of the relationship between the model and the data and often tries to compress that information into a single descriptive number or test result.

In the Quantitative analysis of residuals, the goodness of fit of a model can be judged by coefficient of determination R^2, a statistical measure of how well the regression line approximates the real data points. An R^2 of 1.0 indicates that the regression line perfectly fits the data.

The most general definition of the coefficient of determination is

$$R^2 \equiv 1 - \frac{SS_{err}}{SS_{tot}} \qquad \text{(Eq.5-3)}$$

where $SS_{err} = \sum_i (y_i - y_{mi})^2$, it also called the residual sum of squares and y_i and

y_{mi} are the measured output and modeled (predicted) output respectively. $SS_{tot} = \sum_i (y_i - \bar{y})^2$, the total sum of squares (proportional to the sample variance), $\bar{y}$ is the mean of the measured output.

One promising research direction is the development of low-order modeling strategies that provide a more reasonable compromise between model complexity and prediction accuracy.

5.2 Modeling of QPAWP

Since the welding conditions determine the model, even small change of the conditions − such as the plasma gas, distance and angle between torch and the normal line of the welded workpiece surface, the weld pool position around the pipe − can change the model parameters of the model. On the other hand, a matched initial model is important in the MPC controller, because an unmatched model may cause poor control quality and even make the initial process unstable. In this section, the QKPAW is modeled, based on the parameters given in Table 4-1, both in linear model structure and bilinear structure, and is subsequently validated.

According the process description in Chapter 2, QKPAW should be a nonlinear process. However, nonlinear control systems usually pose substantially higher data, design, implementation, and maintenance demands than linear control systems do. Therefore, before one develops and implements a nonlinear control system, the potential advantages of such a system must be carefully examined in comparison to a linear one. The control schemes of nonlinear MPC which based on the direct use of nonlinear models have been reported [41] [72], but they involved the online solution of higher-order nonlinear optimization problems that are computationally expensive and have a tendency to find a local, rather than a global minimum for non-convex problems. Another approach [73] used a piecewise linearization technique to describe

the nonlinear behavior of a system, so that the model was linearized in each sampling interval. This resulted in the solution of one or more quadratic programming problems − each associated with a corresponding interval, as in the case of linear MPC.

Although many other factors, such as the welding speed, the gas flux, the arc length, can affect the keyhole-establishment time, to simplify the discussion of modeling problem, three assumptions conditions are made here: First, that the welding speed is constant; second, the torch-to-welded workpiece distance is constant; and third, that the orifice and shield gas flux are constant. These conditions can be easily ensured by the proposed QKPAW system, and they do not affect the discussions in the verification experiments in the future, when these parameters will be changed purposely to verify the controller performance.

5.2.1 Linear model

For polynomial models, a general input-output linear model for a single-output system with input *u* and output *y* can be written as shown in Eq.5-4; they may also be good choice for a starting polynomial model because of their simplicity.

$$A(q)y(t) = \sum_{i=1}^{n_u}\left[B_i(q)/F_i(q)\right]u_i(t-nk_i) + \left[C(q)/D(q)\right]e(t) \qquad \text{(Eq.5-4)}$$

here u_i denotes the i_{th} input, A, B_i, C, D, and F_i are polynomials in the shift operator, and nk_i is the time-delays.

Some special cases of the input-output are autoregressive moving average (ARMA), as Eq.5-5, output-error (OE) Eq.5-6, etc.

$$A(q)y(t) = B(q)u(t-nk) + C(q)e(t) \qquad \text{(Eq.5-5)}$$

$$A(q)y(t) = B(q)/F(q)u(t-nk) + e(t) \qquad \text{(Eq.5-6)}$$

Theoretically, the peak current duration $T_p(k)$ is controlled by the heat input rate in the present cycle as determined by $I_p(k)$. When $I_p(k)$ increases, the heat input rate

into the workpiece increases; as a result, the welded metal melts faster thus the keyhole can be established in a shorter period of time, implying that $T_p(k)$ becomes shorter. On the other hand, $T_p(k)$ also depends on the temperature in the area where the keyhole is established, as well as the temperature distribution in the surrounding area. Higher temperature implies that the metal can be melted with less heat input. The temperature depends on the heat input before $T_p(k)$, which is controlled by $I_p(k-i)$, $I_b(k-i)$ and $T_p(k-i)$, $i=1,2,\cdots,n$.

To simplify the model and not lose universal function, here the linear model structure is selected as ARMA, rewritten as Eq.5-7

$$y(k)=\sum_{i=1}^{p} a_i y(k-i)+\sum_{i=0}^{q} b_i u(k-i)+\sum_{i=0}^{r} r_i e(k-i) \qquad \text{(Eq.5-7)}$$

here $y(k)$ represents an output at time k, $u(k)$ is the input at time k, $e(k)$ is the disturbances at time k, and *k-i* represents the i_{th} control cycle before *k*.

5.2.2 Bilinear model structure

Since the empirical modeling approaches can be unreliable and may require a tremendous amount of experimental data to determine the model structure and parameters, and the precise first-principles model is difficult to obtain if the precise mathematical mechanism cannot be derived from the process analysis. Hybrid modeling approaches that combine available first-principles knowledge with empirical modeling have popular application in the industry process modeling. In this research, the process uses a combination of a first-principles model and an empirical model, in order to obtain a best model for the control problem as described below.

On the base of the assumptions in the previous research analysis [74], it shows that T_p is possibly related to the presently and previously applied peak currents $I_p(k-i)$, previous peak current duration $T_p(k-i)$, and previous applied base current $I_b(k-i)$. It can be easily understood that $T_p(k)$ is controlled by the heat input

rate in the present cycle, which is determined by arc current in current cycle $I_p(k)$ and the temperature in the area where the keyhole is established, as well as the temperature distribution in the surrounding area. The temperature surrounding the keyhole depends on the heat input before $T_p(k)$, which is determined by the arc currents and the time arc currents added in the previous cycle, as $I_p(k-i)T_p(k-i)$, $I_b(k-i)T_b(k-i)$, $i=1,2,\cdots,n$.

The physical analysis of the process above suggests that T_p is defined as the output, and I_p is the input of the quasi-keyhole welding system. Thus in this case, the resulting system is SISO, since the $T_p(k)$ is determined by $I_p(k)$, $I_p(k-i)T_p(k-i)$, $I_b(k-i)T_b(k-i)$, $i=1,2,\cdots,n$. An empirical bilinear model under the guidance of system identification theory[75] is proposed:

$$T_p(k)=\sum_{i=1}^{n_y}a_iT_p(k-i)+\sum_{i=1}^{n_{uy}}b_iT_p(k-i)I_p(k-i)+\sum_{i=0}^{n_u}c_iI_p(k-i)$$

$$+\sum_{i=1}^{n_b}d_iT_b(k-i)I_b(k-i)+\zeta \qquad \text{(Eq.5-8)}$$

In the typical QAPWP, T_b and I_b are set to be a constant and remain the same in every period. In that case, the last term in Eq.5-8 is not a variable in the process and can be replaced by a constant ζ, thus the Eq.5-8 can be rewritten into Eq.5-9:

$$T_p(k)=\sum_{i=1}^{n_y}a_iT_p(k-i)+\sum_{i=1}^{n_{uy}}b_iT_p(k-i)I_p(k-i)+\sum_{i=0}^{n_u}c_iI_p(k-i)+\zeta \qquad \text{(Eq.5-9)}$$

where n_y, n_{uy}, n_u are the output horizon lengths , bilinear item and input respectively, which can be determined via open experiment results. Based on this bilinear model, the bilinear controller is designed to control T_p to track the reference trajectory, where its effectiveness is experimentally verified.

To apply to the control algorithm, the model Eq.5-9 can be rewritten into the

input output discrete form:

$$y(k)=\sum_{i=1}^{n_y} a_i y(k-i)+\sum_{i=1}^{n_{uy}} b_i u(k-i)y(k-i)+\sum_{i=0}^{n_u} c_i u(k-i)+\zeta \qquad \text{(Eq.5-10)}$$

here y the output T_p, u the first input I_p.

5.2.3 Parameter identification

After the model structure is selected, the model parameters are still unknown and needed to be determined by parameter identification method.

Since the system model is one of the major components in the design of model predictive control, the model parameters need to be obtained before the close-loop control welding. Some parameters, such as the input and output variable coefficients, can be identified by the least squares algorithm; whilst other parameters, such as n_y, n_u, T_{pr}, T_r and welding speed are needed to be chosen based on the open-loop experiments. In this sub-section, these parameters are selected on the results of the open-loop experiment as follows:

a. Order selection

The purpose of the first open-loop experiment is to select the order and the horizons of the model. In this experiment, the step signals were added into the peak current to test the keyhole-establish time response. Figure 5-2 shows how the step change of peak current affects T_p, i.e. it depicts the responses of T_p to the peak current. In Figure 5-2, when I_p is switched from 100A to 150A and I_b is kept at 30A, T_p decreases with the step, but it becomes stable again after two welding cycles. This result suggests that T_p, and I_p before the two cycles have not much effect on the current T_p. Since the model order, the control length and predictive length affect the calculation burden directly, they should be as short as possible on the base of satisfying control precision in the real-time system. In this control system, the model order can be chosen as $n=2, n_u=n_y=3$ in the experiments and they will be tested in

the model verification phase.

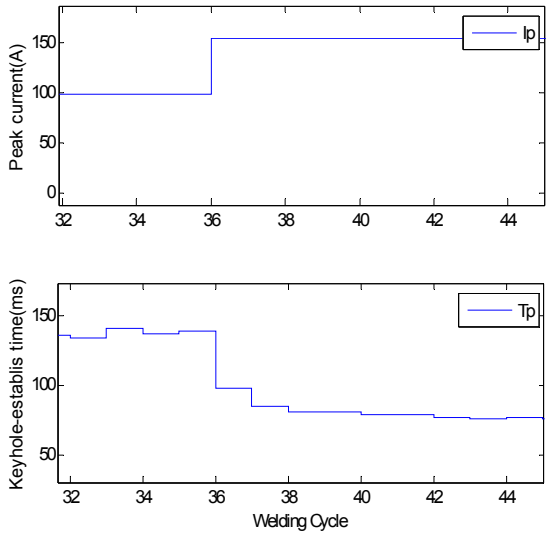

Figure 5-2 T_p response to the peak current

To verify the model selected above, the off-line parameter identification with the open-loop experiments is necessary before the close-loop experiments can begin. The output of system T_p was measured online, and then the model parameters were estimated by using the least square method. With these identified parameters, the process output for the given random input can be simulated. To get the best fit parameters in the model, the detailed identification processes is conducted, as described below.

b. **Test signals for Identification**:

To the linear model, four kinds of standard input − the impulse signal, step signal, Sine signal and Pseudo-Random Multi-level Signal (PRMS) − sequences are usually used as stimulant test signal to identify the parameters [76], they are listed in Table 5-1.

In the nonlinear system, the test signals should have a number of test points to cover as many working conditions as possible. The PRMS has a wide range amplitude distribution with an auto-correlation function similar to white noise. It is suited for identification of nonlinear systems and has the following characters [77]:

- The sequence repeats itself after a period, which can be selected by the user;
- The whole sequence can be determined by only a few parameters. This fact allows the sequence and the whole identification experiment reproduction any time;
- The mean sequence value in a period is zero;
- The first order auto-correlation function is similar in a given shifting time domain to that of the white noise;
- The even order auto-correlation function of the normalized signal, except the binary one, is zero as with the Gaussian white noise;

Table 5-1 Stimulant test signal for linear system

No.	Input sequence	Definition
1	Unit impulse	$u(k)=\begin{cases}0 & k<0\\1 & k=0\\0 & k>0\end{cases}$
2	Unit step	$u(k)=\begin{cases}0 & k<0\\1 & k\geq 0\end{cases}$
3	Standard sinusoid	$u(k)=\sin\left(\frac{k\pi}{n}\right)$
4	Gaussian white noise	$u(k)\sim N(0,1)$

To generate PRMS, there are two methods normally adopted: The first is by multi-level shift registers, as shown in Figure 5-3, which uses the registers to store the information. In this method, every register receives the information from the previous one that is on its left, and uses the clock signal to enable the transformation, then, the state of one of the registers can be considered as the test signal.

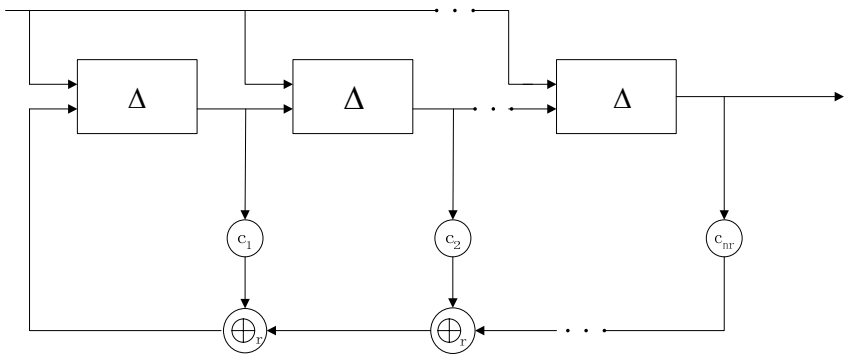

Figure 5-3 shift register

In Figure 5-3, $\oplus_r$ is the modulo addition, where Table 5-2(a) shows the operation in modulo-5 as a example, where $x_1 \oplus_r x_2 = x_1 + x_2$ when $x_1 + x_2 < r$ and $x_1 \oplus_r x_2 = x_1 + x_2 - r$ when $x_1 + x_2 \geq r$.

Another way to obtain the PRMS is by solving difference equations. Since the shift register is a chain of delay operators, if the input to the first register is $x(k)$, then the output of the first register is $x(k-1)$, and the second is $x(k-2)$, etc. Hence, $x(k)$ can be determined by the following difference equation:

$$x(k) \equiv c_1 \otimes_r x(k-1) \otimes_r c_2 \otimes_r x(k-2) \otimes_r \ldots c_{n_r} \otimes_r x(k-n_r) \qquad \text{(Eq.5-11)}$$

$\otimes_r$ in Eq.5-11 is the modulo multiplication, here the word 'modulo' means 'to the modulus'. For any positive integer n, let S be the complete set of residues {0, 1, 2,…, n−1}, then addition modulo n on S is defined as follows. For a and b in S, take the usual sum of a and b as integers, and let r be the element of S to which the result is congruent (modulo n); the sum a+b (mod n) is equal to r. Similarly, multiplication modulo n is defined by taking ab (mod n) to be equal to s, where s is the element of S to which the usual product of a and b is congruent (modulo n). For example, addition and multiplication modulo 5 are given by Table 5-2, in which (a) is modulo addition and (b) is modulo multiplication:

Table 5-2 Operations in modulo-2

+	0	1	2	3	4
0	0	1	2	3	4
1	1	2	3	4	0
2	2	3	4	0	1
3	3	4	0	1	2
4	4	0	1	2	3

(a) Modulo addition

×	0	1	2	3	4
0	0	0	0	0	0
1	0	1	2	3	4
2	0	2	4	1	3
3	0	3	1	4	2
4	0	4	3	2	1

(b) Modulo multiplication

In order to obtain the PRMS in the range of the permissible operations, the PRMS created above needs to be transformed into the operating region before application. Table 5-3 shows the transformation of PRMS in the case that the number of levels is greater than 2. In Table 5-3, U_m is the middle of the operating region and ΔU is the half range of operating region.

In order to get the most matched model, the principle of the model selection is stated as follows: Some possible model structures, linear and nonlinear, were selected to be identified; and after the identification, for each model structure and the corresponding coefficients, the test signals are introduced into the model and the model outputs are calculated. If the calculated output matches the measured output well, it can be concluded that the model can represent the dynamics of the real process and can be used in the control algorithm. If more than one model can represent the dynamics of the process, the model with simpler structure is chosen.

The flowchart of the identification program is as Figure 5-4 shows

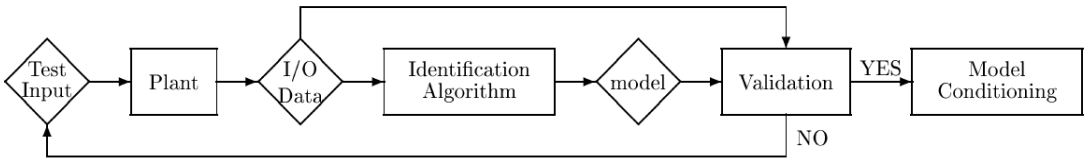

Figure 5-4 the identification flower chart

Table 5-3 Center process for PRMS

PRMS produced by shift register	Transformed PRMS
0	$U_m - \Delta U$
1	$U_m - (r-3)\Delta U/(r-1)$
2	⋮
⋮	$U_m - 4\Delta U/(r-1)$
$(r-1)/2-1$	$U_m - 2\Delta U/(r-1)$
$(r-1)/2$	0
$1+(r-1)/2$	$U_m + 2\Delta U/(r-1)$
$2+(r-1)/2$	$U_m + 4\Delta U/(r-1)$
⋮	⋮
$(r-2)$	$U_m + (r-3)\Delta U/(r-1)$
$(r-1)$	$U_m + \Delta U$

In the bilinear model identification, two groups of PRMS signals are designed. The first group is designed to produce the input signal I_p. From the open-loop welding experiment, in which different I_p is tested in weld for the steel pipe with 1/8" thick wall, it is found that the preferred keyhole establish time is usually in range 100-200ms). From the open-loop experiments, it can be shown that when the peak current is set in 95-125A range, the keyhole establishment time varies around the designed time. To get the output arc current, the control signal range calculated by computer can be 1.8-2.2V. To get the PRMS, *r* is set to 7, thus Figure 5-5 shows the MPRS signal, (a) is the control signal created by computer and (b) is the output

current measured by current sensor.

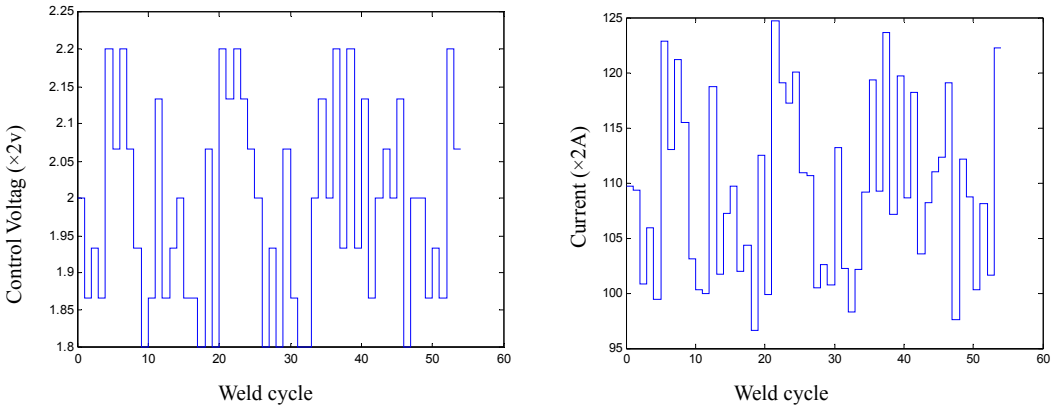

(c) I_p control signal (b) I_p measured signal

Figure 5-5 PRMS for I_p

The second group PRMS is designed for I_b. Based on the open-loop experiments, in this identification, I_b is set to 45-65A. To this end, the control signal is set between 0.87V and 1.13V, and $r = 5$. Figure 5-6 shows the PRMS for I_b, here (a) shows the computer-generated PRMS control signal, (b) is the output current measured by current sensor.

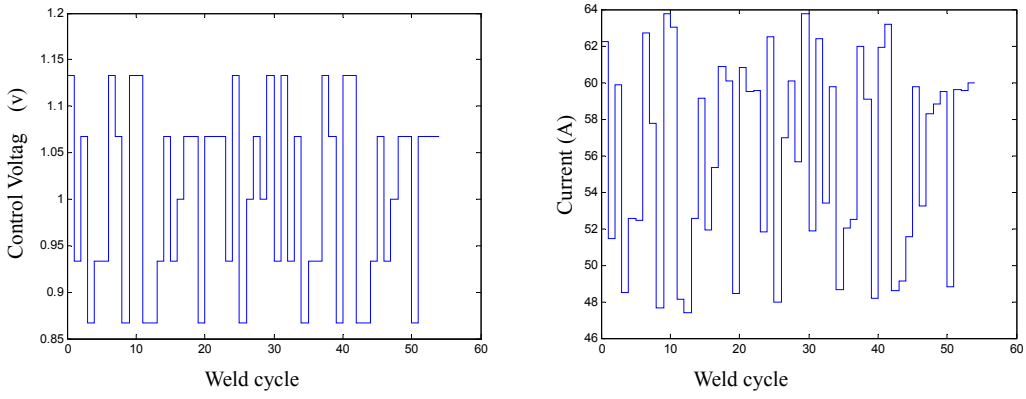

(a) I_b control PRMS (b) I_b measured signal

Figure 5-6 PRMS for I_b

These PRMS above are input to the QKPAW process, and the arc current wave is measured in the experiment and shown in Figure 5-7. After processing the current signal, the peak current times in each weld cycle are obtained as shown in Figure 5-9.

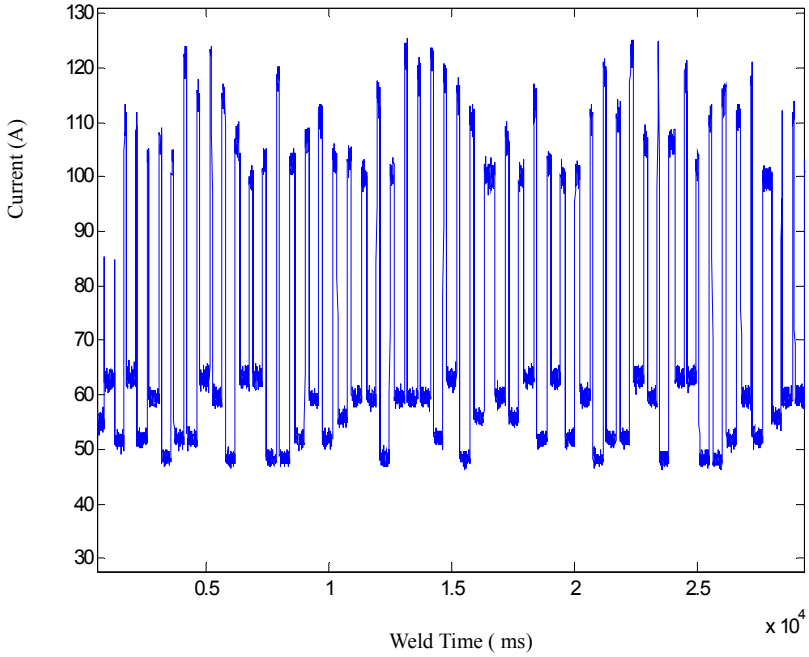

Figure 5-7 Current wave with PRMS

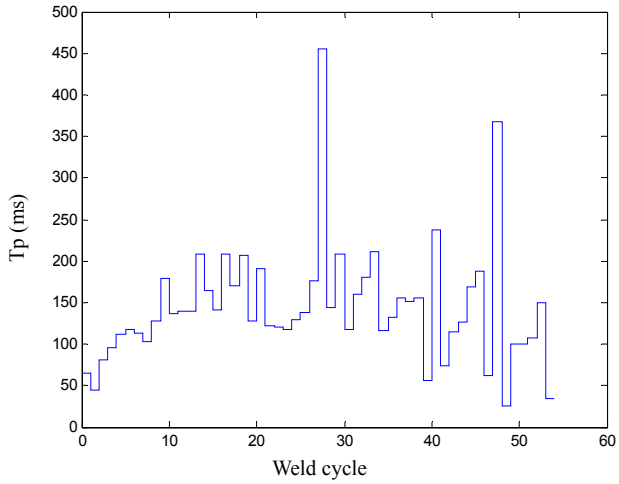

Figure 5-8 Measured T_p in experiment

Based on the inputs (I_p and I_b) and outputs (T_p) obtained above, two-order linear model and two-order bilinear model, are identified respectively as follows:

c. Linear model

The identified linear model is selected with the structure of (Eq.5-8) and with order numbers equal to two, as Eq.5-12:

$$T_p(k) = \sum_{i=1}^{2} a_i T_p(k-i) + \sum_{i=0}^{2} b_i I_p(k-i) + \sum_{i=1}^{2} c_i I_b(k-i) + e \qquad \text{(Eq.5-12)}$$

With the least squares algorithms, Eq.5-12 and the coefficient vector, output vector and memory vector can be written as

$$\hat{\theta} = [a_1, a_2, b_1, b_2, b_3, c_1, c_2, e]^T$$

$$y = [T_P(k), T_P(k-1), \cdots, T_P(k-N+1)]^T$$

$$\phi_{uy}(k) = \left[T_P(k-1), T_P(k-2), I_P(k), I_P(k-1), I_P(k-2), I_b(k-1), I_b(k-2)\right]^T$$

The coefficients of the two-order linear models are identified and are calculated as:

$$a_1 = -0.0443, a_2 = 0.1270, b_0 = -0.0401, b_1 = -0.2775, b_2 = 0.1109, c_1 = -0.1819,$$

$$c_2 = -0.1575, e = 0.8885$$

d. Bilinear model

Similarly, the identified bilinear model is selected as given by Eq.5-13:

$$T_p(k) = \sum_{i=1}^{2} a_i T_p(k-i) + \sum_{i=1}^{2} b_i T_p(k-i) I_p(k-i) + \sum_{i=0}^{2} c_i I_p(k-i) + \sum_{i=1}^{2} d_i I_b(k-i) + \zeta \quad \text{(Eq.5-13)}$$

Then the coefficients are identified as:

$$a_1 = 0.2816, a_2 = 3.3177, b_1 = -0.1757, b_2 = -1.6278, c_0 = -0.0412, c_1 = -0.2536,$$

$$c_2 = 0.3409, d_1 = -0.1827, d_2 = -0.1534, e = 0.3936$$

5.3 Model Validation

To check the performance of the identified models, in this subsection, the models are validated by both graphical analysis and quantitative analysis method, where, with identified coefficients and the selected model structure, the simulation outputs are calculated by inputting the given data sequence.

To compare the different linear and bilinear model results, the validation is divided into two steps, in which two types of data sequence are used to check the performance of both models.

In the first step, the same input data sequence used in the identification is input to

the model to produce the simulation output. Figure 5-9 shows the comparison of simulation output and measured output results, where (a) is the simulation result of the bilinear model, and (b) shows the simulation result of the linear model. From the graphical analysis, simulation output of both linear model and bilinear model match the measured output.

In the residuals analysis, the sum of squared errors, SS_{err}, also is calculated to evaluate the results. Select $SS_{err} = \sum_{i=3}^{50} (y_i - y_{mi})^2$, here i starts from 3 because y_{mi} only can be available from 3 since it are calculated iteratively from y_1, y_2.

With the measured outputs and simulation outputs, for the two-order linear model, $SS_{err} = 0.1226$ and for the two-order bilinear model $SS_{err} = 0.1175$. This result shows the bilinear model can achieve a smaller SS_{err}, implying that it can represent the process better.

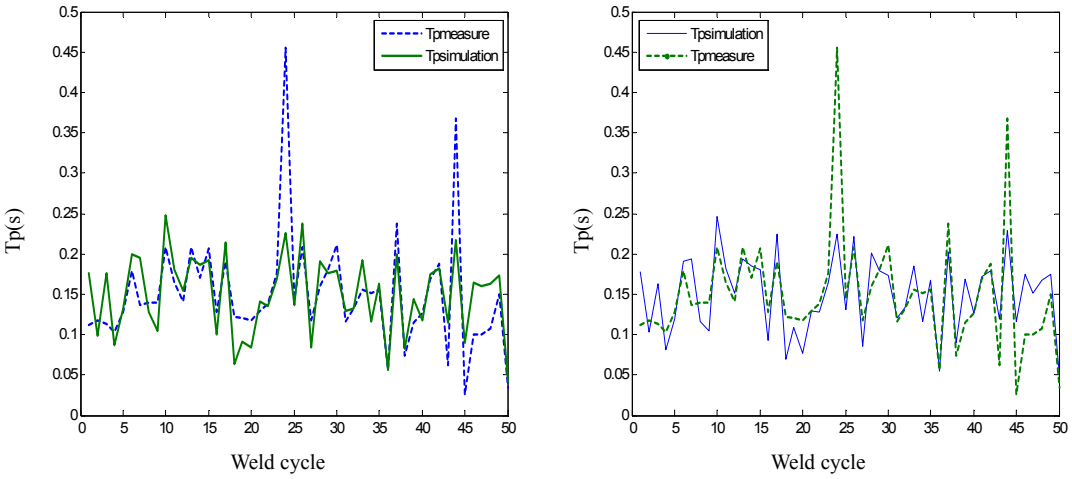

(a) Linear model result (b) Bilinear model result

Figure 5-9 Comparison of the simulated T_p and measured T_p

In the second step, another group PRMS sequence, different from the identification input data, is input to the real process and the output T_P is measured. The new simulation output can be obtained from this PRMS signal sequence and the

model identified above. Finally, the simulated output is compared to the measured output to check the model goodness of fit.

Figure 5-10 shows the PRMS for the validation, (a) is the 5th order PRMS computer generated exciter signal, created before being input to the power supply, and (b) is the output current of the power supply measured by current sensor. Figure 5-11 shows the simulation output and measured output after the signal process, in which (a) is the result of the bilinear model and (b) is the result of the linear model.

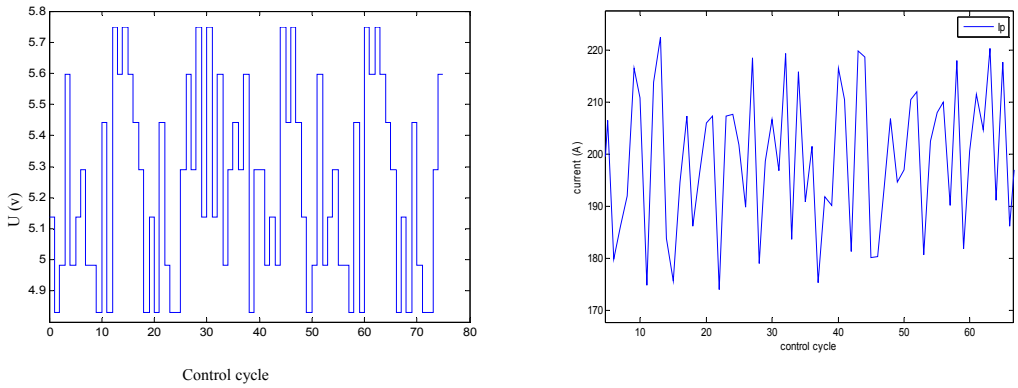

(a) PRMS (b) Measured peak current

Figure 5-10 PRMS for validation

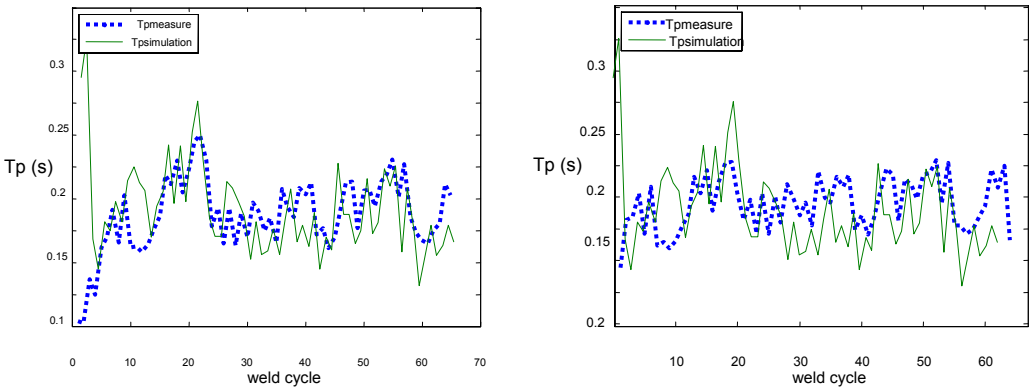

(a) Bilinear model (b) Linear model

Figure 5-11 Comparison of the simulation output and measure output

In the residuals analysis, the sum of squared errors is also calculated from the 10^{th} weld cycle to the 60^{th}. Under the same conditions, *SSerr* is calculated as *SSerr* =

0.1452 for the bilinear model, and $SSerr = 0.1808$ for the linear model. In this respect, the bilinear model better represents the process.

The above validation results show that the bilinear model structure achieves some but not significant improvement. In the following chapter, the both models are adopted in the MPC and used to control the peak current time in the weld experiment.

CHAPTER 6 Linear MPC Algorithm

Despite the fact that most real processes are approximately linear within only a limited operating window, linear MPC approaches are used in the majority of applications, with the feedback mechanism of the MPC compensating for prediction errors due to structural mismatch between the model and the process. In the model predictive controllers that consist only of linear models, the superposition principle of linear algebra enables the effect of changes in multiple independent variables to be added together to predict the response of the dependent variables. This simplifies the control problem to a series of direct matrix algebra calculations that are fast and robust. In this chapter, a linear model structure identified in Chapter 5 is used in the linear MPC in the QKPAW process and is followed by the control result of the experiments to check the performance.

6.1 MPC Design

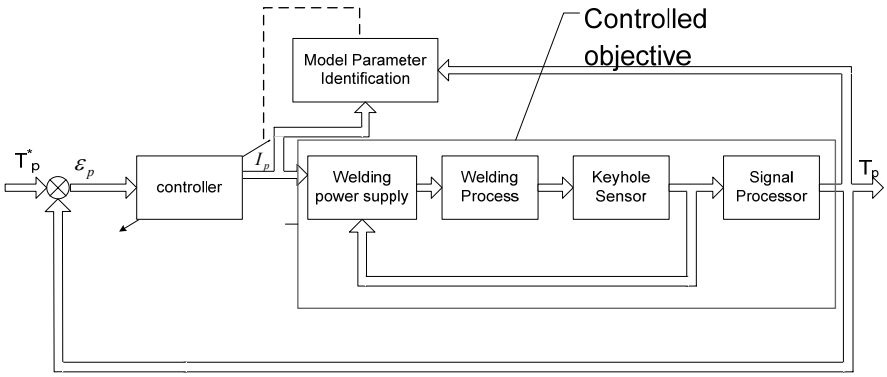

Figure 6-1 Control System

Based on the QKAPW process, the control diagram, shown in Figure 6-1, has been developed to control the peak current duration (T_p) of the process. In this control system, in every weld cycle, the controller calculates the peak current in the next weld cycle. The controlled objective is comprised of welding supplies, the welding process,

the keyhole sensor and the signal analysis. The model parameter identification is added into the system to adjust online the model parameters used in the controllers.

The algorithm of the controller is designed as follows. Extend the linear model Eq.5-7 to n_p future cycles:

$$\begin{aligned} y(k+1) &= \sum_{i=1}^{n} a_i y(k+1-i) + \sum_{i=1}^{n} b_i u(k+1-i) + \xi \\ y(k+2) &= \sum_{i=1}^{n} a_i y(k+2-i) + \sum_{i=1}^{n} b_i u(k+2-i) + \xi \\ &\vdots \\ y(k+n_p) &= \sum_{i=1}^{n} a_i y(k+n_p-i) + \sum_{i=1}^{n} b_i u(k+n_p-i) + \xi \end{aligned} \qquad \text{(Eq.6-1)}$$

here n_p is the predictive horizon. The future variables − the inputs and the outputs in the future that can only be obtained by the prediction, are separated from past variables − the input and the output before the k instants, and they are expressed in matrix form.

$$\begin{aligned} &\underbrace{\begin{bmatrix} 1 & 0 & \cdots & 0 \\ a_1 & 1 & \cdots & 0 \\ a_2 & a_1 & \cdots & 0 \\ \vdots & \vdots & \vdots & \vdots \end{bmatrix}}_{C_a} \underbrace{\begin{bmatrix} y_{k+1} \\ y_{k+2} \\ \vdots \\ y_{k+n} \end{bmatrix}}_{\underset{\rightarrow}{y}_k} + \underbrace{\begin{bmatrix} a_1 & a_2 & \cdots & a_{n+1} \\ a_2 & a_3 & \cdots & 0 \\ a_3 & a_4 & \cdots & 0 \\ \vdots & \vdots & \vdots & \vdots \end{bmatrix}}_{H_a} \underbrace{\begin{bmatrix} y_k \\ y_{k-1} \\ \vdots \\ y_{k-n} \end{bmatrix}}_{\underset{\leftarrow}{y}_k} \\ &= \underbrace{\begin{bmatrix} b_1 & 0 & \cdots & 0 \\ b_2 & b_1 & \cdots & 0 \\ b_3 & b_2 & \cdots & 0 \\ \vdots & \vdots & \vdots & \vdots \end{bmatrix}}_{C_b} \underbrace{\begin{bmatrix} u_k \\ u_{k+1} \\ \vdots \\ u_{k+n-1} \end{bmatrix}}_{\underset{\rightarrow}{u}_k} + \underbrace{\begin{bmatrix} b_2 & b_3 & \cdots & b_n \\ b_3 & b_4 & \cdots & 0 \\ b_4 & b_5 & \cdots & 0 \\ \vdots & \vdots & \vdots & \vdots \end{bmatrix}}_{H_b} \underbrace{\begin{bmatrix} u_{k-1} \\ u_{k-2} \\ \vdots \\ u_{k-n+1} \end{bmatrix}}_{\underset{\leftarrow}{u}_k} + \underset{\rightarrow}{\xi} \end{aligned} \qquad \text{(Eq.6-2)}$$

The equation can be expressed as:

$$C_a \underset{\rightarrow}{y}_k + H_a \underset{\leftarrow}{y}_k = C_b \underset{\rightarrow}{u}_k + H_b \underset{\leftarrow}{u}_k + \underset{\rightarrow}{\xi} \qquad \text{(Eq.6-3)}$$

where $\underset{\rightarrow}{y}_k$ is the vector of the future output predicted at k instant, $\underset{\rightarrow}{u}_k$ is the future input vector that needs to be resolved, $\underset{\leftarrow}{y}_k$ and $\underset{\leftarrow}{u}_k$ are the past output and input vectors that already be known in the k instant, $\underset{\rightarrow}{\xi}$ is a constant vector decided by I_b and T_b.

Then the future output after k instant can be calculated as:

$$\underset{\rightarrow}{y}_k = \left(C_a\right)^{-1} \left(C_b \underset{\rightarrow}{u}_k + H_b \underset{\leftarrow}{u}_k - H_a \underset{\leftarrow}{y}_k + \underset{\rightarrow}{\xi} \right) \qquad \text{(Eq.6-4)}$$

The performance index is selected as:

$$J_p = \left\| \underset{\rightarrow}{r}_k - \underset{\rightarrow}{y}_k \right\|_2^2 + \lambda_p \left\| \Delta \underset{\rightarrow}{u}_k \right\|_2^2 \qquad \text{(Eq.6-5)}$$

here $\underset{\rightarrow}{r}_k$ the future reference output vector and $\underset{\rightarrow}{y}_k$ the predictive output vector, $\Delta \underset{\rightarrow}{u}_k$ is the increase of future control vector, and λ_p is the weight of $\left\| \Delta \underset{\rightarrow}{u}_k \right\|_2^2$. The future vector of *u* can thus be calculated by minimizing this quadratic performance index, comprising the deviations of the output from the desired trajectory and the changes of the future input vector. Take $\underset{\rightarrow}{y}_k$ from Eq.6-4 into the performance index:

$$J_p = \left\| \underset{\rightarrow}{r}_k - \left(C_a \right)^{-1} \left(C_b \underset{\rightarrow}{u}_k + H_b \underset{\leftarrow}{u}_k - H_a \underset{\leftarrow}{y}_k + \underset{\rightarrow}{\xi} \right) \right\|_2^2 + \lambda_p \left\| \Delta \underset{\rightarrow}{u}_k \right\|_2^2 \qquad \text{(Eq.6-6)}$$

here $\Delta \underset{\rightarrow}{u}_k$ can be calculated by the difference between $\underset{\rightarrow}{u}_{k-1}$ and $\underset{\leftarrow}{u}_k$:

$$\begin{aligned} \Delta \underset{\rightarrow}{u}_k &= \begin{bmatrix} u(k)-u(k-1) \\ u(k+1)-u(k) \\ u(k+2)-u(k+1) \\ \vdots \end{bmatrix} = \begin{bmatrix} 1 & 0 & 0 & \cdots \\ -1 & 1 & 0 & \cdots \\ 0 & -1 & 1 & \cdots \\ \vdots & \vdots & \vdots & \vdots \end{bmatrix} \underset{\leftarrow}{u}_k - \begin{bmatrix} 1 & 0 & 0 & \cdots \\ 0 & 0 & 0 & \cdots \\ 0 & 0 & 0 & \cdots \\ \vdots & \vdots & \vdots & \vdots \end{bmatrix} \underset{\rightarrow}{u}_k \\ &= C_f \underset{\rightarrow}{u}_k - C_p \underset{\leftarrow}{u}_k \end{aligned} \qquad \text{(Eq.6-7)}$$

To minimize the performance index, $\Delta \underset{\rightarrow}{u}_k$ is substituted into Eq.6-6, which is then differentiated it with respect to $\underset{\rightarrow}{u}_k$ and the derivative is equated to zero:

$$\frac{dJ_p}{d\underset{\rightarrow}{u}} = 2\left(H^T H + \lambda_p {C_f}^T C_f \right) \underset{\rightarrow}{u} + 2H^T \left[-Q \underset{\leftarrow}{y} + P \underset{\leftarrow}{u} - \underset{\rightarrow}{r} + C_a^{-1} \underset{\rightarrow}{\xi} \right] = 0 \qquad \text{(Eq.6-8)}$$

Solving function Eq.6-8, the input minimizing the performance index Eq.6-5 can be obtained in Eq.6-9:

$$\underset{\rightarrow}{u} = \left(H^T H + \lambda_p {C_f}^T C_f \right)^{-1} H^T \left[\underset{\rightarrow}{r} + Q \underset{\leftarrow}{y} - P \Delta \underset{\leftarrow}{u} - C_a^{-1} \underset{\rightarrow}{\xi} \right] \qquad \text{(Eq.6-9)}$$

here $H = C_a^{-1} C_b$, $P = C_a^{-1} H_b$, $Q = C_a^{-1} H_a$.

Finally, the current input $I_P(k)$ to the system can be obtained from the first scalar of $\underset{\rightarrow}{u}$ as $I_P(k) = [1, 0, 0 \cdots 0] \underset{\rightarrow}{u}(k)$

6.2 Model Coefficients Adaptive Algorithm

Although the identified model can represent the process in the control system, its parameters vary in the pipe welding process. In the welding process, there are many factors that can cause the parameters to deviate from initial parameters obtained as described in last chapter, such as the different initial torch position, the increasing temperature around the weld area in the process, and more importantly − different from the plate weld − the gravitation effect on the weld pool causes the model parameters to keep changing when the weld pool moves around the pipe in pipe weld process, as shown in Figure 6-2. In order to revise the model to match the change in the welding process, the coefficients need to be recursively estimated online during the experiment. To this end, in this paper, the standard recursive least squares (RLS) algorithms [78] is adopted to update the model parameters online.

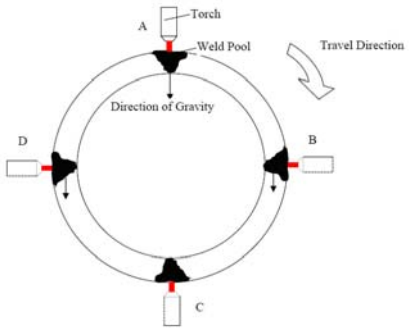

Figure 6-2 Gravity effect in pipe weld

The RLS algorithm is given by Eq.6-10 and Eq.6-11:

$$\hat{\theta}(t+1)=\hat{\theta}(t)+\frac{P(t)\varphi_0(t)}{1+\varphi_0{}^T(t)p(T)\varphi_0(t)}\left[y(t+1)-\varphi_0{}^T\theta_0(t)\right], \quad \text{(Eq.6-10)}$$

$$P(t+1)=P(t)-\frac{P(t)\varphi_0(t)\varphi_0{}^T(t)P(t)}{1+\varphi_0{}^T(t)P(t)\varphi_0} \quad \text{(Eq.6-11)}$$

here $\hat{\theta}(t+1)$ is the modified coefficient vector, $\hat{\theta}(t)$ is the former coefficient vector, P is a matrix initialed as a unit matrix I, φ is the vector of past inputs and outputs.

6.3 Constraints and Signal Process

In order to incorporate the MPC controller designed above into the QKPAW experiment, the measured signals need to be processed before they can be used in the controller.

a. Peak current time process (T_p)

In the experiment, the measure of T_p is important component in the system. Since in each sample time, the system cannot obtain T_p directly. To get an accurate time, a timer component of LabVIEW is used to count the time in every sample time. When the current is switched to the peak current, the time $t_1(k)$ is recorded by the program, and when the keyhole is detected as being established, the time $t_2(k)$ is recorded, and the peak current time is calculated as $T_p(k) = t_2(k) - t_1(k)$.

b. Constraints

The constraints in the system arise from two areas: the functional hardware limits and the constraints added in software to prevent the system damage.

Hardware constraints are the output limits of the power source: the maximum output current of the Miller MAXTRON 450 is 450A, and the corresponding control voltage is 10V, the minimum output current of the power supply is 0A when the corresponding control input voltage is 0V. The output of the power supply has the linear correlation with the control input signal. As the result, the control signal is limited between 0V-10V in the process.

The software constraints are introduced into the program. In contrast to the hardware constraints, the software constraints can be adjusted or exceeded if necessary. It was experimentally confirmed that if the input and the output are too large, such as in the case of T_p is too long or I_p is too high, the torch nozzle would easily be damaged by the heat coming from the arc going through the nozzle. The excessive high heat also can increase the weld pool dimension and the arc pressure

square with the arc can easily cause the burn-through. To avoid the burn-through and protect the torch nozzle, the output constraint is incorporated so that if the keyhole cannot be detected in twice the time of the reference output, the controller switches off the peak current and reestablishes the keyhole after some time. For example, if reference keyhole establish-time T_{pr} is 200ms, the constraint for T_p is T_p<400ms. For the same purpose, the limit of I_p is added in the process, although I_p can up to 450A, it is controlled under 250A in the normal situation.

6.4 Parameters Fuzzy Adjustment

In the MPC designed above, one conflict exists in the parameter selection: in Eq.6-5, λ_p is a primary parameter that determines the response speed of the control system. When it is small, the system can have fast response speed, but may have strong reaction to the noise and disturbance in the system; in contrast, the large λ_p achieves noise inhibition but slows the response speed. To resolve this issue, a simple fuzzy controller is applied to adjust λ_p online.

The fuzzy mathematic and application stemmed from the fuzzy logic, first proposed by L. A. Zandeh in 1965. The fuzzy controller is the most important component in this theory and had its first industrial application in heater control by E.H. Mamdani in 1974. Unlike the traditional control system, the fuzzy control does not need to know the exact model of the controlled process, and imitates the human control strategy to some degree. From this point, the fuzzy control can be treated as a type of intelligent control.

Figure 6-3 shows the block diagram of a fuzzy control system. The system is comprised of the following four components:

1. Rule-base, which contains the knowledge and the goals of the specific application, i.e. fuzzy logics in expert's linguistic description of how to get the

output;

2. Fuzzification, a first step in the fuzzy control, is the process of converting an exact input value to a fuzzy value. These variables include the reference input, process output or state.
3. Fuzzy inference, which is the core of the fuzzy controller. It has the inference ability based on the fuzzy logic.
4. Defuzzification, which transfers the fuzzy control variables, obtained from the fuzzy inference into the real control variables to the control process.

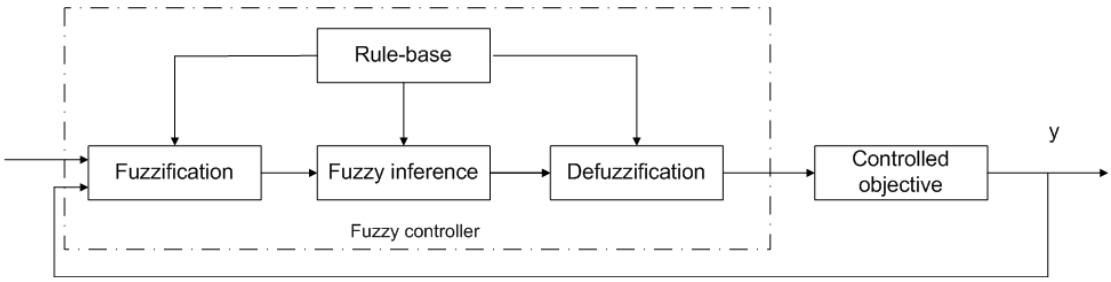

Figure 6-3 Block diagram of fuzzy control

In the fuzzy controller, the expert knowledge is expressed by a group of linguistic descriptions such as IF (satisfy some specified condition) THEN (obtain some specified conclusion). In these sets of IF-THEN rules, the condition and the conclusion are all in fuzzy concept. Since the measured output or states are normally not in fuzzy form, they are needed to be mapped into fuzzy set domain by the fuzzy quantification. One most common fuzzy quantification method is triangle fuzzy function, as Figure 6-4 shows. Here, the membership function $\mu_A(x)$ quantifies the certainty and X is the states input to the fuzzification.

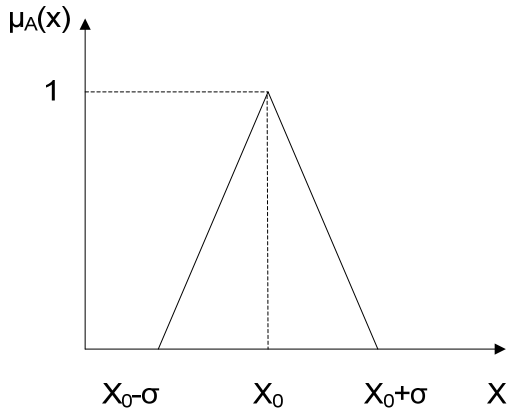

Figure 6-4 Triangle fuzzy membership function

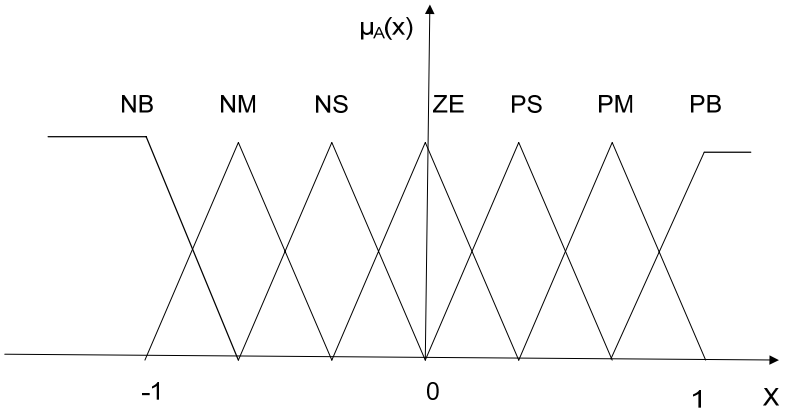

Figure 6-5 Multi-level fuzzy membership functions

If the multi-level fuzzy state quantifies the certainty, it can be classified by multi-triangle fuzzy membership functions. Figure 6-5 shows a 7-level fuzzy quantification, where X is the normalized state. It is classified into NB (negative big), NM (negative middle), NS (negative small), ZE (Zero), PS (positive small), PM (positive middle) and PB (positive big).

In practice, the controller accepts and maps the inputs into their membership functions. These mappings are then fed into the rules, commonly expressed as AND relationships and OR relationships. In the AND relationship between the mappings of the two input variables, the minimum of the two is used as the combined truth value; whereas in the OR relationship, the maximum is used.

Since the control signal obtained from fuzzy inference is a fuzzy value, it needs

to be transferred to an actual (crisp) variable in the defuzzification. A number of defuzzification strategies exist and the most common among them are the following:

1. Max criterion: A crisp output y_{crisp} is chosen as the point on the output, which implies that fuzzy set achieved a maximum in the set.

   $\mu_{\text{Y}}(\text{y}_{\text{crisp}}) \geq \mu_{\text{Y}}(\text{y}) \quad \text{y} \in Y$ here Y is fuzzy set

2. Mean of maximum: a crisp output y_{crisp} is chosen to represent the mean value of all elements whose membership is a maximum in the fuzzy set.
3. Center-average: A crisp output y_{crisp} is chosen using the centers of each of the output membership functions and the maximum certainty of each of the conclusions represented with the implied fuzzy sets.
4. Center of area (COA): A crisp output y_{crisp} is chosen as the center of area for the membership function of the overall implied fuzzy set.

a. Controller structure

In the QKPAW, when T_p, measured in the current weld cycle, is far away from the reference output T_{pr}, the fast response speed is preferred in the process to force T_p to approach to T_{pr} in fast speed. This situation mostly occurs in the beginning of the process or if T_{pr} is changed suddenly, when small λ_p is needed in the algorithm. Otherwise, such as in the stable state, λ_p should be increased to prevent the large variation in the control signal. Another possible case correlated with λ_p is the change of T_p, denoted as $\Delta T_p(k)=(T_p(k)- T_p(k\text{-}1))$. In theory, large $\Delta T_p(k)$ implies that the control signal may change too much and needs to be damped by increasing λ_p; on the other hand, small $\Delta T_p(k)$ may cause the slow response speed, and λ_p need to be reduced.

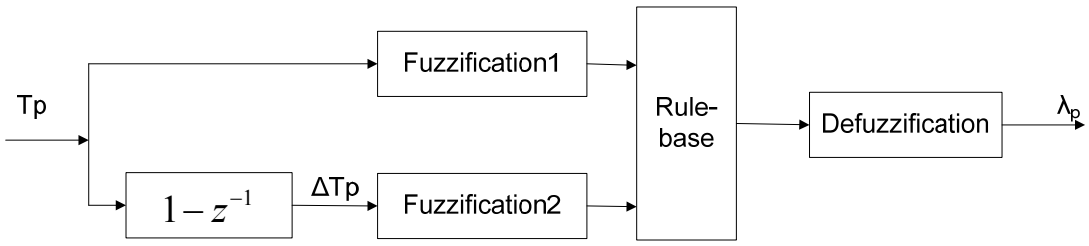

Figure 6-6 Fuzzy controller for λ_p

On the basis of the analysis above, the fuzzy controller is designed as shown in Figure 6-6.

b. Fuzzification

In the fuzzy controller, the fuzzification1 is designed as shown in Figure 6-7. The x-axle is the difference between the measured output and the reference output. In the experimental process, for example, the preferred reference output is selected as $T_r = 200ms$, and the limit $T_p < 400ms$ is added in the process, the minimum and the maximum of T_p-T_r is - T_r and T_r respectively. As a result, T_p is divided into negative big (NB), negative small (NS), zero (ZE), positive small (PS) and positive big (PB) as shown in Figure 6-7.

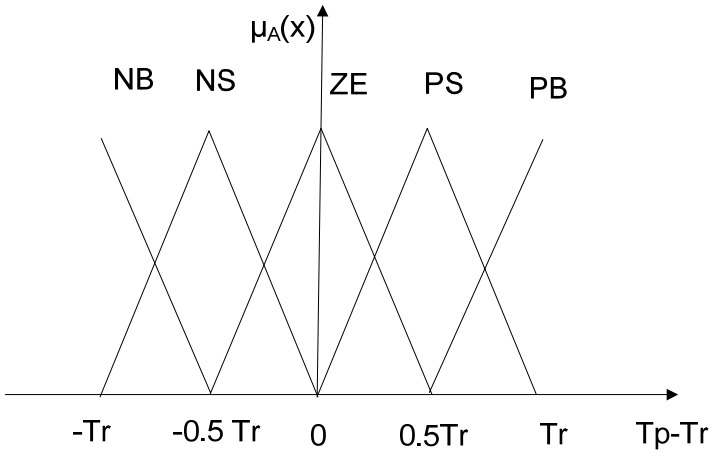

Figure 6-7 Fuzzification of T_p

Figure 6-8 shows the fuzzification of ΔT_p, the range of ΔT_p is between -2T_r, in case of $T_p(k)$=0; and $T_p(k\text{-}1)$ = 2T_r, and 2T_r, in case of $T_p(k)$=2T_r and $T_p(k\text{-}1)$=0. Similarly to T_p, ΔT_p is divided into NB, NS, ZE, PS and PB as shown in Figure 6-8.

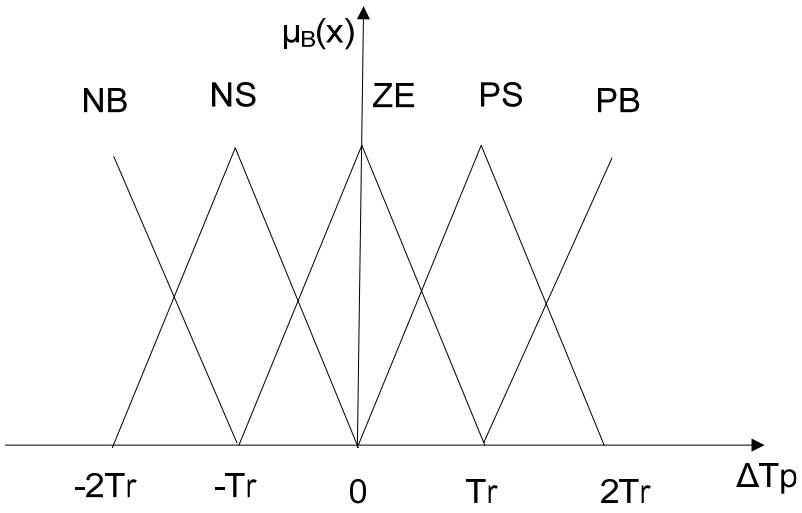

Figure 6-8 Fuzzification of ΔT_p

c. Rule-base

The rule-base, in the fuzzy controller, is designed as presented in Table 6-1:

Table 6-1 Rule-base for fuzzy-controller of λ_p

λ_{pf} / ΔT_p / T_p	NB	NS	ZE	PS	PB
NB	B	M	S		
NS	M	M	M	M	
ZE		M	M	M	
PS		M	M	M	M
PB			S	M	B

In Table 6-1, M denotes the middle value, which is the default value input from the human machine interface (HMI) program. B implies that λ_{pf} is a large value, which is double of middle value; whilst S corresponds to a small value, which is half of the middle value in the controller. In most situations, λ_{pf} is selected as default value M. When ΔT_p is NB (PB) and T_p is NB (PB), it implies that T_p changes too fast. In this case, λ_{pf} needs to be increased to slow the change in T_p. When T_p is NB (PB) and ΔT_p

is ZE, which means T_p cannot follow the reference fast enough. In this case, λ_{pf} is selected as S, a smaller constant to increase the response speed of the controller.

d. Defuzzification

After λ_{pf} if selected from the rule-base, it needs to be transformed to a real number by defuzzification before it is used in MPC. The simple defuzzification in there fuzzy controller is designed as: when λ_{pf} is M, λ_p equals to the default set weight λ_{ps}, when λ_{pf} is B, λ_p is amplified to 2 λ_{ps} and otherwise, λ_p is reduced to a half of λ_{ps}, as Eq.6-12 shows

$$\begin{cases} \lambda_p = 2\lambda_{ps}; & \lambda_{pf} = B \\ \lambda_p = \lambda_{ps}\ ; & \lambda_{pf} = M \\ \lambda_p = 0.5\lambda_{ps}; & \lambda_{pf} = S \end{cases} \qquad \text{(Eq.6-12)}$$

6.5 Experiments

To test the effectiveness of the developed control algorithm, the plasma pipe welding experiments were conducted with the experimental setup shown in Figure 4-1 and the control algorithm described in this Chapter. In the experiment, the welded pipes are schedule 10 A36 carbon steel pipes with 5 inch inner diameters and 0.134 inch wall thickness.

The parameters in Table 4-2 are adopted in the experiments; the travel speed was 2.0mm/s and the initial distance between the torch and welded pipe was 5mm. In the experiments, due to small distortion of the orbital rings and the installation error, the orbital rings are not expected to be exactly concentric with the welded pipes. This non-concentricity results in the gap between the torch and welded pipe and usually has some fluctuation causing the arc length changes during the weld process. The variability of the arc length, measured at around 3mm in the experiments, increases the complexity of the experiment and imposes the robust requirements for the controller.

In order to verify the performance of the controller above, two types of

experiments with different disturbances were conducted. In both, I_b is set as 40A, whilst $T_b = 400ms$ and $\lambda_j = 2$.

The first experiment was conducted to test the tracking performance when the welding speed changed. In this experiment, the set point of the peak keyhole establishment time is a constant T_p=100ms, but the travel speed changes during the experiment. The travel speed of the torch was switched from 2mm/s to 3.5 mm/s at the 60th weld cycle in the welding process. Figure 6-9 shows the curves of T_p and I_p in the experiment. It is observed from the result that when the speed was changed, T_p increased significantly; however the controller increased I_p rapidly forcing T_p to return back to around the 100ms.

The second experiment was conducted to test the tracking performance when the reference trajectory changed. In the middle of the experiment, as shown in Figure 6-10, the desired keyhole duration $T_p^*$was switched from 80ms to 200ms, with other parameters unchanged. It can be seen from Figure 6-10, after T_p^* increased − thus less heat input rate was required to establish the keyhole, I_p began to reduce and T_p followed T_p^* after a few weld cycles.

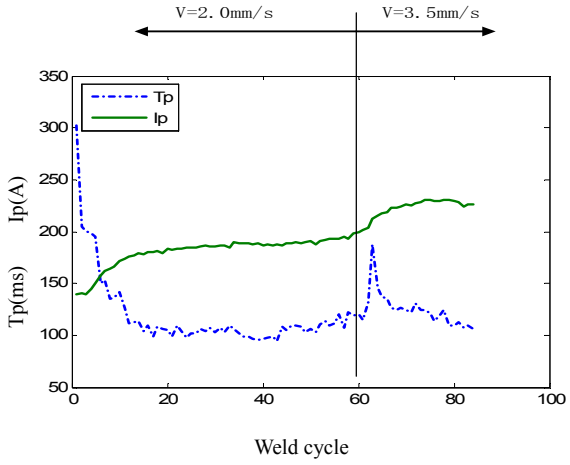

Figure 6-9 Experimental results with travel speed change

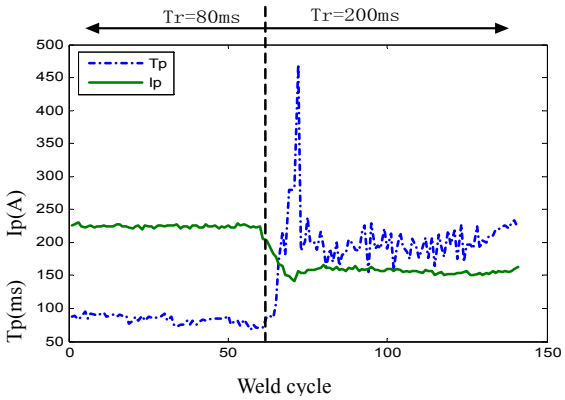

Figure 6-10 Experiment result of tracking performance

For the convenience reason, all the experiments above were conducted with bead-on-plate welds, to test the performance on the butted weld, the standard situation in real application in industry, two pieces 5"ID schedule 10 carbon-steel pipes were butted to be welded in the experiment with the parameters in Table 4-2 and $I_b = 40$A, whilst $T_b = 400ms$. Figure 6-11 shows the entire position butted weld result with linear MPC designed above. Figure 6-11(a) shows the outer surface of the welding line and (b) shows the backside which verified the system can ensure the full penetration and smooth weld line surface, which are the important weld quality in the pipe welding.

(a) Outside weld line (b) Inside weld line

Figure 6-11 Butted weld result

CHAPTER 7 Bilinear MPC

Chapter 6 presents the control performance of linear MPC with a linear model. In the pipe welding, as well as in many other processes, linear models can accurately approximate the process behavior around a single set point, i.e. in a narrow operating range, and the linear MPC is proven to obtain a satisfying result in a limited operating range during the weld experiment. However, an increasing demand for flexibility of many processes requires that these processes are operated over larger operating ranges. Due to the intrinsic nonlinearity of almost all processes, linear models cannot accurately approximate the process behavior over these larger operating ranges and the nonlinear behavior cannot be neglected. In such cases, the nonlinear models are required for accurate approximate modeling [79] [80].

Adaptive control of bilinear systems is important, both in theory and in practice, since many process systems in industry can be better modeled and controlled in wider working ranges if they are treated as bilinear, rather than linear, systems. In this dissertation, an adaptive model predictive control algorithm for bilinear systems was developed and used in the keyhole establish-time control of the QKPAW. The class of discrete-time bilinear input-output models forms a subclass of the nonlinear models, and extends the class of linear models into the models that contain a product term between the past output and the input, as shown in Eq. 5-10.

7.1 Algorithm Introduction

The linear MPC control in QKPAW was introduced in the former work (Chapter 6). In the linear MPC, since there are linear correlations between inputs and outputs, the output and the input can be separated in the control algorithm design, and the future output can be easily predicted with the iterative method. In the bilinear model,

due to its inclusion of bilinear items, the input and the output cannot be separated as in the linear MPC, which limits the MPC application in the bilinear model. Although some research has been reported[81], these works on the bilinear MPC are mainly based on the linearization and added compensation term in the linear model, so it still faces the problem that the linearized model cannot represent the process in a wide working range. In this dissertation, a new bilinear MPC is designed to deal with this bilinear MPC problem and it is introduced as follows:

At first step, the bilinear model Eq.5-10 is expanded to future n_j horizons as linear MPC does:

$$\begin{aligned}
y(k+1) &= \sum_{i=1}^{n_y} a_i y(k+1-i) + \sum_{i=1}^{n_{uy}} b_i u(k+1-i) y(k-i) + \sum_{i=0}^{n_u} c_i u(k+1-i) + \zeta \\
y(k+2) &= \sum_{i=1}^{n_y} a_i y(k+2-i) + \sum_{i=1}^{n_{uy}} b_i u(k+2-i) y(k+2-i) + \sum_{i=0}^{n_u} c_i u(k+2-i) + \zeta \\
&\vdots \\
y(k+n_j) &= \sum_{i=1}^{n_y} a_i y(k+n_j-i) + \sum_{i=1}^{n_{uy}} b_i u(k+n_j-i) y(k+n_j-i) + \sum_{i=0}^{n_u} c_i u(k+n_j-i) + \zeta
\end{aligned} \qquad \text{(Eq.7-1)}$$

where n_j predictive horizon of the algorithm.

The following steps are then taken: transfer the items in Eq.7-1 grouped by future output, pass output, future input, and pass input. Rewrite them into the matrix form:

$$\begin{aligned}
&\underbrace{\begin{bmatrix} 1 & 0 & \cdots & 0 \\ -\tilde{a}_{21} & 1 & \cdots & 0 \\ -\tilde{a}_{32} & -\tilde{a}_{31} & \cdots & 0 \\ \vdots & \vdots & \vdots & \vdots \end{bmatrix}}_{\tilde{C}_a} \underbrace{\begin{bmatrix} y(k+1) \\ y(k+2) \\ \vdots \\ y(k+n) \end{bmatrix}}_{\underline{y}_k} + \underbrace{\begin{bmatrix} -\tilde{a}_{11} & -\tilde{a}_{12} & \cdots & -\tilde{a}_{1n+1} \\ -\tilde{a}_{22} & -\tilde{a}_{23} & \cdots & 0 \\ -\tilde{a}_{33} & -\tilde{a}_{34} & \cdots & 0 \\ \vdots & \vdots & \vdots & \vdots \end{bmatrix}}_{\tilde{H}_a} \underbrace{\begin{bmatrix} y(k) \\ y(k-1) \\ \vdots \\ y(k-n+1) \end{bmatrix}}_{\underline{y}_k} \\
&= \underbrace{\begin{bmatrix} c_0 & 0 & \cdots & 0 \\ c_1 & c_0 & \cdots & 0 \\ c_2 & c_1 & \cdots & 0 \\ \vdots & \vdots & \vdots & \vdots \end{bmatrix}}_{C_b} \underbrace{\begin{bmatrix} u(k+1) \\ u(k+2) \\ \vdots \\ u(k+n) \end{bmatrix}}_{\underline{u}_k} + \underbrace{\begin{bmatrix} c_1 & c_2 & \cdots & c_{n+1} \\ c_2 & c_3 & \cdots & 0 \\ c_3 & c_4 & \cdots & 0 \\ \vdots & \vdots & \vdots & \vdots \end{bmatrix}}_{H_b} \underbrace{\begin{bmatrix} u(k) \\ u(k-1) \\ \vdots \\ u(k-n+1) \end{bmatrix}}_{\underline{u}_k} + \underbrace{\begin{bmatrix} \zeta \\ \zeta \\ \vdots \\ \zeta \end{bmatrix}}_{\zeta}
\end{aligned} \qquad \text{(Eq.7-2)}$$

where $\tilde{a}_{ij} = a_j + b_j u(k+i-j)$, when $i < j$, $u(k+i-j)$ is unknown control variables to be predicted, and in case of $i \geq j$, $u(k+i-j)$ is the past variables retained in memory.

The performance index is selected as Eq.7-3:

$$J_p = \sum_{i=1}^{n_p} \left\| y_r(k+i) - \hat{y}(k+i) \mid k \right\|_2^2 + \lambda \sum_{i=1}^{n_c} \left\| \Delta u(k+i) \mid k \right\|_2^2 \qquad \text{(Eq.7-3)}$$

where y_r is set point, $\hat{y}$ is predictive output,

$\Delta u(k+i) \mid k = u(k+i) \mid k - u(k+i-1) \mid k$.

It is apparent that in this bilinear model, the coefficient matrices $\tilde{C}_a$ and $\tilde{H}_a$ depend on $\underset{\rightarrow}{u}_{k-1}$ obtained from the model. Since $\underset{\rightarrow}{u}_{k-1}$ is the future control vector determined by the control algorithm, $\tilde{C}_a$ and $\tilde{H}a$ are unknown in the current instant, thus MPC cannot be used to resolve the problem as in the linear model control system. If $\tilde{a}_{ij}$ in Eq.7-2 could be found, $\tilde{C}_a$ and $\tilde{H}_a$ would be determined and thus the bilinear MPC would be resolvable as in linear model method. To this end, the author proposes an iterative search method that selects initial values for $\underset{\rightarrow}{u}_k$ in $\tilde{C}_a$ and $\tilde{H}_a$, then obtains the analytic solution for the resultant quadratic cost function. The analytic solution can then be used in the iterative search computation until the optimal solution is found. For our application in PAW of pipes, the set-point does not continuously change rapidly. This method can result in convergence in the iterative computation to find, with controlled accuracy, an approximate for the input vector that minimizes the non-linear cost function. In the following derivation, the initially selected input in $\tilde{C}_a$ and $\tilde{H}_a$ is noted as $\underset{\rightarrow}{u}_s$; but in the control variable vector, $\underset{\rightarrow}{u}_{k+1}$ to be determined by the MPC is denoted as $\underset{\rightarrow}{u}^*$ and it can be calculated as:

$$\underset{\rightarrow}{u}^* = \left(H^T H + \lambda C_f^T C_f \right)^{-1} \left(H^T \left(\underset{\rightarrow}{r}_k - P \underset{\rightarrow}{u}_k + Q \underset{\rightarrow}{y}_k \right) + \lambda C_f^T C_P \underset{\rightarrow}{u}_k \right) \qquad \text{(Eq.7-4)}$$

where $H = \tilde{C}_a^{-1} C_b, \quad P = \tilde{C}_a^{-1} H_b, \quad Q = \tilde{C}_a^{-1} \tilde{H}_a$

To resolve the problem formulated in the proposed bilinear MPC algorithm above, a search algorithm is performed to find a converged solution, $\underline{u}^*_{k-1} \approx \underline{u}_S$. As a result, an approximation of the optimal solution for the control signal can be obtained.

In the proposed search algorithm, the search range of $\underline{u}_s$ is constrained between u_{min} and u_{max}, a search range that depends on the welding conditions, and a small $\gamma > 0$ is chosen for the convergence criterion $\left|\underline{u}_k - \underline{u}^*\right| < \gamma$.

The proposed search algorithm for the bilinear MPC can be summarized into following steps:

1. Determine the initial $\underline{u}_s$ (to be discussed immediately below) and set the step length $\alpha(i) = 1$;
2. Compute $\underline{u}^*$ by solving linear MPC (Eq.7-4), If $\left\|\underline{u}^* - \underline{u}\right\| < \gamma$ then terminate the search by going to step 5;
3. Calculate the new $\underline{u}_S$ by $\underline{u}_{sn}(i) = \underline{u}_s(i) + \alpha(i)(\underline{u}^*(i) - \underline{u}_s(i))$; replace $\underline{u}_s$ in $\tilde{C}_a$ and $\tilde{H}_a$ with $\underline{u}_{sn}$; call (Eq.7-4) again to calculate a new $\underline{u}^*$ noted as $\underline{u}^*_n$. If $\left|\underline{u}^*_n(i) - \underline{u}_{sn}(i)\right| > \left|\underline{u}^*(i) - \underline{u}_s(i)\right|$ (i.e., $\underline{u}_{sn}$ is a worse updated initial than $\underline{u}_s$), update $\alpha(i) = \lambda_s\ \alpha(i)$ and repeat 3; otherwise go to step 4;
4. Replace $\underline{u}_s$ with $\underline{u}_{sn}$, reset $\alpha(i) = 1$ and go to step 2.
5. Stop and output $\underline{u}^*$

Here (i) presents the i_{th} variable in the vector and $i = 1, 2$ since the horizons in the model is 2. λ_s is the scale coefficient for search step. Here α is a vector determining the search step length.

The initial $\underline{u}_s$ is an important parameter that determines the convenience of the proposed search algorithm. Before beginning the research, the initial $\underline{u}_s$ need to be

known, it is better that they are chosen near $\underset{\rightarrow}{u}^*$ obtained from the above algorithm to decrease the search times and achieve fast convergence speed. To this end, at the beginning of the search, the following algorithm is called to find the initial $\underset{\rightarrow}{u}_s$:

1. Combine the bilinear factors and the input factors in (4) together, and then the bilinear model (4) is transferred into:

$$\begin{aligned}
y(k+1) &= \sum_{i=1}^{n_y} a_i y(k+1-i) + \sum_{i=0}^{\max(n_u, n_{uy})} \left[b_i y(k+1-i) + c_i \right] u(k+1-i) + \zeta \\
y(k+2) &= \sum_{i=1}^{n_y} a_i y(k+2-i) + \sum_{i=0}^{\max(n_u, n_{uy})} \left[b_i y(k+2-i) + c_i \right] u(k+2-i) + \zeta \\
&\vdots \\
y(k+n_j) &= \sum_{i=1}^{n_y} a_i y(k+n_j-i) + \sum_{i=0}^{\max(n_u, n_{uy})} \left[b_i y(k+n_j-i) + c_i \right] u(k+n_j-i) + \zeta
\end{aligned} \qquad \text{(Eq.7-5)}$$

2. Separate the future variables from the past variables and express it into matrix form

$$\begin{aligned}
&\underbrace{\begin{bmatrix} 1 & 0 & \cdots & 0 \\ -a_1 & 1 & \cdots & 0 \\ -a_2 & -a_1 & \cdots & 0 \\ \vdots & \vdots & \vdots & \vdots \end{bmatrix}}_{C_a} \underbrace{\begin{bmatrix} y_{k+1} \\ y_{k+2} \\ \vdots \\ y_{k+n} \end{bmatrix}}_{\underset{\rightarrow}{y}_k} + \underbrace{\begin{bmatrix} -a_1 & -a_2 & \cdots & -a_{n+1} \\ -a_2 & -a_3 & \cdots & 0 \\ -a_3 & -a_4 & \cdots & 0 \\ \vdots & \vdots & \vdots & \vdots \end{bmatrix}}_{H_a} \underbrace{\begin{bmatrix} y_k \\ y_{k-1} \\ \vdots \\ y_{k-n+1} \end{bmatrix}}_{\underset{\rightarrow}{y}_k} \\
&= \underbrace{\begin{bmatrix} \tilde{b}_{11} & 0 & \cdots & 0 \\ \tilde{b}_{21} & \tilde{b}_{22} & \cdots & 0 \\ \tilde{b}_{31} & \tilde{b}_{32} & \cdots & 0 \\ \vdots & \vdots & \vdots & \vdots \end{bmatrix}}_{\tilde{C}_b} \underbrace{\begin{bmatrix} u_{k+1} \\ u_{k+2} \\ \vdots \\ u_{k+n} \end{bmatrix}}_{\underset{\rightarrow}{u}_k} + \underbrace{\begin{bmatrix} \tilde{b}_{12} & \tilde{b}_{13} & \cdots & \tilde{b}_{1n} \\ \tilde{b}_{23} & \tilde{b}_{24} & \cdots & 0 \\ \tilde{b}_{34} & \tilde{b}_{35} & \cdots & 0 \\ \vdots & \vdots & \vdots & \vdots \end{bmatrix}}_{H_b} \underbrace{\begin{bmatrix} u_k \\ u_{k-1} \\ \vdots \\ u_{k-n+1} \end{bmatrix}}_{\underset{\rightarrow}{u}_k} + \underbrace{\begin{bmatrix} \zeta \\ \zeta \\ \vdots \\ \zeta \end{bmatrix}}_{\zeta}
\end{aligned} \qquad \text{(Eq.7-6)}$$

$$\text{where} \begin{cases} \tilde{b}_{ij} = b_{i-j} y(k+j) + c_{i-j} & i \geq j \\ \tilde{b}_{ij} = b_{j-1} y(k-j+i+1) + c_{j-1} & i < j \end{cases}$$

In the MPC, if the process is well modeled and controlled, the output should be equal or close to the reference output, y may thus be replaced by the reference output y_r such that one can use the linear MPC to calculate the initial $\underset{\rightarrow}{u}_s$.

$$\begin{cases} \tilde{b}_{ij} = b_{i-j} y_r(k+j) + c_{i-j} & i \geq j \\ \tilde{b}_{ij} = b_{j-1} y_r(k-j+i+1) + c_{j-1} & i < j \end{cases}$$

$$\underset{\rightarrow}{u}_s = \left(\tilde{H}^T\tilde{H} + \lambda C_f^T C_f\right)^{-1}\left(\tilde{H}^T\left(\underset{\rightarrow}{r}_k - P\underset{\rightarrow}{u}_k + Q\underset{\rightarrow}{y}_k\right) + \lambda C_f^T C_P \underset{\rightarrow}{u}_k\right)$$

where $\tilde{H} = C_a^{-1}\tilde{C}_b$, $P = C_a^{-1}\tilde{H}_b$, $Q = -C_a^{-1}H_a$

7.2 Simulation

To verify the effect of the search algorithm in the bilinear MPC, with a type of two-order bilinear model Eq.5-10 and a set of parameters introduced in Chapter 6, a software simulation has been conducted to track a reference square wave y_r which is switched from 150ms to 300ms at both 50th and 10th cycle. The search termination condition is set to one tenth of the difference between $\underset{\rightarrow}{u}_k^*$ and $\underset{\rightarrow}{u}_k$, $\gamma = \left\|\underset{\rightarrow}{u}_k^* - \underset{\rightarrow}{u}_k\right\|/10$. Figure 7-1(a) is the simulation result of the bilinear MPC without the self-search algorithm and Figure 7-1(b) shows the result with the same model and parameters, but the self-search algorithm is called in the simulation. It can be seen that after adding the self-search algorithm, $u^*(k)$ approached $u(k)$ and as the result, the overshoot and oscillation are decreased, which implies that the controlled process is more stable.

The simulation result also shows, in Figure 7-1 (c), the corresponding search times called by the controller. When the steps occur in the reference signal, $u^*(k)$ has a relative departure from $u(k)$, as a result, the self-search algorithm is called, and the larger departure causes more searching times. When the reference signal is stable, $u^*(k)$ will be close to $u(k)$, and fewer or even no self-search algorithm calls are made in this situation.

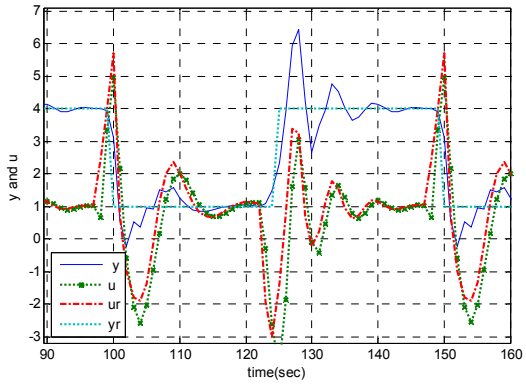

(a)Simulation without self-search algorithm

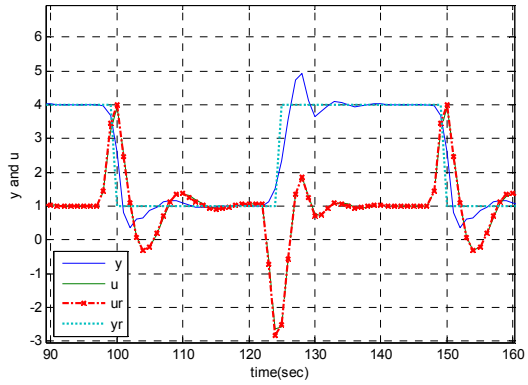

(b) Simulation with self-search algorithm

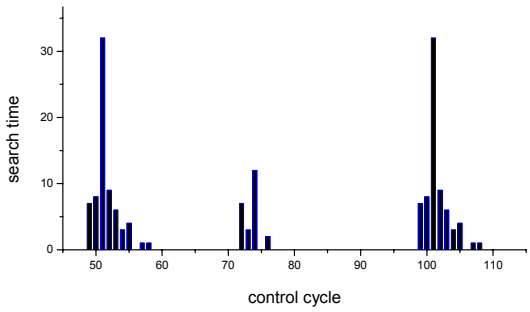

(c) Search times plot

Figure 7-1 Bilinear tracking simulations

7.3 Experiments

To test the effectiveness of the developed bilinear MPC controller, the plasma piping welding experiments were conducted on the experimental system set up in Figure 4-1. The welded pipes were 5" ID, schedule 10, A36 carbon steel pipes with 0.134 inch wall thickness. The travel speed was 2.0mm/s, if not specifically mentioned, and the initial distance between nozzle and welded pipe was 5 mm.

To verify the control performance, three types of experiments with different disturbances were conducted, in which the constraint of input control signal was set to (120A, 220A) and the base current was set I_b=40A.

The first experiment was conducted to test the tracking performance when the reference trajectory changed. In the middle of the experiment, the desired keyhole duration T_{pr} was switched from 150ms to 100ms at 62nd cycle, with other parameters unchanged. Figure 7-2 shows the input and the output, in which the peak current increases after the reference T_{pr} changes and T_p is controlled to follow new T_{pr} as the result.

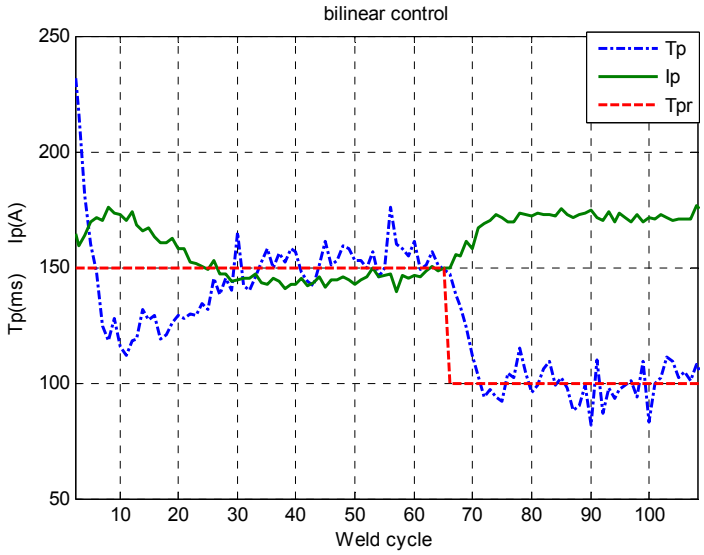

Figure 7-2 Experimental result of tracking performance

The second experiment was conducted to test the controller performance robustness. The reference keyhole establishment time was set to a constant in the experiment $T_{pr} = 150ms$ and the travel speed was switched from 2.0mm/s to 3.0mm/s around the 80th welding cycle. Figure 7-3 shows the I_p and T_p result of the experiment. It is observed that, when speed increased, T_p increased greatly, however the controller decreased the current rapidly forcing T_p to return back to around $150ms$.

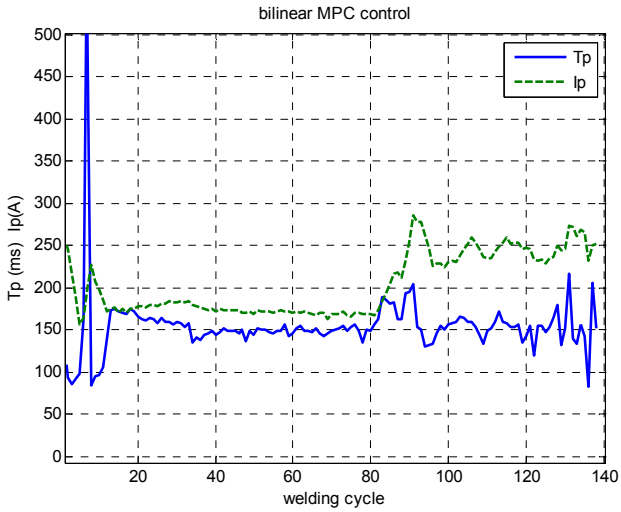

Figure 7-3 Experimental result of change of speed

The third experiment was conducted to verify the control performance when the characteristics of the objective were changing. To this end, the surface of the welded pipe was grooved before the experiments. Thus, the surface of the pipe was uneven, as shown in Figure 7-4. The deepest depth of the groove is around 1mm. Since the thickness of the welded pipe was 3.2mm before grooving, the thickness of the grooved welded pipe varied from 2.2mm to 3.2mm. The objective in this experiment was to control T_p when the workpiece thickness changed. Since the thickness of the pipe wall was one of the most important factors to keyhole establishment time in the

keyhole welding, thinner pipe wall implies that less current is needed to establish the keyhole than in a thicker pipe wall pipe weld. The controller should reduce the arc current when the weld pool enters the grooved area.

Figure 7-5(a) and (b) shows the weld result of the bilinear MPC, Figure 7-6 shows that controller adjusted I_p so that T_p can be controlled around the reference keyhole establish time (150ms) when the welding thickness changed.

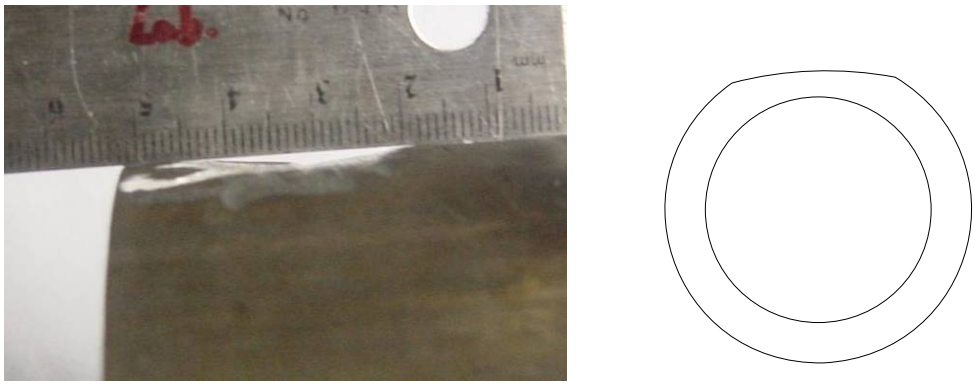

(a) Depth of the cave (b) The grinded pipe wall

Figure 7-4 Cave on the pipe before weld

(a) Outside of weld line (b) Backside of the weld line

Figure 7-5 Pipe weld result

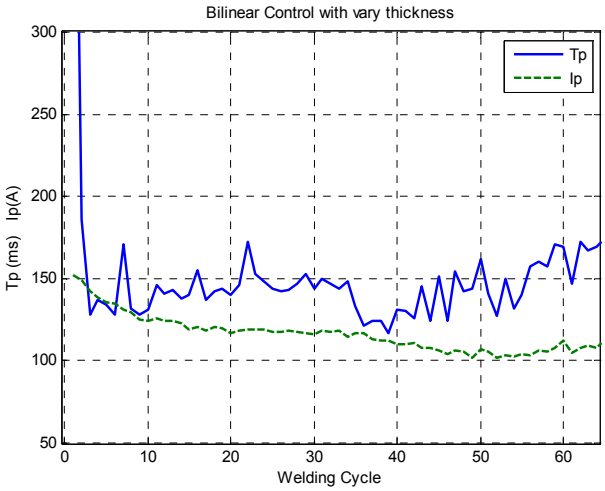

Figure 7-6 Experiment of change of thickness

One of the advantages of the bilinear control is that the model can represent the process better than a linear model does, especially in the changing working conditions. In the tracking performance experiment, the reference output T_{pr} changed from 150ms to 200ms at 100th weld cycle, and the coefficients were identified by the RLS algorithm Eq.6-10 online and recorded during the experiment. Figure 7-7(a) shows the change of the parameters in the bilinear model experiment and Figure 7-7 (b) shows the change of the parameters of two-order linear model linearized into $T_p(k) = \sum_{i=1}^{2} a_i T_p(k-i) + \sum_{i=1}^{2} b_i I_p(k-i) + \sum_{i=1}^{2} c_i I_b(k-i) + \zeta$. It is obvious that when T_{pr} was changed, the bilinear model parameters had smaller vibration than linear model did.

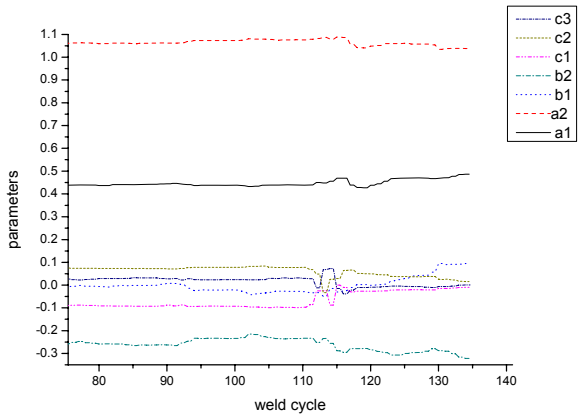

(a) Bilinear model

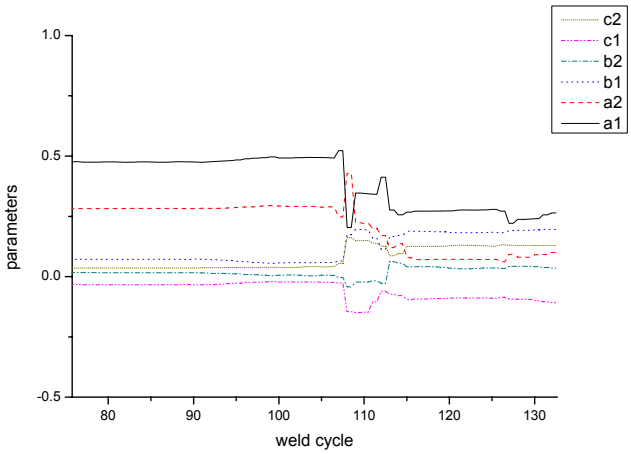

(b) Linear model

Figure 7-7 Model coefficients in the experiment

CHAPTER 8 Process Optimization

Since the heat affected zone (HAZ) is one weak spot in the entire welding joint zone of the super-high strength steel, effect of the weld heat input on the impact energy in the HAZ is given close attention by many investigators. Other authors [82] have shown the impact energy required to fracture a part subjected to shock loading, as in an impact test, and hardness tend to decrease when the weld heat input increases.

The intense arc heat increases the temperature of the metal beneath the arc, which therefore reaches the melting point very quickly. In the arc weld, if weld speed is a constant, the heat input is mainly controlled by the arc setting, such as the arc current and arc length.

In this chapter, the optimal algorithm is introduced to find an optimal base current to decrease the heat input in the process.

8.1 Linear MPC Optimization

In a typical quasi-keyhole process control, I_b is set to be a constant and I_p is the only controlled input to adjust T_p. Since both I_p and I_b affect T_p, I_b is also an important factor to determine the keyhole establishment time and may achieve an additional goal in the weld. In this paper, this additional goal is to reduce of the heat input during the weld. Based on the QAPWP system introduced in previous chapters, the automatic control system diagram, shown in Figure 8-1, has been proposed to control the peak current duration (T_p) control process. In this control system, there are two controllers connected in series. The first controller, called the base current controller, is used to calculate the base current to minimize the heat input into the workpiece. Based on the base current, the second controller, called peak current controller, is used to calculate the peak current in the current control period to keep the output of the system T_p

tracking the desired trajectory T_{pr}. The controlled objective is comprised of welding supply, the welding process, the keyhole sensor, and the signal analysis. The model coefficient identification is added into the system to adjust the model parameters used in the controllers. Since the adjustment of I_b must affect the control performance, such as the convergence of the peak current controller, this effect is prominent when the process is in the unsteady state, such as the beginning of the process, the change of weld speed, or reference keyhole establishment time. In this situation, the tracking performance is more important than the optimization in the control system. To this end, the base current is only calculated in the steady state, during which the $I_p(k)$ does not change, obviously with constant $I_b(k)$.

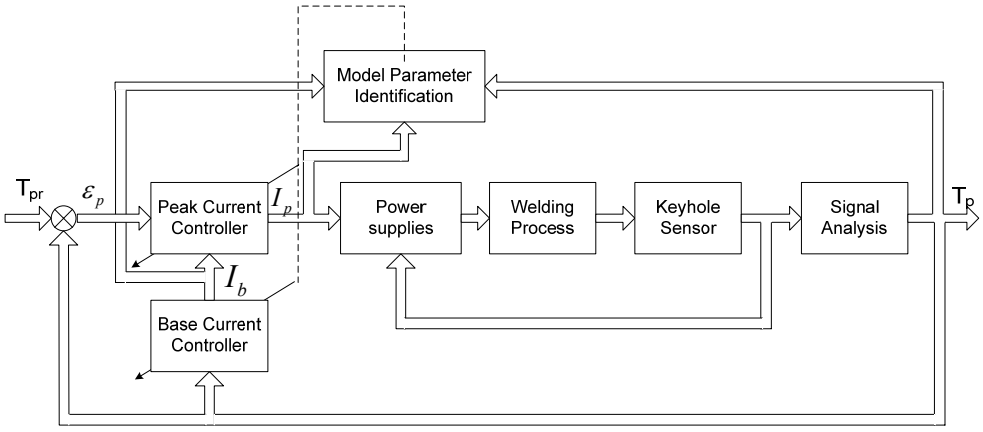

Figure 8-1 Optimization Control System

In order to optimize the heat input by adjusting base current, I_b is introduced into the linear model as shown in Eq.8-1.

$$T_p(k) = \sum_{i=1}^{2} a_i T_p(k-i) + \sum_{i=0}^{2} b_i I_p(k-i) + \sum_{i=1}^{n_c} c_i I_b(k-i) + \zeta \qquad \text{(Eq.8-1)}$$

The orders of the T_p and I_p have been determined and introduced in Chapter 6, in order to determine n_c, the order of I_b, an open-loop experiment has been conducted, in which with the other parameters remaining constant, the base current is switched from 35A to 65A. The corresponding change of peak current is shown in Figure 8-2, in which T_p begins to fall when the I_b is stepped up, but goes to a stable state again after three cycles. This means that I_b in the first three cycles has a small effect on the

current instant T_p and the order of I_b can be selected $n_c = 3$.

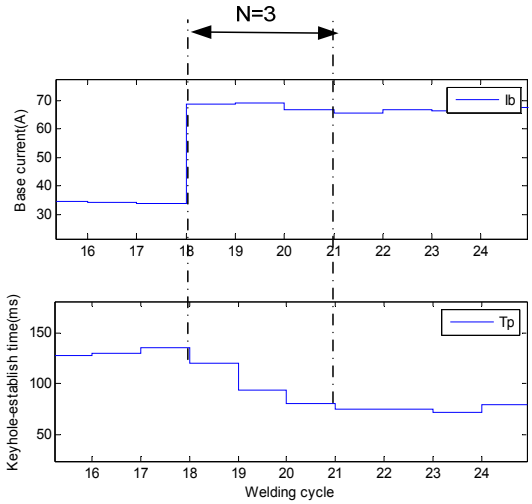

Figure 8-2 T_p response to I_b

8.2 Base Current Algorithm

In the welding process, the heat input in unit length can be calculated by

$$Q = \eta IU / V \qquad \text{(Eq.8-2)}$$

where Q stands for the heat input to the workpiece in unit length, subsequently referred to as heat input in this dissertation; I is the welding current, U is the welding voltage, V is welding velocity and η is heat efficiency [14].

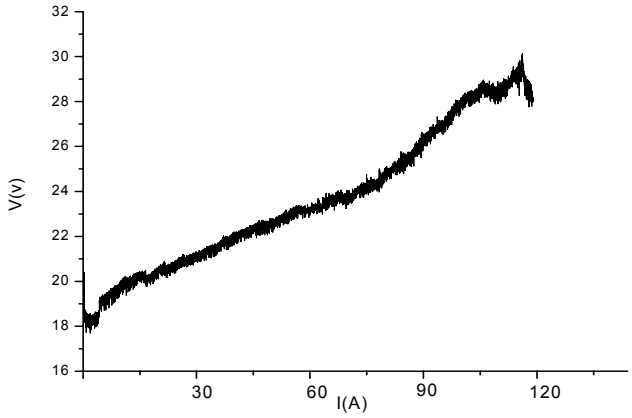

Figure 8-3 Plot of arc voltage and current

In order to get the relationship between the arc voltage and arc amperage, one open–loop experiment was conducted. In this experiment, one hot rolled steel pipe with 6"ID, schedule 40 and 0.28" wall thickness was welded with continually increased plasma arc, and the measured arc voltage and amperage were recorded to find their relationship. The reason of using the thick wall pipe is that the heat can disperse in the pipe faster than in a thin wall pipe, thus it can withstand the higher arc current than thin wall pipe before the weld pool is sunken, which increases the arc length. In this experiment, the distance between the torch and the pipe is kept at 5 mm and the torch moving speed is 4 mm/s. Figure 8-2 shows the curve of the arc voltage (y axis) vs. arc current (x axis) when the arc current linearly increased from 0A to 120A. From the result, it can be found that, with the same arc length, the relationship between the output voltage and output current of the power supply in the constant arc length is an approximately linear slope. The slope ratio of the V-I curve $r = \Delta V / \Delta I$ is almost constant for $I < 90A$. The small increase of *R* when $I > 90A$ is caused by the weld pool, where the metal is melted and blown away by the plasma arc resulting the arc length increases, and as the result, increases the voltage between the ends of the arc. The relationship between arc voltage and current can be expressed as $V = rI + m$ where *r* is the slope ratio of I-V curve, $r = \Delta V / \Delta I$, depicted in Figure 8-3, $r = 0.078$, and *m* is intercept on V-axis, i.e. the voltage when *I* tends to zero.

Based on Eq.8-2, the heat input in T_p and in T_b can be respectively calculated as

$$\begin{aligned} Q_p &= \eta_p I_p(k) U_p(k) / V_p(k) = \eta_p I_p(k)(rI_p(k) + m) / V_p(k) \\ Q_b &= \eta_b I_b(k) U_b(k) / V_b(k) \ = \eta_b I_b(k)(rI_b(k) + m) / V_b(k) \end{aligned} \qquad \text{(Eq.8-3)}$$

Since in the weld process, the heat input per unit length in one weld cycle can be expressed as the sum of the heat input during T_b and T_p:

$$Q = \frac{\left(\dfrac{\eta I_p(k)(rI_p(k) + m) T_p(k)}{V_p(k)} + \dfrac{\eta I_b(k)(rI_b(k) + m) T_b(k)}{V_b(k)} \right)}{\left(T_p(k) + T_b(k) \right)} \qquad \text{(Eq.8-4)}$$

Since the weld speed during T_b and T_p is same, the heat input for optimization can be expressed in Eq.8-5:

$$Q = \frac{\eta}{\left(T_p(k)+T_b(k)\right)V}\left(I_p(k)(rI_p(k)+m)T_p(k)+I_b(k)(rI_b(k)+m)T_b(k)\right)$$
$$= \frac{\eta}{\left(T_p(k)+T_b(k)\right)V}\left((rI_p{}^2(k)+mI_p)T_p(k)+(rI_b{}^2(k)+mI_b(k))T_b(k)\right) \quad \text{(Eq.8-5)}$$

In the PKW, when the system is in a steady state, the output and input of the system should be maintained constant, thus $T_p(k) = T_p(k-1) = T_p(k-2)$, $I_p(k) = I_p(k-1) = I_p(k-2)$, $I_b(k-1) = I_b(k-2) = I_b(k-3)$ and the model in the steady state can be expressed as given by Eq.8-6:

$$T_p = \left(\sum_{i=1}^{2} a_i\right)T_p + \left(\sum_{i=0}^{2} b_i\right)I_p + \left(\sum_{i=1}^{3} c_i\right)I_b + \zeta \quad \text{(Eq.8-6)}$$

The peak current in the steady state is given by Eq.8-7 and the differential of peak current with respect to the base current can be calculated using Eq.8-8.

$$I_p = \frac{1}{\sum_{i=0}^{2} b_i}\left(\left(1-\sum_{i=1}^{2} a_i\right)T_p - \sum_{i=1}^{3} c_i I_b - \zeta\right) \quad \text{(Eq.8-7)}$$

$$\frac{\partial I_p}{\partial I_b} = -\sum_{i=1}^{3} c_i I_b \Big/ \sum_{i=0}^{2} b_i \quad \text{(Eq.8-8)}$$

From the Eq.8-5, the differential of heat input with respect to base current can be calculated using Eq.8-9

$$\frac{dQ}{dI_b} = \frac{\eta}{\left(T_p+T_b\right)V}\left((2rI_p\frac{dI_p}{dI_b}+m\frac{dI_p}{dI_b})T_p+(2rI_b+m)T_b\right) \quad \text{(Eq.8-9)}$$

In order to find the optimized I_b minimizing the Q,

Eq.8-7 and Eq.8-8 are input into Eq.8-9, which is then equated to zero.

$$\frac{dQ}{dI_b} = 0 \quad \Rightarrow$$

$$I_b = \frac{1}{2r\left(\frac{C^2}{B}T_p + BT_b\right)}\left\{\frac{2rT_pC\left[(1-A)T_p - \zeta\right]}{B} + mT_pC - mBT_b\right\} \qquad \text{(Eq.8-10)}$$

where $A = \sum_{i=1}^{2} a_i$, $B = \sum_{i=0}^{2} b_i$, $C = \sum_{i=1}^{3} c_i$

In order to ensure the optimized I_b is feasible in the control system, the restriction conditions are necessary. Before the calculated I_b is used in the peak current controller, two types of restriction are applied, the range and the differential restrictions.

To ensure the keyhole can be filled during the T_b, I_b cannot too be high, in order to prevent the undercut or even a burn-through. To this end, an upper limit is added as $I_b < 65A$.

The purpose of the differential restriction is to prevent the instability caused by the fast variation of I_b. In the experiment, the difference of I_b between the adjacent cycles cannot exceed 10A: $\left|I_b(k) - I_b(k-1)\right| < 10A$

After I_b is obtained from the above calculation, the linear MPC, introduced in Chapter 7 can be called to calculate the peak current I_p to realize the optimization control of the weld process.

8.3 Experimental Results

To verify the optimization performance designed above, the following experiment was conducted on the A36 steel pipe with 5"ID and 0.134" wall thickness. The parameters are given in Table 5-3. In this experiment, the optimal algorithm was disabled at the beginning and the initial I_b was set to be constant (5A). In the middle of the experiment (40th cycle), the optimal algorithm was enabled to determine the optimal I_b that minimizes the cost function. As can be observed from the result

shown in Figure 8-4, I_b increased to around 40A and the I_p reduced from 210A to 150A, and T_p was kept around 100ms. The output power of power supply $J = UI$ was decreased from around 80×10^2 W to around 50×10^2 W by the optimal control. Since weld speed V and heat efficiency is constant, the heat input Q is decreased by the optimization controller. When I_b is adjusted by the controller, the oscillation of T_p increases significantly and when I_b becomes stable, T_p converges to the reference output again.

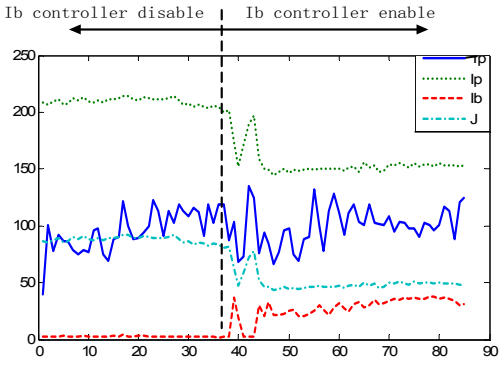

Figure 8-4 Optimal output results

CHAPTER 9 Double-Sided Arc Welding

Although the experiments above have proved the performance of the proposed QKPAW system, most of them are conducted in plasma keyhole welding mode using the steel pipe with 0.13" pipe wall. Since the quasi-keyhole welding includes the double-sided arc welding, in this chapter, the designed system works under double-sided arc welding mode to verify the performance of the system.

Because DSAW is performed on a thick workpiece weld, the DSAW experiments in this chapter are conducted on the 6" ID, schedule 40 carbon steel pipes with 0.256" pipe wall. The process is modeled and controlled with the similar method to that introduced in previous chapters.

To switch the QKPAW system from the keyhole PAW mode to DSAW mode, the keyhole sensor electrode is used to work as the backside electrode to provide the double-side arc current as well as to monitor the establishment of the keyhole in DSAW. This transformation can be realized by the software and does not require any changes in the hardware, previously mentioned as one advantage of the designed QKPAW.

9.1 Process Parameters

To check the robustness of the controller, in these thick pipes weld experiments, the 6"ID schedule 40 carbon steel pipes with 0.256 inch thickness are welded, and the process parameters, selected from repeating open-loop experiments are described in Table 9.1.

9.2 Determination of Order

Similar to the order determination of 0.13" thick pipe, the structures of the model are developed from Eq. 5-7. In the open-loop experiment, the peak current stepped down from 175A to 140 A in the middle of the process. Figure 9-1 shows the step signal and experimentally measured T_P, where T_P became stable after two weld cycles. On the bases of the open-loop experiment results, the model order, predictive horizon and control horizon are selected as 2, 3 and 3 respectively.

Table 9-1 Process parameters in DSAW

Pipe wall thickness	0.256 inch
Pipe length	3 inch
Pipe inner Diameter	6 inch
Orifice diameter	2.6 mm
Plasma gas	Pure argon
Shielding gas	Pure argon
Inner Shielding gas	Pure argon
Plasma gas flow	4 L/Min
Shielding gas flow	20 L/Min
Double-side current I_d	40 A
Base current time	400 ms
Peak current delay T_{pd}	30 ms
Arc gap T_g	30 ms
Welding speed	1 mm/s
Retraction of tungsten	1.5mm

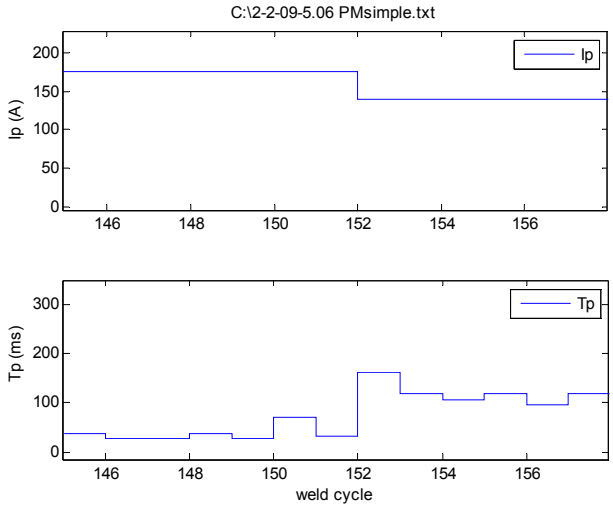

Figure 9-1 T_p response to the peak current

The model used in the thick pipe DSAW is selected with a second-order linear model evolved from Eq.5-12. As Eq.10-1 shows, the base current I_b in the Eq.5-12 is replaced by double-side arc current I_d.

$$T_p(k) = \sum_{i=1}^{2} a_i T_p(k-i) + \sum_{i=0}^{2} b_i I_p(k-i) + \sum_{i=1}^{2} c_i I_d(k-i) + e \qquad \text{(Eq.9-1)}$$

Since the double-side arc current I_d is a constant in the normal DSAW, the third item in the right side of Eq.9-1, $\sum_{i=1}^{2} c_i I_d(k-i)$, can be treated as a constant, as a result, Eq.9-1 can be rewritten as Eq.9-2:

$$T_p(k) = \sum_{i=1}^{2} a_i T_p(k-i) + \sum_{i=0}^{2} b_i I_p(k-i) + \zeta \qquad \text{(Eq.9-2)}$$

9.3 Coefficient Identification

Similar to the coefficients identification process in thin pipe weld, the coefficients of the thick pipe QKAPW are identified with LSA. Since I_b is a constant and I_p is the only variable controlling the T_p, in this experiment, the base current is set to a constant 20A, and I_d = 45A.

In the identification, the excitation signals are selected as PRMS with r = 5. The

amplitude of the PRMS control signal is 1 and it is shifted with offset 5.75V before being sent to the power supply. Figure 9-2 shows the PRMS, (a) shows the control signal changed between 5.25V and 6.25V, and (b) shows, under the control signal, the experimentally measured output peak current I_p. The peak current changed between 170A and 220A. Using the current sensor designed as described in the last chapter, with 1ms sample period, the current wave can be measured as shown in Figure 9-3 (a). After the signal process, the output and the input signal used to identify the model can be obtained, as shown in Figure 9-3 (b).

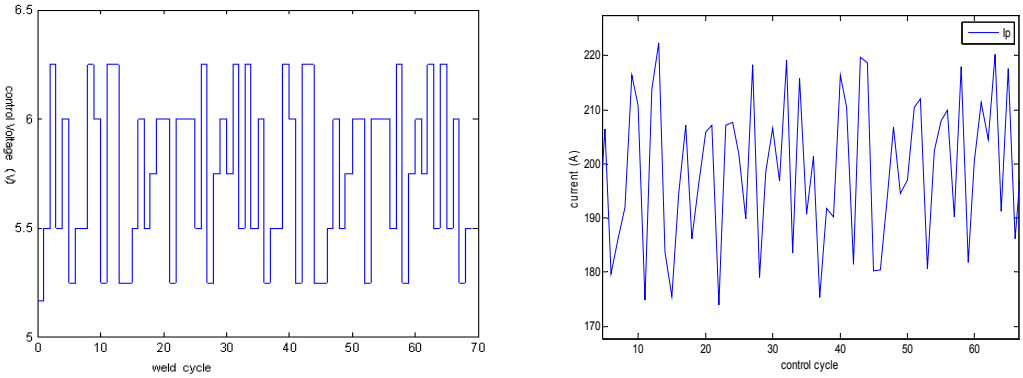

(a) PRMS for identification (b) Measured peak current

Figure 9-2 PRMS in thick pipe weld

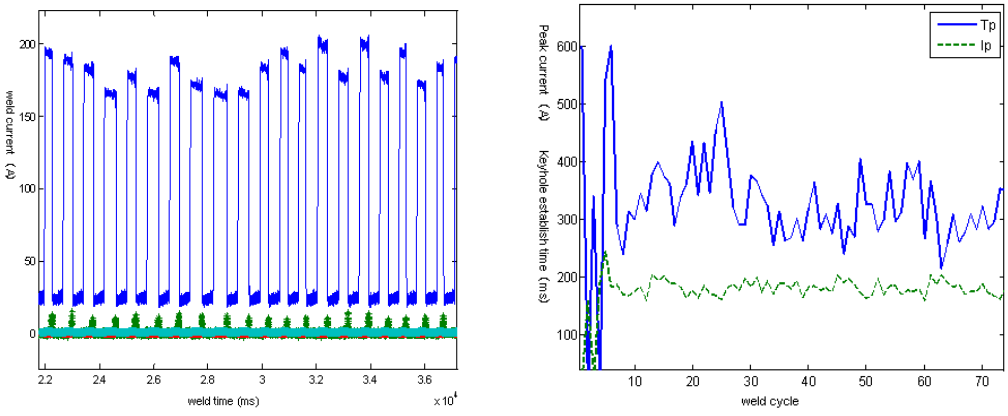

(a) Current wave measured in experiment (b) Input and output measured in experiments

Figure 9-3 PRMS in thick pipe weld

The second-order linear model and bilinear model are chosen as Eq.9-3 and

Eq.9-4:

$$T_p(k) = \sum_{i=1}^{2} a_i T_p(k-i) + \sum_{i=0}^{2} b_i I_p(k-i) + \zeta \quad \text{(Eq.9-3)}$$

$$T_p(k) = \sum_{i=1}^{2} a_i T_p(k-i) + \sum_{i=1}^{2} b_i T_p(k-i) I_p(k-i) + \sum_{i=0}^{2} c_i I_p(k-i) + \zeta \quad \text{(Eq.9-4)}$$

For linear model Eq.9-3, with LSA, the model coefficients are identified as:

$a_1 = 0.2564, a_2 = 0.4815, b_1 = -0.1191, b_2 = 0.0128, b_3 = 0.0581, \zeta = 0.3452$.

As a result, the second-order linear model is expressed as:

$$\begin{aligned} T_p(k) &= 0.2564 T_p(k-1) + 0.4815 T_p(k-2) - 0.1191 I_p(k) \\ &\quad + 0.0128 I_p(k-1) + 0.0581 I_p(k-2) + 0.3452 \end{aligned} \quad \text{(Eq.9-5)}$$

For the bilinear model, the model coefficients are identified as:

$$a_1 = 1.1242, a_2 = 0.4011, b_1 = -0.1521, b_2 = 0.0165, c_0 = -0.1223, c_1 = 0.0558,$$
$$c_2 = 0.0512, \zeta = 0.1523$$

Thus the second-order bilinear model can be expressed as:

$$\begin{aligned} T_p(k) &= 1.1242 T_p(k-1) + 0.4011 T_p(k-2) - 0.1521 T_p(k-1) I_p(k-1) \\ &\quad + 0.0165 T_p(k-2) I_p(k-2) - 0.1223 I_p(k) + 0.0588 I_p(k-1) \\ &\quad + 0.0512 I_p(k-2) + 0.1523 \end{aligned} \quad \text{(Eq.9-6)}$$

To check the performance of the identified models, in this subsection, the models are validated by both graphical analysis and quantitative analysis method; where using identified coefficients and the selected model structure, the simulation outputs are calculated by inputting the given data sequence.

To compare the linear and bilinear model results, the validation is divided into two steps, in which two types of data sequence are used to check the performance of the two models, introduced as below.

In the first step, the same input data sequence used in the identification is input to the model to get the simulation output. Figure 9-4 shows the comparison of simulation output and measured output results, (a) is the simulation result of the bilinear model

Eq.9-6, and (b) shows the simulation result of the linear model Eq.9-5.

In the residuals analysis, in order to avoid the error arising from the beginning of several weld cycles, unstable in the beginning of the process, the sum of squared errors is calculated between the 10^{th} and the 60^{th} weld cycle. For the bilinear model, *SSerr*=0.0449, whilst for the linear model, with the same condition *SSerr* is calculated as *SSerr*=0.0456. In this respect, there is no significant difference between the linear and bilinear model.

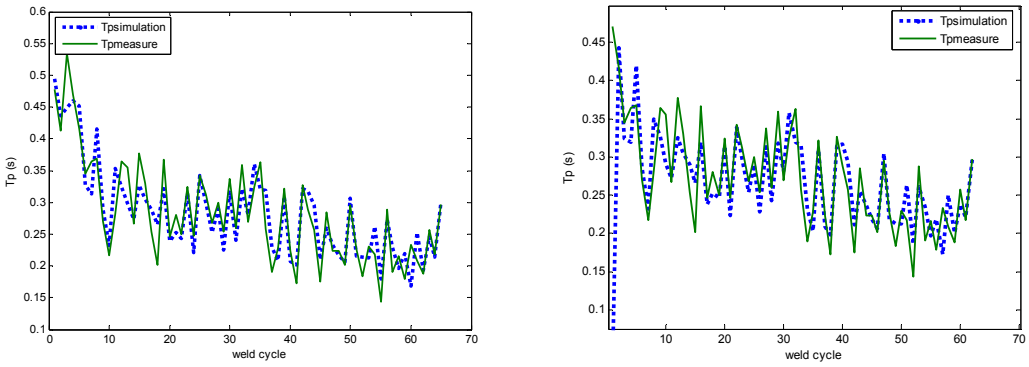

(a) Bilinear model result (b) Linear model result

Figure 9-4 Simulation result with identification input data sequence

In the close-loop experiment, the bilinear model is used in the bilinear MPC to control the peak current time in the DSAW process. The coefficients are revised online with RLS and their initial values are the coefficients identified off-line in the experiment above.

9.4 Verification of Experiments

To verify the performance of QKPAW system in the DSAW mode, the following experiments were conducted to track reference outputs in the bead on pipe weld. Since the welded pipe has different size to those in the previous experiment, the process parameters are required for the DSAW experiment. Based on the open-loop experiments, the process parameters in Table 9-1 are used.

The first experiment was designed to track the constant output, T_r=200ms. Figure

9-5 shows the current wave form measured in the experiment. After signal processing, the controlled peak current and the output peak current time are obtained as shown in Figure 9-6. The oscillation of the peak current time is larger than in the plasma keyhole weld mode for the thin workpiece weld. This is caused by the thick workpiece characteristic in which the weld pool is larger when the thickness of the welded workpiece increases. Since the fluctuation of the weld pool fluid becomes stronger with the increase of its size, the stability of T_p is worse than in the thinner workpiece weld, but in the weld result, the average T_p is well maintained around reference time 200ms, verifying the performance of the control system.

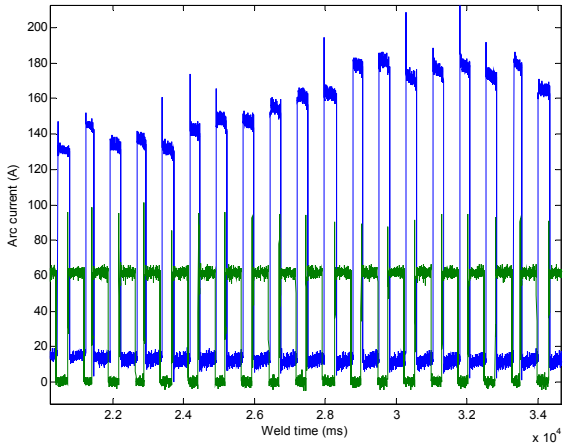

Figure 9-5 Current wave of DSAW

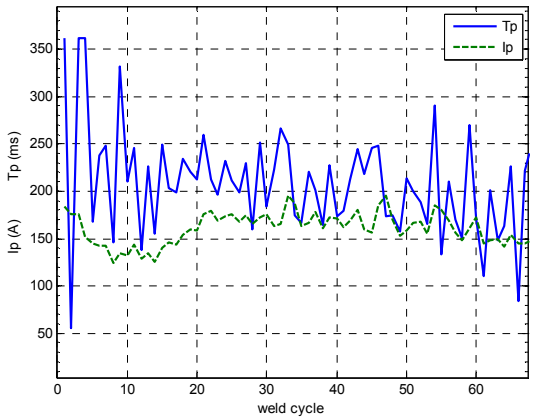

Figure 9-6 Peak current and peak current time in the DSAW

Figure 9-7 shows the welded seam as the weld result, in which (a) is the outside surface and (b) is the inside surface of the weld line.

To test the system adaptive performance , in the second experiment, the weld speed was switched from 1mm/s to 0.5 mm/s during the experiment (30^{th} weld cycle) and Figure10-8 shows the change of I_p and T_p measured in the experiment. When the speed is reduced, the temperature around the point where keyhole is established is higher and the keyhole is easily opened. As a result, T_p drops when the speed is reduced, but under the control, it follows the reference output after several weld cycles due to the decrease of peak current, which is controlled by the controller.

(a) Outside of the welded line

(b) Inside of the welded line

Figure 9-7 Weld result of DSAW

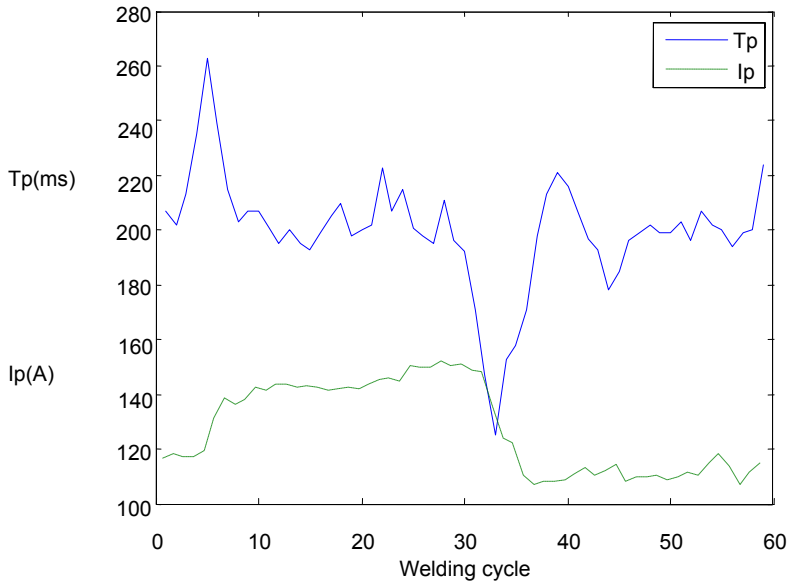

Figure 9-8 Experiment with speed change

To test the system robustness, in the third experiment, the welded pipe was ground before the experiment; Figure 9-9 shows the ground pipe surface. The depth of the ground area is around 0.1", implying that the smallest thickness of the weld area is around 0.16". Figure 9-10 shows T_p and I_p change when the weld pool goes through the grooved area. When the pipe wall thickness is reduced, the keyhole is easily opened, thus T_p begins to decrease and the controller reduces the peak current to prevent the T_p from diverging away from T_{pr}. On the other hand, when the pipe wall thickness increases, the peak current is enhanced by the controller to force the keyhole establishment, hence the time stays around T_{pr}.

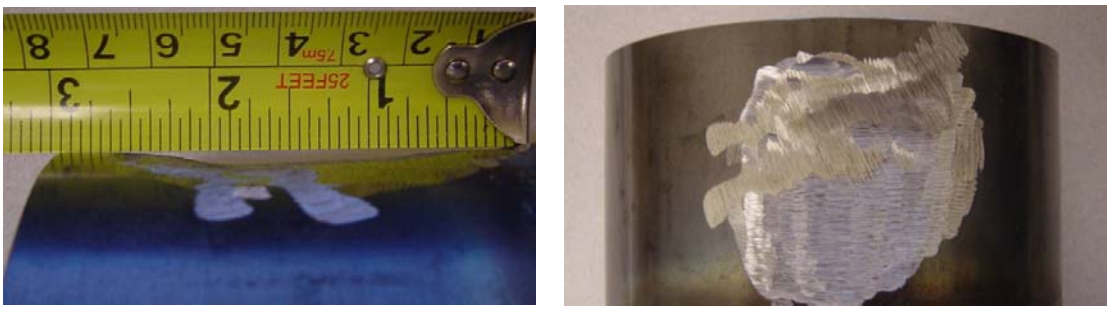

Figure 9-9 Grooved pipe before weld

Figure 9-11 (a) and (b) show the weld result in the experiment, which shows that even when the thickness of the welded pipe wall was reduced to 2/3 of original thickness, the weld result was still well maintained, as T_p is well controlled in the process.

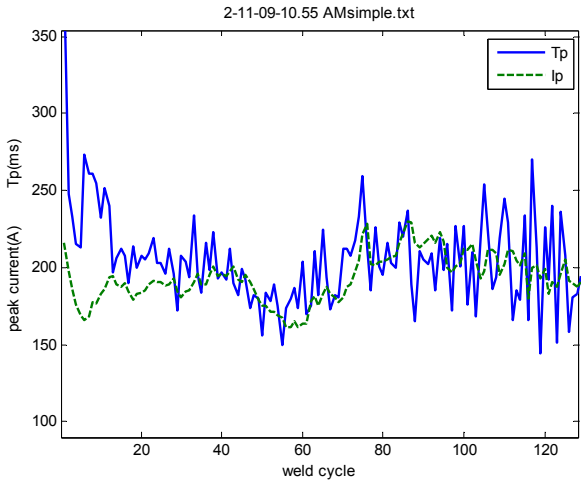

Figure 9-10 Peak current and peak current time

(a) Weld result (outer surface)

(b) Weld result (inner surface)

Figure 9-11 Experimental result with thickness change

From the experiments above, the proposed QKAPW can be used in double-sided arc welding mode and satisfying control results can be achieved in these experiments. When the working conditions are changed, such as varying the weld speed and the welded pipe thickness during the process, the control system can adequately maintain the keyhole-establish time to tracking the reference output set by operator.

CHAPTER 10 Conclusion and Future Work

10.1 Conclusion

Welding, especially pipe welding is a labor-intensive job when performed in a manual control mode. Automated orbital arc pipe weld system, where the torch is fixed on a computer controlled weld head and moved on an orbit around the motionless welded pipes, is a labor intensity reducing and productivity enhancing solution in the pipe welding.

The Quasi-keyhole welding, comprised of the plasma keyhole and the double-sided arc welding, is a special plasma welding mode. It uses a recessed electrode to reduce the arc dispersion and achieve concentrated plasma energy to establish the keyhole on the welded workpiece. After the keyhole is confirmed, the arc current is switched off letting the melted metal to fill the keyhole and solidify in it to produce the weld. It has many advantages compared to other arc welding methods in respect of weld quality and cost.

In this dissertation, a new automation orbital keyhole pipe weld system is proposed, including the system integration and the control algorithm, to realize the automation orbital pipe weld. The contents of the thesis are arranged as follows: In the first part, the relevant background and knowledge is introduced (Chapters 2 and 3), followed by the integration of the QKPAW system (Chapter 4). The system modeling and simulation (Chapter 5), the linear MPC algorithm and system control (Chapter 6), the Bilinear MPC (Chapter 7), the control process optimization (Chapter 8) and the double-sided arc mode control experiment (Chapter 9) are subsequently covered.

The main achievements and contributions of this research study are summarized as follows:

1. A novel design of a QKPAW system for the automation orbital pipe weld.

This QKPAW system can work in two keyhole weld modes: plasma keyhole weld mode and double-sided arc welding mode, without hardware modification, and both weld performances are verified in experiments introduced in the thesis. In practical application, the weld operator can change the weld mode by modifying parameters of the program.

2. Model of the QKPAW process with arc current amperage and keyhole establish-time is developed. Based on the model, MPC algorithm is designed to control the weld process peak current time to improve the weld process, and experiments are conducted to verify the control system performance.
3. Bilinear MPC algorithm based on the bilinear model of QKPAW process is proposed. Although this algorithm is based on the QKPAW MPC research, its use is not limited to the QKPAW control. It can be applied to other short horizon bilinear MPC problems.
4. On the basis of the QKPAW system MPC controller, an optimization strategy is proposed to decrease the energy of the plasma arc created by power supplies in the weld process. Since this energy directly affects the heat input to the weld workpiece, the optimization might reduce the heat input to the workpiece and improve the strength of the welded area.

10.2 Future Work

Although the QKPAW system was proved to obtain satisfactory weld results in the experiments introduced above, it was validated in the laboratory environment, set up for research purposes. To enable practical application of this research in industry field welding, further work is needed to improve the system performance and simplify the system structure, including:

1. New rear electrode development.

   The rear electrode, in the current QKPAW system, is a water-cooled

copper pipe held by the axis in centric position of the welded pipe, and its length is three inches. In practical pipe welding in the field, the welded pipe is usually too long to insert a centric axis to the weld area. Another disadvantage preventing the practical implementation of this approach is that the rear protective gas is supplied from one end of the pipe and the other end is plugged up, which is also unpractical in the field pipe welding. To overcome this issue, a new rear electrode needs to be developed before applying QKPAW in industry.

2. Embedded controller development

In the current QKPAW system, the controller is realized by a real-time target PC. It has many advantages in the laboratory environment, such as lower real-time control system cost, excellent extending potential and ease of programming complex algorithms and program debugging , but its short-comings are also obvious: The big size of the controller, the poor anti-interference performance and the potential damage of the PC based controller in the hostile environment in the field operation. To enable practical system application, a reliable controller is necessary in the industry application. One proposed design is using an embedded controller such as digital signal processor (DSP) or Microcomputer combined with control panel as the human machine interface (HMI) terminal. The controller can be placed inside the power supply and parameters can be input from the control panel.

3. System simplification

The industry application needs a simple and reliable system, in the proposed QKPAW, three power supplies are used to supply pilot arc, main current (peak current and base current) and double-side current. The pilot arc power supply can be removed if a special plasma power supply providing the

pilot arc as well as main arc is used as the main power supply. The main arc and the double-side arc might be supplied by one power source if a sensor and high speed switch circuit are designed and used in the system, as shown in Figure 10-1, in which the high speed switch might be realized by the insulated-gate bipolar transistor (IGBT). After these improvements, the system can be significantly simplified with only one power supply.

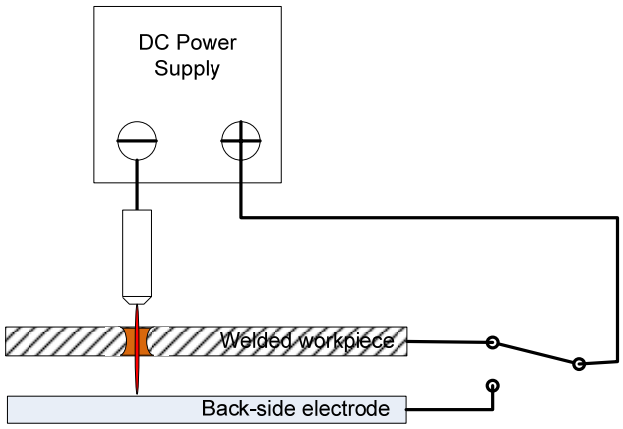

Figure 10-1 Single power supply DSAW system structure

4. Model and control algorithm research

The welding system is a complex system and many factors can affect the weld result, such as the weld speed and base current time. In this dissertation, they are set to constants, but they might be adjusted, as in the manual welding, in the weld process to improve the weld quality. So the model of the process, especially the multi-input/multi-output model and corresponding controller might be the important aspect in the future research.

REFERENCE

1. American Welding Society, *Welding Handbook*, Vol.2, 1990, Miami, USA.

2. Y. M. Zhang and S. B. Zhang, "*Method of arc welding using dual serial opposed torches",* U.S. Patent, 1999.

3. Y. M. Zhang and Y. C. Liu, "*Modeling and control of quasi-keyhole arc welding process",* Control Engineering Practice, 2003, **11**(12): p. 1401-1411.

4. Y. M. Zhang, S. B. Zhang and M. Jia, "*Sensing and control of double-sided arc welding",* Journal of Manufacturing Science and Engineering, 2002, **124**: p. 695-701.

5. W. Lu, Y. M. Zhang and W. Y. Lin, "*Nonlinear interval model control of quasi-keyhole arc welding process",* Automatica, 2004, **40**: p. 805-813.

6. Y. M. Zhang and Y. C. Liu, "*Control of dynamic keyhole welding process",* Automatica, 2007, **43**: p. 876-884.

7. J. C. Allwright and G. C. Papasiliow, "*On-linear programming and robust model-predictive control using impulse-responses",*Systems and Control Letters, 1992. **18**: p. 159-164.

8. Y. M. Zhang and R. Kovacevic, "*Robust control of interval plants: A time domain method",* IEE Process Control Theory Application, 1997, **144**(4): p. 347-353.

9. Y. M. Zhang, S. B. Zhang and M. Jia, "*Keyhole double-sided arc welding process",* Welding Journal, 2002, **81**(11): p. 28-255.

10. E. Craig, "*The plasma arc process-A review",* Welding Journal, 1988, **67**(2): p. 19-26.

11. http://en.wikipedia.org/wiki/Gas_metal_arc_welding

12. H. B. Cary and S. C. Helzer, *Modern Welding Technology*, 2005, NJ: Pearson Education.

13. http://en.wikipedia.org/wiki/Gas_tungsten_arc_welding

14. K. Weman, *Welding Processes Handbook*, 1st Edition, 2003, CRC Press.

15. http://en.wikipedia.org/wiki/Plasma_arc_welding

16. Y. M. Zhang, W. Lu and Y. C. Liu, "*Guided arc enhances GTAW*", Welding Journal, 2003: 82 (12), p. 40-45.

17. Y. M. Zhang and Y. C. Liu, "*Modeling and control of quasi-keyhole arc welding process",* Control Engineering Practice, 2003, **11**: p. 1401–1411.

18. H. Rampaul, *Pipe welding procedures*, 2nd Edition, 2003, Industrial Press.

19. S. J. Qin and T. A. Badgwell, "*An overview of nonlinear model predictive control applications"*, In IFAC Workshop on Nonlinear Model Predictive Control, Assessment and Future Directions, 1998, Ascona (Switzerland).

20. E. S. Meadows and J. B. Rawlings, *Model Predictive Control*, 1997, NJ: Prentice Hall.

21. M. A. Henson, "*Nonlinear model predictive control: current status and future directions",* Computers and Chemical Engineering, 1998, **23**: p. 187-202.

22. R. K. Pearson, *Discrete-time Dynamic Models*. 1999: Oxford University Press.

23. J. A. Rossiter, *Model-based Predictive Control,* 2003, London: CRC Press.

24. A. Janczak, *Identification of Nonlinear Systems Using Neural Networks and Polynomial Models*, 2005: Springer.

25. S. Boyed and L. O. Chua, "*Fading memory and the problem of approximating nonlinear operations with Volterra series",* IEEE Transactions on Circuits and Systems, 1985, **32**: p. 1150-1161.

26. Yeong K. Yeo and Dennis C. Williams, "*Bilinear model predictive control",* Industrial & Engineering Chemistry Research, 1987, **26**(11): p. 2267-2274.

27. A. A. Al-zahrani and M. M. Noorwali, "*An adaptive bilinear model-predictive control algorithm for a plate heat exchanger*", Developments in Chemical

Engineering and Mineral Processing, 1994, **2**(2-3): p. 158-170.

28. D. W. Clarke, C. Mohtadi and P. S. Tuffs, "*Generalized predictive control-part I: The basic algorithm*", Automatica, 1987, **23**(2): p. 137-148.

29. B. D. O. Anderson and J. B. Moore, *Optimal Control,* 1990: Prentic-Hall.

30. A. Bemporad, F. Borrelli and M. Morari, "*Model predictive control based on linear programming—the explicit solution*", IEEE Transaction on Automatic Control, 2002, **47**(12): p. 1974-1985.

31. D.Q. Mayne, J.B. Rawlings, C.V Rao and P.O.M Scokaert, "*Constrained model predictive control: Stability and optimality",* Automatica, 2000, **36**: p. 789-814.

32. S. N. Huang, K. K. Tan and T. H. Lee, *Applied Predictive Control-Advances in Industrial Control*, 2002, London: Springer.

33. M. Morairi and J. Lee, "*Model predictive control: past, present and future",* Computers and Chemical Engineering, 1999, **23**(4-5): p. 667-682.

34. D. W. Clarke, C. Mohtadi and P. S. Tuffs, "*Generalized predictive control-I: The basic algorithm",* Automatica, 1987, **23**: p. 137-148.

35. D. W. Clarke, C. Mohtadi and P. S. Tuffs, "*Generalized predictive control-II: Extensions and interpretations*", Automatica, 1987, **23**: p. 149-160.

36. J. Richalet, A. Rault, J. I. Testod, and J. Paon, "*Model predictive heuristic control: Applications to industrial processes",* Automatica, 1978, **14**: p. 413-428.

37. C. R. Cutler and B. L. Ramaker, "*Dynamic matrix control-A computer control algorithm",* Proc Joint Automatic control Conf, 1980.

38. R. M. C. De Keyser and A.R. Van Cuawenberghe, "*Extended prediction self-adaptive control", IFAC Symposium on Identification and System Parameter Estimation*, 1985, York, UK.

39. S. Joe Qin, Thomas A. Badgwell, "*An overview of industrial model predictive control technology",* Control Engineering Practice, 2003. **11**(7): p. 733-764.

40. D. Shu, *Predictive Control System and Application*, 1996, Beijing: Mechanical industry.

41. T. A. Badgwell and S. J. Qin, "*Nonlinear predictive control, chapter review of nonlinear model predictive control applications",* IEE Control Engineering series, 2001.

42. K. S. Narendra and K. Parthasarathy, "*Identification and control of dynamical systems using neural networks",* IEEE Transactions on Neural Networks, 1990, **1**: p. 4-27.

43. Y. L. Huang, H. Lou, J.P. Gong and T. F. Edgar, "*Fuzzy Model Predictive Control",* IEEE Transactions on Fuzzy System, 2000, **8**(6): p. 665-679.

44. S. Sastry, *Nonlinear Systems: Analysis, Stability and Control*, 1999, New York: Springer.

45. J. B. Rawlings and K. R. Muske, "*The stability of constrained multivariable receding horizon control",* IEEE Transactions on automatic control, 1993, **38**: p. 1512-1520.

46. M. V. Kothare, V. Balakrishanan and M. Morari, "*Robust constrained model predictive control using linear matrix inequalities",* Automatica, 1996, **32**: p. 1361-1379.

47. S. S. Keerhi and E. G. Gilbert, "*Optimal infinite-horizon feedback laws for a general class of constrained discrete-time systems: Stability and moving-horizon approximation",* Journal of Optimization Theory and Application 1988, **57**: p. 265-293.

48. E. S. Meadows, M. A. Henson, J. W. Eaton and J. B. Rawlings, "*Receding horizon control and discontinuous state feedback stabilization",* International Journal of Control 1995, **61**: p. 1217-1229.

49. E. Polak and T. H. Yang, "*Robust receding horizon control of linear systems with input saturation and plant uncertainty",* International Journal of Control, 1993, **58**: p. 613-663.

50. S. Kanev and M. Verhaegena, "*Robustly asymptotically stable finite-horizon MPC",* Automatica, 2006, **42**: p. 2189-2194.

51. D. Limon, T. Alamo, F. Salas and E. F. Camacho, "*On the stability of constrained MPC without terminal constraint",* IEEE Transactions on automatic control, 2006, **51**(5): p. 832-843.

52. H. Michalska and D. Q. Mayne, "*Robust receding horizon control of constrained nonlinear systems",* IEEE Transaction on Automatic Control, 1993, **38**: p. 1623-1633.

53. A. Bemporad, L. Chisci, and E. Mosca, "*On the stabilizing property of SIORHC",* Automatica, 1994, **30**(12): p. 2013-2015.

54. K. Qian and Y. M. Zhang, "*Optimal model predictive control of plasma pipe welding process"*, in 4th IEEE Conference on Automation Science and Engineering, 2008, Key Bridge Marriott, Washington DC, USA.

55. http://www.millerwelds.com/products/tig/dynasty_350/

56. http://www.sti.nasa.gov/tto/spinoff1996/66.html

57. P. Li, and Y. M. Zhang, "*Analysis of arc light mechanism and its application in sensing of GTAW Process",* Welding Journal, 2000, **79**(9): p. 252-260.

58. W. Chen and B. A. Chin, "*Monitoring joint penetration using infrared sensing techniques",* Welding Journal, 1990, **69**(4): p. 181-185.

59. P. Banerjee, "*Infrared sensing for on-line weld geometry monitoring and control",* ASMW Journal of Engineering for Industry, 1995, **117**(3): p. 323-330.

60. Y. H. Xiao and O. G. Den, "*Weld pool oscillation during GTA welding of mild steel",* Welding journal Welding Research Supplement, 1993, **72**(2): p. 428-434.

61. D. Hardt, and J. Katz, "*Ultrasonic measurement of weld penetration",* Welding journal Welding Research Supplement, 1988, **67**(11): p. 239-246.

62. Y. M. Zhang and S. B. Zhang and Y. C. Liu, "*Plasma cloud charge sensor for pulse keyhole process control",* Measurement Science and Process Control, 2001, **12**(8): p. 1365-1370.

63. B. E. Losch and Y. M. Zhang, "*Fuzzy classification of plasma reflection for keyhole sensing and control"*, In Proceedings of the 2002 IEEE International Conference on Control Applications, 2002: Glasgow, Scotland, U.K.

64. Y. M. Zhang and S. B. Zhang, "*Efflux plasma charge based sensing and control of joint penetration during keyhole plasma arc welding",* Welding Journal, 2001. **80**(7): p. 157-162.

65. W. Lu, "*Robust sensing and control of weld pool surface in gas tungsten arc welding and its modifications"*, in *College of Engineering*, 2004, University of Kentucky: lexington.

66. http://sine.ni.com/nips/cds/view/p/lang/en/nid/13742

67. http://www.ni.com/pdf/products/us/20044546301101dlr.pdf

68. L. Ljung, *System Identification — Theory for the User,* 2nd Edition, 1999, Upper Saddle River N.J: Prentice Hall.

69. J. Richalet, A. Rault, J. I. Testod, and J. Paon, "*Model predictive heuristic control: Applications to industrial processes",* Automatica, 1978, **14**: p. 413-428.

70. C. R. Cutlor and B. L. Ramaker, "*Dynamic matrix control-A computer control algorithm*", In Proceedings of the joint automatic control conference, 1980

71. J. B. Rawlings, "*Tutorial overview of model predictive control"*, in IEE Control Systems Magazine, 2000, p. 38-52.

72. O. A. G.Sentoni, A. Desages, and J. Romagnoli, "*Approximate models for nonlinear process control",* AIChE J, 1996, **42**: p. 2240-2250.

73. H. Peng, K. Nakano, and H. Shioya, "*Nonlinear predictive control using neural nets- based local linearization ARX model-stability and industrial application",* IEEE Transactions on control systems technology, 2007. **15**(1): p. 130-143.

74. Y. C. Liu, "*Control of dynamic keyhole welding process"*, Dissertation, in Department of Electrical and Computer Engineering, 2004, University of Kentucky: Lexington.

75. L. Ljung, "*System identification-Theory for the user",* Upper Saddle River, 1997, NJ: Prentice-Hall.

76. R. K. Pearson, *Discrete-Time Dynamic Model,* 1999, New York: Oxford University Press.

77. H. K. KAHLIL, *Nonlinear Systems,* 2002, New Jersey: Prentice Hall.

78. R. Isermann, "*Identification dynamic System",* 1992, Berlin: Springer Verlag.

79. H. H. J. Bloemen, V. Verdult, T. J. J. Van Den Boom and M. Verhaegen, "*Bilinear versus Linear MPC: Application to a polymerization process"*, In 15th Triennial World Congress, 2002: Barcelona, Spain.

80. G. C. Goodwin, "*A brief overview of nonlinear control"*, In 3rd International Conference on Control Theory and Applications, 2001

81. A. D. B. Fontes, A. L. Maitelli and A. L. D. O. Cavalcanti," *Bilinear compensed generalized predictive control: An adaptive approach"*, in 5th Asian Control Conference. 2004: Melbourne, Australia, p.1781-1785.

82. J. Wang, Y. J. Li and P. Liu, "*Effect of weld heat input on toughness and structure of HAZ of new super-high strength steel",* Bull. Mater. Sci, 2003, **26**(3): p. 301-305.

83. D. M. Prett and R. D. Gillette, "*Optimization and constrained multivariable control of catalytic cracking unit*", *In Proceedings of the joint automatic control conference*, 1980.

VITA

Kun Qian was born on July 15th, 1977 in Nancheng, Jiangxi Province, China.

EDUCATION

Beijing Institute of Control Engineering, China 07/2002

M.S in Control Theory and Application Engineering

Beijing Institute of Technology, China 07/1998

B.S. in Fluid Transmission & Control Engineering

PUBLICATION

1. K. Qian, Y. M. Zhang, *Optimal Model Predictive Control of Plasma Pipe Welding Process*, in 4th IEEE Conference on Automation Science and Engineering. 2008: Key Bridge Marriott, Washington DC, USA.
2. K. Qian, Y. M. Zhang, *Model Predictive Control of Plasma Pipe Welding Process*, Trends in welding research, proceeding of the 8th International Conference.2008: Pine Mountain, Georgia, USA.
3. K. Qian, Y. M. Zhang, *Bilinear Model Predictive Control of Plasma Keyhole Pipe Welding Process,* Mechatronics2010, ETH Zurich, Switzerland.
4. X. P. Liu, Y. S. Liu, K. Qian, Y. M. Zhang, *Nonlinear Modeling and Control of Full-Penetration Dual Bypass Gas Metal Arc Welding of Aluminum,* Information Control Problems in Manufacturing, 2009: V.A. Trapeznikov Institute of Control Sciences, Russia.